

**A Modified Framework for Seismic Fragility Assessment of School
Buildings in High-Intensity Seismic Zones of Pakistan**



By

Muhammad Zain

Regn No: NUST201590302PSCEE1515F

Thesis Supervisor: Dr. Muhammad Usman

Co-Supervisor: Dr. Syed Hassan Farooq

Department of Structural Engineering

NUST Institute of Civil Engineering

School of Civil and Environmental Engineering

National University of Sciences and Technology

Islamabad, Pakistan

(2022)

**A Modified Framework for Seismic Fragility Assessment of School
Buildings in High-Intensity Seismic Zones of Pakistan**



By

Muhammad Zain

Regn No: NUST201590302PSCEE1515F

A thesis submitted to the National University of Sciences and Technology, Islamabad
in partial fulfillment of the requirements for the degree of

Doctor of Philosophy in
Structural Engineering

Thesis Supervisor: Dr. Muhammad Usman

Co-Supervisor: Dr. Syed Hassan Farooq

Department of Structural Engineering

NUST Institute of Civil Engineering

School of Civil and Environmental Engineering

National University of Sciences and Technology, Islamabad

(2022)

THESIS ACCEPTANCE CERTIFICATE

Certified that final copy of PhD Thesis written by Mr. Muhammad Zain (Registration No. NUST201590302PSCEE1515F), of Department of Structural Engineering has been vetted by undersigned, found complete in all respect as per NUST Statutes/ Regulations/ PhD Policy, is free of plagiarism, errors, and mistakes and is accepted as partial fulfillment for award of PhD degree. It is further certified that necessary amendments as point out by GEC members and foreign/ local evaluators of the scholar have also been incorporated in the said thesis.

Signature: 

Name of Supervisor: Dr. Muhammad Usman

Date: 24-10-22

Signature (HOD): 

Date: 24-10-22

Signature (Dean/ Principal): 

PROF. DR. MUHAMMAD IRFAN
Principal & Dean
SCEE, NUST

Date: 25 Oct, 2022



Annex L
Form PhD-7
DOCTORAL PROGRAMME
OF STUDY
(Must be type written)

National University of Sciences & Technology REPORT OF DOCTORAL THESIS DEFENCE

Name: Muhammad Zain NUST Regn No: NUST201590302PSCEE1515F

School/College/Centre: NICE (SCEE)

Title: A Modified Framework for Seismic Fragility Analysis of School Buildings in High-Intensity Seismic Zones of Pakistan

DOCTORAL DEFENCE COMMITTEE

Doctoral Defence held on 7th October, 2022

	QUALIFIED	NOT QUALIFIED	SIGNATURE
GEC Member-1: <u>Dr. Rao Arsalan Khushnood</u>	<input checked="" type="checkbox"/>	<input type="checkbox"/>	
GEC Member-2: <u>Dr. Ather Ali</u>	<input checked="" type="checkbox"/>	<input type="checkbox"/>	
GEC Member (External): <u>Dr. Faheem Butt</u>	<input checked="" type="checkbox"/>	<input type="checkbox"/>	
Supervisor: <u>Dr. Muhammad Usman</u>	<input checked="" type="checkbox"/>	<input type="checkbox"/>	
Co Supervisor (if appointed): <u>Dr. Syed Hassan Farooq</u>	<input checked="" type="checkbox"/>	<input type="checkbox"/>	
External Evaluator-1: <u>Dr. Muhammad Ilyas</u> (Local Expert)	<input checked="" type="checkbox"/>	<input type="checkbox"/>	
External Evaluator-2: <u>Dr. Aslam Faqeer Mohammad</u> (Local Expert)	<input checked="" type="checkbox"/>	<input type="checkbox"/>	
External Evaluator-3: <u>Dr. Chuanlin Hu</u> (Foreign Expert)	<input type="checkbox"/>	<input type="checkbox"/>	
External Evaluator-4: <u>Dr. Cong Lu</u> (Foreign Expert)	<input type="checkbox"/>	<input type="checkbox"/>	

FINAL RESULT OF THE DOCTORAL DEFENCE (Appropriate box to be signed by HOD)

PASS

FAIL

The student Muhammad Zain Regn No NUST201590302PSCEE1515F is / is NOT accepted for Doctor of Philosophy Degree.

Dated: 13 Oct, 2022

Dean/Commandant/Principal/DG
PROF DR MUHAMMAD IRFAN
Principal & Dean
NUST

Distribution:

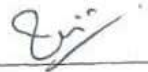
01 x original copy each for PGP Dte, Exam Branch Main Office NUST and Student's dossier at the School/College/Centre.
01 x photocopy each for HoD, Supervisor, Co-Supervisor (if appointed), sponsoring agency (if any) and 05 copies for insertion in Dissertation.
Note: Decision of External Evaluators (Foreign Experts) will be sought through video conference, if possible, on the same date and their decision will be intimated (on paper) to HQ NUST at a later date.

CERTIFICATE OF APPROVAL

This is to certify that the research work presented in this thesis, entitled "A Modified Framework for Seismic Fragility Assessment of School Buildings in High-Intensity Seismic Zones of Pakistan" was conducted by Mr. Muhammad Zain under the supervision of Dr. Muhammad Usman.

No part of this thesis has been submitted anywhere else for any other degree. This thesis is submitted to the Department of Structural Engineering in partial fulfillment of the requirements for the degree of Doctor of Philosophy in the field of Structural Engineering, NUST Institute of Civil Engineering, School of Civil and Environmental Engineering, National University of Sciences and Technology, Islamabad

Student Name: Muhammad Zain

Signature: 

Examination Committee:


a. External Examiner 1:

Prof. Dr. Muhammad Ilyas
Professor, Department of Civil Engineering, Lahore
Leads University, Lahore, Pakistan

Signature: 


b. External Examiner 2:

Dr. Aslam Faqeer Mohammad
Assistant Professor
Department of Civil Engineering
NED University of Engineering and Technology,
Karachi, Pakistan

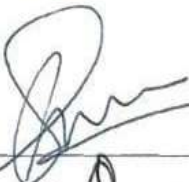
Signature: 

c. Internal Examiner:

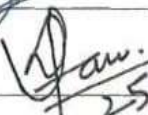
Dr. Rao Arsalan Khushnood
HOD Research
NUST Institute of Civil Engineering,
National University of Sciences and Technology
(NUST), Islamabad

Signature: 
24/1/22

Supervisor Name: Dr. Muhammad Usman

Signature: 

Dean HOD:

Signature: 
25/1/22
PROF DR MUHAMMAD IRFAN
Principal & Dean
SCEE, NUST

AUTHOR'S DECLARATION

I, Muhammad Zain, hereby state that my PhD thesis titled "A Modified Framework for Seismic Fragility Analysis of School Buildings in High-Intensity Seismic Zones of Pakistan" is my own work and has not been submitted previously by me for taking any degree from National University of Sciences and Technology, Islamabad, Pakistan or anywhere else in the country/world.

At any time if my statement is found to be incorrect even after my Graduation, the university has the right to withdraw my PhD degree.

Signature 

Student Name: Muhammad Zain

Date: 25/10/2022

PLAGIARISM UNDERTAKING

I solemnly declare that research work presented in the thesis titled “A Modified Framework for Seismic Fragility Analysis of School Buildings in High-Intensity Seismic Zones of Pakistan” is solely my research work with no significant contribution from any other person. Small contribution/ help wherever taken has been duly acknowledged and that complete thesis has been written by me.

I understand the zero-tolerance policy of the HEC and the University (National University of Sciences and Technology, Islamabad, Pakistan) towards the plagiarism. Therefore, I as an author of the above titled thesis declare that no portion of my thesis has been plagiarized and any material used as reference is properly referred/cited.

I undertake that if I am found guilty of any formal plagiarism in the above titled thesis even after award of PhD degree, the University reserves the rights to withdraw/revoke my PhD degree and that HEC and the University has the right to publish my name on the HEC/University website on which names of students are placed who submitted plagiarized thesis.

Signature _____



Student Name: Muhammad Zain

Dedication

This thesis is dedicated to my beloved Parents

(Altaf Iqbal & Nargis Shaheen)

for their endless love, prayers, and support of all kinds,

And **Z. Kalita** for being the main inspiration in my life, and motivation
behind this work (Thank you with all my heart).

Acknowledgment

I am grateful to Almighty whose countless blessings gave me strength to accomplish this research work. I sincerely thank my mentor and advisor Assoc. Prof. Dr. Muhammad Usman, Department of Structural Engineering at NUST Institute of Civil Engineering (NICE) for his advice, untiring guidance, incredible patience and supervision. He has always inspired me through his perseverance, professionalism, diligence and sincerity, and inspired me to always possess a positive attitude towards life. I am really grateful to him for his encouragement, motivation and a super-nice soft-spoken & tremendously cooperative attitude, that urged me to achieve the best during this research program, and has really inspired me to live by helping other humans on earth. I sincerely pray for his good health and success in all walks of life.

I would also like to thank my Co-Supervisor, and my research committee members: Dr. Rao Arsalan Khushnood, Dr. Ather Ali, and Dr. Faheem Butt, for their support and valuable guidance during my research.

I extend my gratitude and special thanks to Dr. Fawad Najam who extended his unconditional guidance, precious time and valued input towards my research.

I am also thankful to my parents, and sisters for their unwavering support during these times and helping me go through my journey during my failures.

I am also thankful to my not younger brother, Muhammad Zaid, for teasing me a lot to always inject vital dose of moral support and encouragement, and giving me picks-and-drops from intra-city bus terminals while disturbing his asleep, very early in the mornings.

I am truly thankful to my brother-like friend, Waleed Khan, who has been extremely generous to me all the time, and always extended his help in an unparalleled manner. I truly wish him best for all his life and future endeavors, and I pray for his success.

Last but not the least, I thank a very special person of my life, Z. Kalita, who has been the main motivation for me to pursue my doctorate. I have been truly impressed with Kalita's endurance towards life, and the way Kalita has treated me. Regardless of ups & downs, Kalita has always remained extremely true to me, and always supported me in my life, morally & emotionally, and kept me going with life. I pray for Kalita's success always.

Table of Contents

List of Figures	x
List of Tables.....	xiv
Abstract	xv
Chapter 1: Introduction.....	1
1.1. Background.....	1
1.2. Identification of Research Gap and Objectives of Research	3
1.3 Scope and Limitations of study	4
1.4. Workflow of thesis.....	4
1.5. Thesis Overview:	6
Chapter 2 : Literature Review	7
2.1. Overview.....	7
2.2 Consequence Based Engineering (CBD) – An Overview	7
2.3 Fragility Curves	9
2.3.1 Types of Fragility Curves.....	9
2.3.2 Structural Response and Seismic Excitation Intensity Parameters for Fragility Studies	13
2.3.3 Limit States of Structures for Fragility Assessment.....	15
Chapter 3 : Data Collection & Typology Identification.....	18
3.1. Overview:.....	18
3.2. Data Collection	19
3.2.1 Field Survey Procedure	19
3.2.2 Data Collection in Considered Area.....	20
3.2.3. Definition of building typologies	22
Chapter 4 : Vulnerability Assessment of School Buildings	34
4.1. Overview.....	34

4.2. Vulnerability Assessment of Reinforced Concrete (RC) Schools	35
4.2.1. Uncoupled Modal Response History Analysis (UMRHA) for elastic and inelastic systems (Conversion of 3D structure to SDOF Systems).....	35
4.2.2. Proposed methodology for seismic vulnerability assessment of RC schools	38
4.2.3. Application of proposed methodology	41
4.3. Validation of Proposed Methodology	66
4.3.1. Validation of proposed methodology through PEER’s benchmark building.....	66
4.3.2. Validation of proposed methodology through a high-rise structure	75
4.3. Vulnerability Assessment of Stone Masonry Schools.....	84
4.3.1. Structural modelling of a representative stone masonry school building	84
4.3.2. Structural analysis, performance assessment, and fragility development.....	87
4.4. Vulnerability Assessment of Brick Masonry Schools	96
4.4.1. Structural modelling of brick masonry schools	97
4.4.2. Pushover analysis	100
4.4.3. Nonlinear time history analysis and fragility derivation.....	103
Chapter 5: Conclusions and Recommendations.....	108
5.1. Conclusions.....	108
5.2. Recommendations.....	110
References.....	113

LIST OF FIGURES

Figure 1.1: Workflow of thesis.....	5
Figure 2.1: Hierarchy of Consequence-Based Engineering [5].....	8
Figure 2.2: Derived fragility curves for 3 story RC buildings in turkey for 5 damage states Using Pushover Analysis [19]	12
Figure 3.1: Story-Wise number of schools visited during data collection	21
Figure 3.2: No. of schools depending upon the construction material.....	21
Figure 3.3: Number of schools under each of 19 RC School building categories	24
Figure 3.4: Photograph of a school in Muzaffarabad district, showing disintegration of infill wall panels from RC Frame.....	25
Figure 3.5: Photographs of a school having cracked structural members: a) Isometric view of school in Neelam District; b) Cracked beam; c) cracked column.....	26
Figure 3.6: Diagonal adjoining cracks due to stress concentration near openings: (a) isometric view of school in Pangran District; (b) Shear cracking due to stress concentration near openings	26
Figure 3.7: General layout of the construction of stone masonry schools	28
Figure 3.8: Plan view of a single unit of stone masonry schools, comprising two classrooms	28
Figure 3.9: Illustrative diagram of stone masonry classroom blocks in considered region	29
Figure 3.10: Photographs of a 5-bay 1-story stone masonry building: (a) isometric view of school (b) Damaged corner wall, susceptible to out-of-plane failure (c) disintegration of corridor in front of the classrooms.	30
Figure 3.11: photographs of a 1-story, 3-bay stone masonry school: (a) isometric view (b) fallen wooden planks because of earthquake (c) crack propagating from the roof to the window	30
Figure 3.12: photograph of an abandoned 1-story school in Poonch District; (a) isometric view, showing out-of-plane failure of wall (b) falling out of stones from the school's corner (c) inside view showing fallen roof planks and cracks in wall.....	31

Figure 3.13: Plan view of a typical brick masonry school in considered region	32
Figure 3.14: 3-Dimensional analytical model of brick masonry school structure	32
Figure 4.1: Plan view of BLR-11	42
Figure 4.2: Elevation view of BLR-11, indicating the bay widths, story heights, and total height	42
Figure 4.3: Typical representation of Fibers for beams and columns [44]	44
Figure 4.4: Nonlinear static pushover analyses curves for first two modes in the weaker direction	46
Figure 4.5: Cyclic pushover behavior of considered school building	47
Figure 4.6: Comparison of roof drift, obtained from UMRHA and 3D model subjected to NLRHA	48
Figure 4.7: IDA Curves for maximum global drift v/s PGA (g)	55
Figure 4.8: IDA Curves for maximum global drift v/s Spectral Acceleration scaled at the time periods of first two modes ($S_a @ T_1, T_2$)	56
Figure 4.9: Hazard-Damage Relationship: PGA v/s Global Drift	57
Figure 4.10: Hazard-Damage Relationship: S_a v/s Global Drift	57
Figure 4.11: Derived fragility curve using fundamental mode only against PGA as an IM	60
Figure 4.12: Derived fragility curve using fundamental mode only against $S_a @ T_1$ as an IM	60
Figure 4.13: Fragility curves with 2nd mode's contribution (UMRHA framework) using PGA as an IM	62
Figure 4.14: Fragility curves with 2nd mode's contribution (UMRHA framework) using $S_a @ T_1, T_2$ as an IM	63
Figure 4.15: Comparison of fragility curves developed through analyses in fundamental mode only with the curves developed using presented methodology, considering two modes, against PGA as an IM	64

Figure 4.16: Comparison of fragility curves developed through analyses in fundamental mode only with the curves developed using presented methodology, considering two modes, against $S_a @ T_1, T_2$ as an IM	65
Figure 4.17: Plan view of PEER’s benchmark building	67
Figure 4.18: Elevation view of PEER’s benchmark building	68
Figure 4.19: Concrete model (a) unconfined and confined backbone curve (b) hysteretic behavior	72
Figure 4.20: Hysteresis loop for steel by Guiffre-Menegotto-Pinto, used by PEER	72
Figure 4.21: Fragility curve developed by PEER against collapse level LS	73
Figure 4.22: Comparison of Fragility curves developed by PEER and proposed methodology	74
Figure 4.23: Isometric view of 3-Dimensional nonlinear analytical model	76
Figure 4.24: Hysteretic behavior of considered building (Cyclic POA)	77
Figure 4.25: Roof drifts obtained through 3D model and UMRHA procedure (Proposed methodology)	78
Figure 4.26: Comparison of fragility relationships, developed with and without the contribution from higher modes: a) Fragility curves against PGA b) Fragility curves against $S_a @ 0.2$ sec. c) Fragility curves against $S_a @ 1.0$ sec.	82
Figure 4.27: A photograph of typical stone masonry block, showing the adjoining toilet, repaired door, and flexible diaphragm	84
Figure 4.28: Experimental investigation to determine material characteristics of stone: (a) Core extraction for testing; (b) Core testing	85
Figure 4.29: Plan view of considered stone masonry school building	86
Figure 4.30: 3-Dimensional view of the stone masonry school and corresponding macroelements	87
Figure 4.31: Pushover curves of a typical stone masonry school building structure in seismic zone 4 of Pakistan, representing structural capacity in terms of base shear, V_b , v/s global displacement	88

Figure 4.32: Results of seismic performance-based assessment in terms of du/dt	90
Figure 4.33: Ground motion spectra of considered GM histories in terms of Period (T) ..	93
Figure 4.34: Results of GM history analyses	93
Figure 4.35: Fragility curves for typical stone masonry school buildings in considered region.....	95
Figure 4.36: Plan view of considered brick masonry school.....	97
Figure 4.37: 3-Dimensional analytical model of brick masonry school structure in considered area	98
Figure 4.38: 3-Dimensional model of brick masonry school, showing macro elements .	100
Figure 4.39: Color legend of brick masonry results	101
Figure 4.40: (a) Plan view showing considered wall to check damage (b) Deformed shape of wall in EFM.....	101
Figure 4.41: (a) Plan view showing considered wall to check damage (b) Deformed shape of considered wall in EFM	102
Figure 4.42: Pushover curve of considered brick masonry school building, showing maximum capacity of structure as 21.59 mm (less than 1 inch)	103
Figure 4.43: Fragility relationships for brick masonry school building.....	106

LIST OF TABLES

Table 3.1: No. of Stories of School Buildings depending upon the material used in their construction	22
Table 3.2: General properties of buildings in developed database	23
Table 4.1: Reinforcement details of structural members.....	43
Table 4.2: Loading values and material strengths for analytical structural model.....	45
Table 4.3: Selected natural ground motion histories	50
Table 4.4: Numerical threshold values of global drifts for limit states in first two modes	54
Table 4.5: Lognormal distribution parameters for fragility curves against PGA and Sa@T1	61
Table 4.6: Controlling parameters for fragility curves, developed using presented methodology	63
Table 4.7: PEER’s criterion for GM selection for benchmark structure	69
Table 4.8: Selected ground motions for PEER benchmark building.....	69
Table 4.9: Geometrical features of considered high-rise building	75
Table 4.10: Material characteristics for structural components.....	76
Table 4.11: Modal mass participation ratios	77
Table 4.12: Selected ground motions for high-rise building	78
Table 4.13: Quantitative thresholds for considered limit states for considered modes	80
Table 4.14: Material characteristics of stone and mortar	85
Table 4.15: Selected ground motions for stone masonry school buildings in seismic zone 4 of Pakistan	91
Table 4.16: Quantitative values of limit states for stone masonry school buildings	95
Table 4.17: Material characteristics of brick masonry	98
Table 4.18: Modal analysis results for brick masonry school building.....	100
Table 4.19: Ground motions for brick masonry school building	104

ABSTRACT

The current research is targeted to develop analytical fragility curves for school buildings in seismic zone 4 of Pakistan. Data was collected from Muzaffarabad, Poonch, and Neelam Districts from Azad & Jammu Kashmir region that has been categorized as high-intensity seismic zone in Building Code of Pakistan. 2417 schools were visited and three building typologies; Reinforced Concrete (RC) schools, Stone Masonry schools, and Brick Masonry schools, were defined accordingly. RC schools comprised 79% of total school building stock in considered districts. On the other hand, stone masonry schools were mostly found to be abandoned, while brick masonry schools were mostly opened in houses by small-scale investors, lacking spirit of an educational facility. A new framework has been proposed and demonstrated in current research for assessing seismic fragility of RC school buildings. Developed methodology considers uncoupled modes of structure, employing nonlinear single degree of freedom structures and defines distinct limit states for each mode separately. By using presented methodology, response of higher modes was incorporated in fragility curves. For elucidation, a two-story RC school building structure was selected from seismic zone 4 of Pakistan. Presented methodology reduced computational time required for developing fragility curves of considered school building, using a regular computer. Presented methodology had been validated for its efficacy by applying it to two other case studies; a benchmark structure, developed by Pacific Earthquake Engineering Research Center, and a high-rise building with substantial modal contribution from higher modes. It has been inferred that established methodology is generic and can be conveniently employed to assess structural vulnerabilities of all sorts of RC buildings, subjected to any mixed use. Presented methodology inherently considers the effect of higher building modes in structural response and utilizes Uncoupled Modal Response History Analysis. For determining seismic fragility of stone and brick masonry schools, conventional methodology has been followed that focuses on response of fundamental mode only. Obtained results from proposed methodology prove effectiveness and simplicity of established methodology for determining seismic vulnerability with accuracy.

Keywords: High-Intensity Seismic Zones, Seismic Vulnerability, Fragility Assessment, Reinforced Concrete Structures, Unreinforced Masonry

CHAPTER 1: INTRODUCTION

1.1. Background

Pakistan has faced numerous devastating earthquake in recent years, which have shaken the confidence of local engineering community, and consequently, there is an immense need to address the shortcomings of structural systems, employed in different types of buildings, to ensure the structural safety and comfort levels of inhabitants.

It is globally apprehended that wrong conceptions in design and the collapse of poorly-constructed buildings are the major causes for large number of casualties in earthquakes. The engineering design codes ensure the safety of life by fulfilling certain criterions, nevertheless, the implied parochial requirements of codes relay on a broader grouping of structures and their occupancies, and are mostly explained in the form of numbers, arbitrary factors, and fixed values which are unable to explicitly cover the risks involved in the dynamic response of the structures. Such limitations of design codes have led to the development of “Consequence-Based Engineering (CBE)” that allows a designer to explicitly capture the uncertainties and risks involved in the dynamic response of structures. Thus, an unequivocal consideration of risks provides the foundations for the development of a framework for seismic vulnerability assessment, and seismic fragility curves are the most widely accepted and adopted method for the describing the vulnerability information. Fragility curves are one of the assimilated portions of CBE and they deliver the conditional probabilities of a structure exceeding a particular damage state at given intensities of ground motion. They can be employed for pre-earthquake planning and also for the post-earthquake losses estimation. Analogously, fragility curves can also be utilized to assess the effectiveness of different retrofiting strategies, if employed. But so far, no research has been conducted to incorporate the contribution of higher modes in structural vulnerability.

In Pakistan, the October 2005 Muzaffarabad earthquake enriched the awareness about the increasing seismic vulnerability in Pakistan. As a whole, it resulted in approximately 87000 casualties, including 19,000 school going children, and posed severe economic repercussions. Earthquake Engineering Research Institute Report, United States (US), stated complete destruction was faced by around 67% of schools in the affected area. However, the earthquake instigated a new spirit and slogan of “Build Back Better” in Pakistan, and resultantly, the Building Code of Pakistan (BCP)–Seismic Provisions 2007 emerged.

However, no comprehensive document till date exists to portray the seismic vulnerability information of public infrastructure, in particular the school buildings specifically in seismic zone 4 (very high seismic intensity zone) of Pakistan. The presented document provides a new framework to determine their structural vulnerability. Relevant information and data has been collected from three districts i.e. Muzaffarabad, Neelam, and Poonch.

The presented study is focused towards assessing the seismic vulnerability of existing school buildings in seismic zone 4 of Pakistan. The considered area experienced most colossal fiscal and socio-economic damage during the 2005 Kashmir earthquake, and therefore, in prevailing scenario, it is vital to assess the structural vulnerabilities in the considered area.

In presented work, the vulnerability for the existing school buildings has been assessed by developing a new methodology. Established methodology can also be applied to all other sorts of RC structures for assessing their vulnerability. It distinctively captures the contribution of higher modes in the overall structural vulnerability, and thus in opposition to conventional procedures that mostly define the limit states on the basis of fundamental mode only, the presented methodology allows the separate qualitative and quantitative definition of limit states for different structural modes of a same structure as it utilizes the Uncoupled Modal Response History Analysis (UMRHA), initially proposed by Chopra.

It is pertinent to mention that research for the vulnerability assessments is still lacking in the underdeveloped and developing world. Presented work attempts to fill in the research void by contributing in the process to develop the analytical vulnerability information of RC, stone, and brick masonry schools in seismic zone 4 of Pakistan by establishing a methodology that could reduce the computational effort. Presented relationships can be employed for pre-earthquake planning and for the post-earthquake losses estimation. Analogously, fragility curves can also be utilized to assess the effectiveness of different retrofitting strategies, if employed for structural interventions.

For elucidation of proposed methodology, an RC school building has been taken as a case-study out of the considered RC structural typology that has 18 other structural configurations, established after a rigorous data-collection in Neelam Valley, Muzaffarabad District, and Poonch District of Azad and Jammu Kashmir region in Pakistan. All the considered areas had been severely affected by 2005 Kashmir Earthquake, and rebuilding efforts are still

ongoing to date. Specific details about the collected data, establishment of structural typologies, and field observations have been provided in Chapter no. 3.

1.2. Identification of Research Gap and Objectives of Research

The current study primarily focuses on the development of a rational framework for seismic vulnerability assessment of school buildings in seismic zone 4 of Pakistan to obtain an insight of the structural behavior so that safety of life of the students, and other occupants can be ensured; and so that the domestic authorities may employ the presented procedure for establishing vulnerability information of other public infrastructural facilities e.g. hospitals, etc. Conventionally, the governmental authorities, and international bodies administer the school safety programs throughout the world i.e. (i) Reducing Vulnerability of School Children to Earthquakes, A project of School Earthquake Safety Initiative (SESI) of 2009, (ii) Comprehensive School Safety by United Nations Development Program (UNDP) in 2012, (iii) Disaster Risk Reduction for Schools in Nepal by Asian Development Bank (ADB), in 2013, (iv) Seismic Safety of Schools in Italy, 2018, funded by the Italian Government, and several other initiatives and programs for ensuring the societal and structural safety of schools. However, in Pakistan, no such program was developed by the governments or any international funding agency till 2017. In 2017, Pakistan's National Disaster Management Agency developed a Pakistan School Safety Framework. The framework does assert the need of vulnerability assessment of school buildings, however, it does not suggest any discreet methodology for it. The current work fills the gap by adding in a new methodology for Pakistan to swiftly evaluate the analytical vulnerability of schools so that decision makers may utilize it to form decisions about required interventions. Following are the objectives that will be precisely achieved as results of the proposed research study:

1. To conduct data-collection of schools from selected areas of Seismic Zone 4 of Pakistan for identification of their structural typologies and subsequent vulnerability assessment.
2. To conduct systematic seismic vulnerability assessment of representative school buildings from every typology using conventional methods.
3. To propose an improved framework and methodology for swift evaluation of analytical vulnerability of existing school buildings in selected areas of Seismic Zone 4 of Pakistan.

1.3 Scope and Limitations of study

The school buildings accommodate many students from different families of a community; therefore, if an earthquake causes damage to a school, it directly imposes enormous social losses along with the fiscal losses over the whole community. The proposal of a novel framework in current study is only related with and limited to the reinforced concrete school buildings of seismic zone 4 in the context of above mentioned objectives, and it does not cover any other residential or commercial building types in the said region. However, for the purpose of establishing a document that can portray the vulnerability of all types of school buildings typologies, the presented work also provides the fragility relationships of unreinforced stone and brick masonry typical schools. This work is particularly focused towards the development of fragility curves for existing school buildings and does not consider any other infrastructural facility in considered region; however, the proposed methodology in this work is generic in its nature, and thus, can be widely applied to any sort of RC structures, anywhere across the globe.

1.4. Workflow of thesis

The workflow of thesis is provided in figure 1.1. The research study starts with the data collection of school buildings from the seismic zone 4 of Pakistan. Eventually, desk study has been conducted to identify the structural typologies of schools. Afterwards, a framework for fragility analysis of RC schools has been presented and demonstrated by means of a case study, and subsequently, the proposed procedure for fragility analysis has been validated by applying it for two other case studies. Furthermore, the fragility has also been assessed for brick and stone masonry schools for the process of establishing a wholesome document, portraying the prevailing seismic vulnerability of schools in considered region. Finally, the conclusions have been drawn and recommendations have been proposed for future research in the area of seismic fragility.

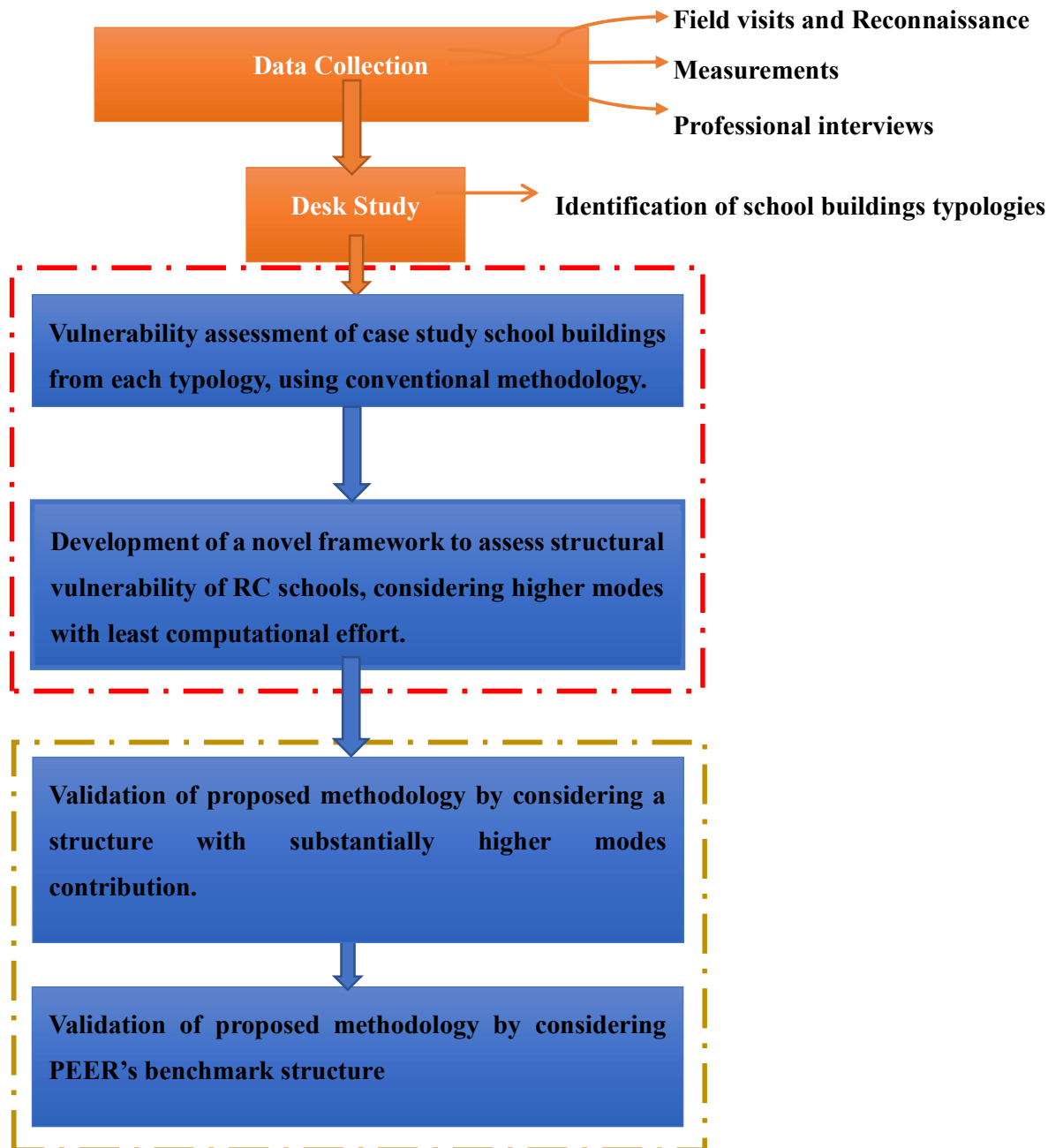


Figure 1.1: Workflow of thesis

1.5. Thesis Overview:

Chapter 1 provides the background of presented research, the problem statement, objectives, scope and limitations of the work. The whole workflow of thesis has also been provided in this chapter.

Chapter No. 2 includes the literature review and presents a review on the state of the art research, being conducted in the field of seismic fragility analysis.

Chapter No. 3 elucidates the statistics of school buildings data, collected from the field, indicating their typologies

Chapter no. 4 presents the framework for assessing the seismic vulnerability of reinforced concrete (RC) schools, and demonstrates the application of proposed framework on a case study RC school building. The results obtained from the application of the proposed procedure have also been discussed in the same chapter accordingly for convenience of readers. Furthermore, same chapter contains the seismic fragility analysis of brick and stone masonry schools, conducted using conventional procedure, as elucidated in the chapter, and the results have been discussed and elaborated accordingly.

Chapter 5 comprises the derived inferences from the work, and provides recommendations for subsequent research.

CHAPTER 2 : LITERATURE REVIEW

2.1. Overview

The classification of losses from earthquake excitations are well recognized, and the most important one is the magnitude of fatalities, which has triggered the development, as well as the refinement, of the minimum standards and design codes for structural engineers. Apart from number of casualties, the fiscal losses, either from the repairs of structures or from their complete loss, also serve as a huge concern [1].

The presence of any of such losses poses a great risk which must be identified to develop better concepts for the design and retrofiting of the structures. Consequence-Based Engineering, and advanced form of Performance-Based Engineering, permits an engineer to assess and consider that risk in a probabilistic manner. The current study utilizes the concept of CBE, and is focused towards developing a framework for assessing the structural vulnerability associated with the stocks of school buildings in AJK by considering the response from higher modes of the building structures.

2.2 Consequence Based Engineering (CBD) – An Overview

CBE is a frame work that quantifies the risk associated with an individual system, or a component of a system through a selective intervention process, and this process also helps in evaluating the significance of different mitigation measures in terms of their influence on the performance of the built facility through a continuum of earthquake risks on the reduction of the consequences through the whole system [2].

The basic equation that is involved in expressing the seismic risk can be written as:

$$\text{Seismic Risk} = \text{Hazard} \times \text{Vulnerability}$$

The above equation represents two different components which are associated with each other to pose associated risks. The “Hazard” part is usually expressed in the form of a hazard map, whereas, the remaining portion of the equation illustrates the possible exposure of a system to that hazard in the form of fragility curves [3]. CBE covers, almost, every aspect of the equation from engineering, as well as, from social and environmental point of view. Figure 2.1 illustrates the whole framework of CBE.

The CBE enables an engineer to capture the dominant factors that contribute to risk through probabilistic safety assessment for evaluating the associated uncertainties. The process begins by the selection of a system, the definition of hazards, and the establishment of the particular limit states (LS) for that system in which it discontinues to perform its anticipated function [4]. The process concludes at the probabilistic assessment of social and economic consequences, whereas, the development of fragility curves is an integral portion of the full framework that describe the associated conditional probability of exceeding a particular limit state given a seismic intensity indicator. In a structural engineering context, limit states can be either deformation related or strength related, while from a broader socioeconomic perspective, limit states can be related to fiscal losses, or even the number of casualties.

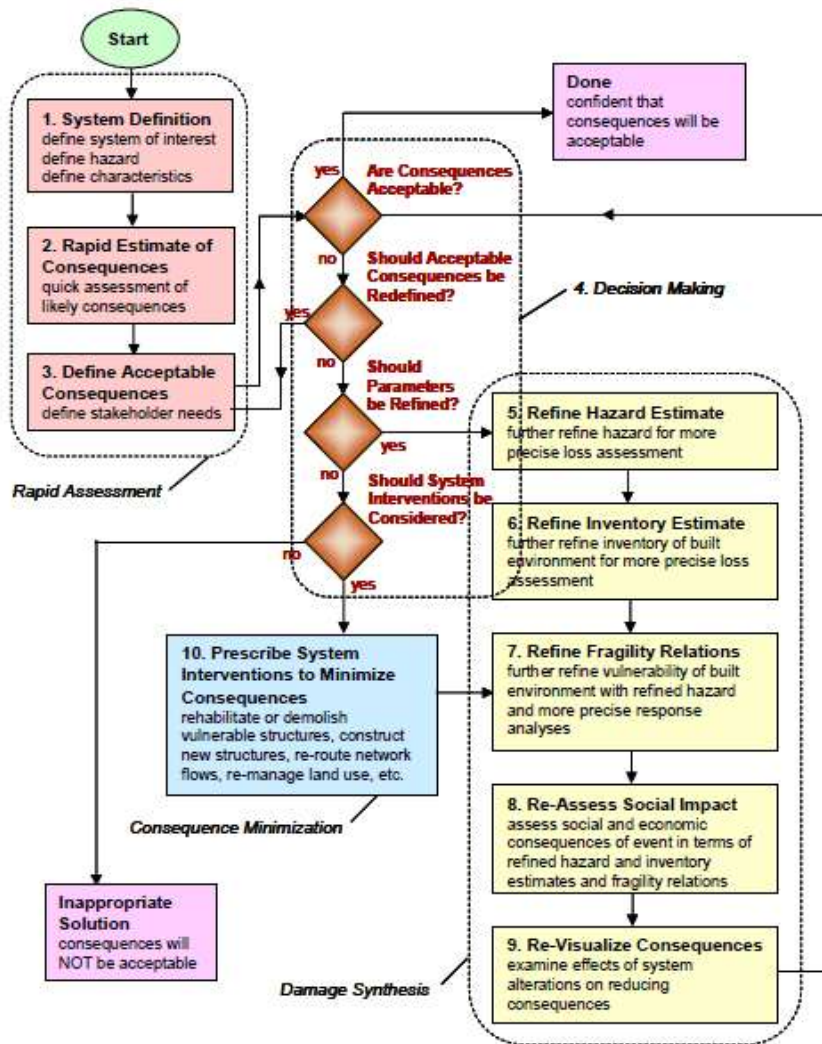


Figure 2.1: Hierarchy of Consequence-Based Engineering [5]

2.3 Fragility Curves

Fragility curves are one of the widely accepted approaches to represent the vulnerability information, specifically when multiple sources of uncertainties exist for example, seismic demands, soil-structure interaction, structural characteristics, etc.

Fragility curves or functions describe the conditional probability of reaching or exceeding a particular limit state, also known as damage state, for a given intensity of seismic excitation, and can be written in the following form as illustrated by Zain et al.[6] ;

$$P(\text{fragility}) = P [\text{LS}|\text{IM} = x]$$

Where LS indicates a specific limit or damage state of a structure, and IM is the intensity measure i.e. the intensity of ground excitation, given a particular intensity indicator which can be peak ground acceleration (PGA), spectral acceleration (Sa) at 0.2 sec., spectral acceleration at 1.0 sec., spectral velocity (Sv), spectral displacement (Sd) etc. (Ajamy et al. 2018) established the fragility relationships for jacket type offshore platforms considering two damage states i.e. extensive damage state and a collapse state. Analogously, (Giaccu and Caracoglia 2018) provided a novel algorithm to analyze the dynamic response of slender towers under turbulent winds, by using a Monte Carlo simulation based algorithm and produced fragility curves against the wind loads. However, it is quite evident from the literature that fragility curves are widely developed against the earthquake loadings and hold a limited application in the field of wind engineering. The curves can be conveniently produced by employing nonlinear static and nonlinear dynamic analyses (Alam, Kim, and Choi 2017, Tran et al. 2018, Lestuzzi et al. 2018), while nonlinear dynamic analysis is considered as most reliable method for developing fragility relationships (Bakalis and Vamvatsikos 2018). Depending upon the nature of fragility curves, they are divided into four categories which are explained in the proceeding section of the chapter.

2.3.1 Types of Fragility Curves

Existing fragility functions are classified into four types, as follows;

1. Empirical Fragility Curves
2. Judgmental Fragility Curves
3. Analytical Fragility Curves, and;

4. Hybrid Fragility Curves

The classification of fragility functions depends upon the data being used in their formation. The sources of data can be post-earthquake surveys, numerical and analytical simulations, opinion of experts, or even a combination of all these [7]. Every data source has its own intrinsic pros and cons.

2.3.1.1. Empirical Fragility Curves

In empirical fragility functions, the relationship of seismic excitation and limit states is usually established by employing the post-earthquake loss statistics [8]. Conventionally, the post-earthquake surveys pertaining to the performance of buildings are considered to be the most effective and valid actuarial source of loss as all aspects of ground motion i.e. earthquake source, variety and characteristics of path, damages of structural and non-structural components are represented in the sample.

These observations, based on one or more earthquakes, are efficiently considered significant to probabilistically evaluate the vulnerability of buildings and other assets for varying seismic excitation intensities occurring in future events, however, empirical vulnerability curves may not yield reliable predictions given the typically poor eminence and quantity of available observations. Moreover, various damage states can be defined for a same building because each observer can have different definitions for damage states, and empirical fragility curves which are constructed on the basis of data obtained from a single earthquake may not suitably provide justification for the variation in the structural response due to highly unpredictable nature of ground shaking. Such considerations make the empirical vulnerability relationships inept at predicting the vulnerability of a particular building class effected by future events. Researches performed by [9]–[11] are some of the latest examples for empirical fragility relationships.

2.3.1.2. Judgmental Fragility Curves

Judgmental fragility curves, also known as expert opinion based fragility relationships, are developed on the basis of the judgement and the expertise of the experts who provide an estimate of the likelihood of damage for different types and classes of structures at varying intensities of ground motion. Applied Technology Council (ATC) developed the empirical fragility relationships for the first time in 1985 and evaluated the possibility of 7 level of damage on bridges in terms of Modified-Mercalli Intensity (MMI), and all this was

completed with the help of collected data, obtained from several experts to forecast seismic response [12]. Such relationships are not significantly affected by the limitations pertaining to the eminence and quantity of the actuarial structural damage data, nevertheless, the relationships are strictly associated with the experience of the experts [13].

2.3.1.3. Analytical Fragility Curves

Analytical fragility curves are generated by employing the numerical simulations of the structures to anticipate the probability of exceedance of particular damage states of structures. In simple words, the structural system behavior, including the disparities and fluctuations in the structural demand and capacity, is simulated by employing the numerical techniques, and finally the probability distributions for the damage related to particular damage measures and intensity measures are evaluated [6]. The curves generated through numerical analysis are considered impartial and usually considered as the most reliable vulnerability estimate, however, despite of the reliability of such curves, few analytical curves have been developed for reinforced concrete buildings because of the involvement of extensive computational effort in the analysis and the limitations of software that are used to develop analytical and mathematical models of the structures, while recent developments in structural engineering industry have led to the inclusion of number of features such as soil-structure interaction, concrete confinements, axial-shear-flexure interaction, local and global buckling of steel members, etc. in the numerical analysis, and such advances has elevated the popularity of analytical fragility relationships in terms of their efficiency [7]. D. Forcellini, N. Giordano et al., and Sadraddin [14]–[17] have provided the outcomes of their vulnerability assessment in terms of the analytical fragility curves.

Several procedures have been developed and employed for the generation of such relationships which vary from the linear static analysis to most versatile, non-linear dynamic analysis. Karimzadeh et al. [18] developed the fragility curves for masonry buildings in Eastern Turkey using simulated ground motions, and compared them with results obtained from real ground motions, and eventually concluded that simulated ground motions yield somewhat higher probabilities of exceedance for damage states indicating severe damage.

Di Cesare and Ponzio [19] derived fragility curves for 3 story RC buildings in turkey for 5 damage states Using Pushover Analysis, a nonlinear static analysis. Their research

considered the effects of infill walls during the fragility analysis. Figure 2.2 shows the established building configuration and resulting fragility curves by their work.

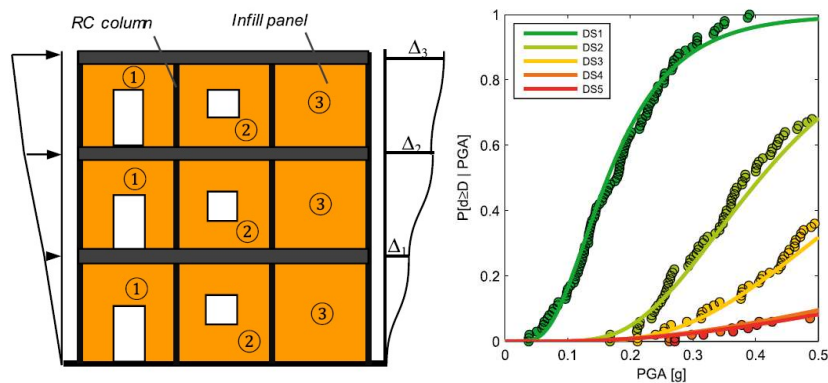


Figure 2.2: Derived fragility curves for 3 story RC buildings in turkey for 5 damage states Using Pushover Analysis [19]

The structural analysis procedures, idealization techniques, hazards and attenuation models; employed by different experts for a same facility, effect the properties of analytical fragility relationships.

2.3.1.4. Hybrid Fragility Curves

Hybrid fragility relationships are developed by combining analytical, empirical and judgmental fragility approaches, and they provide more rational estimate of vulnerability. Hybrid fragility curves are used when there is insufficient data for the empirical and experimental methods, and analytical fragility assessment becomes difficult due to limitations in the modelling capabilities [20]. Recent examples of hybrid fragility curves can be found in the work of Sandoli et al. [21] in which they had utilized Bayesian technique for upgrading the contemporary analytical fragility curves for low rise frames by utilizing the damage data, obtained by inspecting approximately 84 buildings, influenced by the Northridge earthquake. Thus, the combination of analytical fragility and observational-based (judgmental fragility) fragility relationships can be considered as a distinctive example of hybrid fragility curves.

The current study focuses on the development of analytical fragility curves for low rise school buildings located in Muzaffarabad region which is highly prone to seismic excitations

in Pakistan. These buildings were severely affected during the AJK 2005 Earthquake, and their collapse caused several casualties during the seismic excitation.

2.3.2 Structural Response and Seismic Excitation Intensity Parameters for Fragility Studies

While executing the dynamic analysis, the demand on a system is described by the intensity of the ground excitation, whereas, the limit states of a structure correspond to the structural response against the dynamic motion of the ground, and since both of them are essentially required for performing the fragility analysis, the following sections provide an insight to the work of different researchers who employed different structural response indicators and seismic intensity indicators while deriving the analytical fragility relationships

2.3.2.1. Seismic Intensity Indicators

Several seismic intensity indicators e.g. peak ground acceleration (PGA), spectral acceleration (Sa) at 0.2 seconds, spectral acceleration at 1.0 second, peak ground velocity (PGV), etc. has been employed in deriving the fragility relationships that can correlate well with the anticipated structural response, and there exists a lot of contentious debate in their selection. Altug and Serdar [22] used PGA, PGV, and spectral displacement (Sd) at fundamental mode time periods for 28 low-rise and mid-rise concrete buildings in Turkey. Analogously, Güneyisi [7], used PGA, Sa, and Sd as for indicating the seismic intensity during the fragility analysis of a 12 story reinforced concrete frame structure on a stiff soil. Some of the conventional parameters that have been employed in various researches to demonstrate the amplitude of the ground motion include Root Mean Square (RMS) Acceleration, spectral intensity, Modified-Mercalli Intensity, and Arias Intensity (AI) [23]. Zhai et al. [23], used PGA and Sa as earthquake intensity indicators while developing the analytical fragility curves for civil structures, considering soil-structure interaction. Ercolino et al. 2018; Wu et al. [24-[25] used Sa at the fundamental time period of the structures as their intensity measure.

United States Geological Survey (USGS) suggests that PGA is a good index to seismic hazard for short buildings that consist of up to 7 stories, that essentially means if some measure of structural response e.g. the total base shear or inter-story drift, is plotted against PGA, for a number of different earthquakes and buildings, a strong correlation among them

can be observed. USGS also suggests that PGV is particularly suitable for taller buildings, nevertheless, it is still not very clear that how the velocity should be related to force in for designing a tall building.

Furthermore, USGS also states that spectral acceleration would also be a good index as it is more closely related to the building's structural behavior in comparison with the peak ground motion parameters, however, the design forces are likely to be more convoluted to evaluate as the modal time periods must also be considered during calculations.

An investigation performed by Pejovic and Jankovic [26], yielded that PGA provides greatest dispersion in results in comparison with the peak ground velocity, spectral acceleration, and spectral displacement, scaled at the fundamental time period of structure. The research portrayed the efficacy of spectral response parameters, i.e. $S_a @ T_1$ and $S_d @ T_1$ as such IMs were able to incorporate the dynamic characteristics of the structures.

The current study considers spectral acceleration and PGA, both, intensity measures. PGA is the most widely considered intensity measure because of its easiness to be comprehended by the people with no technical background, while spectral acceleration as an IM incorporates corresponds with the structural features during analyses.

2.3.2.2. Structural Response Indicator

The selection of different structural response indicators (also known as 'Engineering Demand Parameter (EDP)', and 'Damage Indicators') depends upon whether the fragility is intended to be developed at global level, or local (member) level. Abraik and Youssef [27] used maximum inter-story drift ratios as response indicator to define four different damage states; slight, moderate, major, and complete collapse. Wu et al. [28] employed story drift capacities to generate analytical fragility functions for a three story reinforced concrete frame, designed to resist gravity loading only, before and after it's retrofitting by increasing the column-to-beam ratios and consequently, quantified the seismic risk in China. Siva et al. [29] used the nonlinear response history analysis to assess the response of a ten story reinforced concrete structure at varyingly increasing ground motion intensities, and selected peak floor acceleration at all story levels along with the inter story drift ratio at all floors of the building to indicate the structural response against the seismic excitations during their research work.

Zain et al. [6] stated that the intended type of performance assessment i.e. structural damage assessment or non-structural damage assessment, also influences the selection of damage indicators, for instance, maximum inter-story drift ratios are most widely used for co-relating the structural damage response with the seismic demands while developing the fragility curves, whereas, peak roof accelerations are usually used for evaluating the non-structural damages.

Sadraddin [17] developed the analytical fragility relationships for 3 buildings, each having 12 number of stories but different structural configuration, by using Incremental Dynamic Analysis (IDA), and employed maximum inter-story drift ratio as a damage measure to compare the structural damage of the buildings.

Flexural strength of members was used to characterize the first limit state (LS1) by Casotto et al. [30], while their research employed the limit of 3% for inter-story drift for second limit state which indicated the flexural collapse. Subsequently, LS2 indicated collapse of beam in their work. 1%, 2% and 4% Inter-story drift ratios were used as the DIs to relate structural performance with three different performance levels. Al Mamun et al. [31] also employed the drift ratio to assess the seismic vulnerability of existing Canadian buildings. The selection of the damage indicator for this particular study is discussed in the proceeding chapter.

2.3.3 Limit States of Structures for Fragility Assessment

Limit state or damage state of a structure describes a particular level of damage experienced by a structure given a specific seismic excitation, nevertheless, a structure can have many damage states, ranging from no or minor damage to complete collapse. The limit states in the literature are classified into two categories; the one is qualitative as employed by the FEMA 273 i.e. Immediate Occupancy (IO), Life Safety (LS), and Collapse Prevention (CP), while the other category holds quantitative limit states which are characterized by numerical values of structural damage measures e.g. forces, deformations, inter-story drift ratios, etc. HAZUS, a software package developed by FEMA to assess the regional seismic risk, uses a color index to characterize the buildings' damage states into four categories. In HAZUS software package, the green color describes undamaged or minor structural damage state, the yellow color is related to moderate structural damage, and the orange color corresponds with an extensive structural damage, while the red color represents the full dynamic instability or complete structural damage.

Karimzadeh et al. [18] defined three limit states; serviceability (LS1), damage control (LS2), and collapse prevention (LS3), characterize by the stiffness of the structure which corresponded with the softening index (SI).

Serdar Kirçil and Polat [32] developed the fragility curves for mid-rise buildings, ranging from 3 to 7 stories, in Turkey for yielding and collapse capacity by employing incremental dynamic analysis with artificial ground motions.

Bakalis and Vamvatsikos [33] executed IDA with a scaled suit of 20 ground motions at different intensities to develop the analytical fragility functions for three limit states i.e. immediate occupancy, collapse prevention, and global dynamic instability, which were characterize by the numerical values of maximum inter-story drift ratios obtained from the results of IDA.

Ji et al. [34] developed the analytical fragility functions for a RC frame and shear wall building for three damage states, namely as serviceability, damage control, and collapse prevention, and these limit states were dependent upon the numerical values of inter story drift ratio and inter-story pure translation ratio (ISPT) which were used as damage measures. Fardis et al. [35] used two damage states i.e. member yielding and ultimate condition in flexure and shear, and employed chord rotation at the member's end as a damage measure in flexure, and the shear force outside and inside the plastic hinge as a damage measure for shear in ultimate condition. Three damage states, ranging from slight damage to complete collapse were used by Ghimire and Chaulagain [36] to develop empirical fragility relationships for buildings in Nepal. Both of the researches eventually related their results with the damage levels specified in FEMA356, which stipulates three damage or limit states i.e. Immediate Occupancy, Life Safety, and Collapse Prevention; characterized by 1%, 2%, and 4% inter-story drift ratios respectively.

The current study employs three damage states for presented work. The data and details about the adopted damage/limit states are discussed in 4th chapter. The current study primarily focuses on the development of a rational framework for seismic vulnerability assessment of school buildings in seismic zone 4 of Pakistan to obtain an insight of the structural behavior so that safety of life of the students, and other occupants can be ensured; and so that the domestic authorities may employ the presented procedure for establishing vulnerability information of other public infrastructural facilities e.g. hospitals, etc.

Conventionally, the governmental authorities, and international bodies administer the school safety programs throughout the world i.e. (i) Reducing Vulnerability of School Children to Earthquakes, A project of School Earthquake Safety Initiative (SESI) of 2009, (ii) Comprehensive School Safety by United Nations Development Program (UNDP) in 2012, (iii) Disaster Risk Reduction for Schools in Nepal by Asian Development Bank (ADB), in 2013, (iv) Seismic Safety of Schools in Italy, 2018, funded by the Italian Government, and several other initiatives and programs for ensuring the societal and structural safety of schools. However, in Pakistan, no such program was developed by the governments or any international funding agency till 2017. In 2017, Pakistan's National Disaster Management Agency developed a Pakistan School Safety Framework. The framework does assert the need of vulnerability assessment of school buildings, however, it does not suggest any discreet methodology for it. The current work fills the gap by adding in a new methodology for Pakistan to swiftly evaluate the analytical vulnerability of schools so that decision makers may utilize it to form decisions about required interventions.

CHAPTER 3 : DATA COLLECTION & TYPOLOGY IDENTIFICATION

3.1. Overview:

This chapter presents the procedure and statistics of collected data from considered region. Three districts, Poonch Valley, Neelam Valley, and Muzaffarabad District were selected to collect the data of school buildings. The school buildings in these areas were visited, inspected, and resultantly, building typologies were identified on the basis of material used in their construction. All three districts fall under the seismic zone 4 of Pakistan according to Building Code of Pakistan –Seismic Provision 2007. This chapter presents the procedure developed and adopted for data collection in considered districts. The collected data revealed substantial information about the architectural and structural design of schools in considered areas. During the data collection, professional interviews were conducted to obtain architectural and primarily the structural drawings of as built structures. Three school building typologies were identified i.e. reinforced concrete (RC) frame structures, stone masonry schools, and brick masonry schools.

The existence of the Himalayan Range with the world's highest peaks is evidence of the continued tectonic activities beneath the country. As a result, considered areas, Muzaffarabd, Neelam, and Poonch districts, are seismically highly active and prone regions in Pakistan. They have a long and vast history of destructive earthquakes, while the most devastating earthquake in the latest history is the Hazara Kashmir Earthquake 2005. The majority of the reported destruction from the said earthquake occurred in Khyber Pakhtunkhwa (KPK), and out of the reported casualties, more than 25000 school going children died because of school building collapse and timing of earthquake which was 0850 hrs. in the morning [37]. This event confirmed that, because of its geological characteristics, KPK is susceptible to enhanced damage during an earthquake.

Despite of such high risk of earthquakes, the school buildings' designs in KPK are deprived of the seismic structural safety, and they are designed and constructed very informally like common residential buildings without any seismic design considerations.

Presently, no effort has been made to evaluate the earthquake risk of public schools in KPK, and consequently, there is a dire need to conduct the seismic vulnerability assessment of existing school buildings in public and private sectors to determine their seismic

vulnerability for suggesting the appropriate retrofit designs to enhance their seismic performance. Apparently it is quite evident that majority of school buildings are quite vulnerable to any sort of seismic activity that is admonishing.

3.2. Data Collection

3.2.1 Field Survey Procedure

For developing the fragility functions for a general building stock, versatile sets of generic building models are of vital importance. These generic building models reflect the dynamic response of different buildings in the stock and its relative variation. To create the generic models that can accurately predict the structural response, it is essential to clearly understand the local building designs and the different construction practices of the considered area, and for this purpose, a field survey has been conducted on the study area to acquire the indispensable information.

To gather the information about the buildings, the field survey was conducted on the questionnaire developed by *FEMA 154 Report*. The collected data was eventually used to develop the statistics and to identify different typologies of school buildings in visited areas; while a detailed analytical vulnerability assessment was conducted by considering one school building from each building typology to assess the structural vulnerability against seismic activities.

For collecting the data, initially a reconnaissance survey was conducted for every school building where all the information had been collected by the visual inspections only from the outside of sample buildings.

Since, the reconnaissance is conventionally an easy task, the time required to attain data from a sample building was short, and consequently, the field team was able to acquire adequate information about the architectural configurations of schools in considered region.

After reconnaissance sidewalk was conducted for every school; however, complete tape measurements (measurement of structural member dimensions, span lengths, etc.) were taken from inside and outside of the building after getting proper permission from the concerned stakeholders.

1st-floor plan sketches, which were helpful in recording the total number of bays and their respective span lengths, the cross sectional dimensions and locations of the columns (if any),

and the thickness of load bearing walls and infill walls and their locations were recorded at this stage. For inducing adequate quality in collected data and to accommodate various sources of data and domestic construction practices, as-built drawings were collected from domestic renowned construction supervision firm, National Engineering Services of Pakistan (NESPAK) that works with Earthquake Reconstruction and Rehabilitation Authority (ERRA) of Pakistan, formed after 2005 Kashmir-Hazara earthquake. It is pertinent to mention that NESPAK could provide only three types of architectural and structural configurations for school buildings in the considered region. It was observed that there wasn't a general or any consolidated authority that could regularize the construction of schools.

3.2.2 Data Collection in Considered Area

In regional seismic loss assessments, a large number of buildings are considered, rendering the derivation of fragility functions for each building nearly impossible due to huge computational effort. To cope with this difficulty, the buildings with analogous characteristics are grouped together, and the fragility curves are derived in this work for each of the group of the building without a significant loss of accuracy. The details for vulnerability assessment are provided in proceeding chapter. Following the procedure prescribed in preceding section, the data has been collected from Muzaffarabad, Neelam, and Poonch districts.

Precisely, 2417 schools were visited. Out of total 2417 schools, 1158 were single-story schools, 847 were two-story schools, while 412 were three-story schools. Figure 3.1 provides the pictorial representation of collected data. Figure 3.2 describes the number of school buildings depending upon the primary material used for their construction. From figure 3.2, it can be acutely observed that there were a total of 1900 RC frame school buildings, 417 brick masonry buildings, and only a total of 100 stone masonry school buildings. Table 3.1 depicts all the information in terms of percentage. It is apposite to elaborate that only one stone masonry building was found to be a two-story school, while rest of the stone masonry schools were only single story structures. Out of total 1900 reinforced concrete (RC) frames, 804 were single-story, 684 were double-story, while 412 were three-story. The two-story schools had maximum number of pupils, while three-story structures had better-allied facilities i.e. laboratories, library, etc. Out of total 417 brick masonry schools, 255 structures

were double-story, while 162 were single-story. In counting the number of stories, top roof and water storage tanks, situated at the roof, were not considered. It was observed that almost all brick masonry schools were privately owned and were opened in house buildings instead of purpose-built infrastructure. It was also observed that such schools charged heavily, and when private investors ran out of investment to run schools, schools were used to be closed permanently. Therefore, brick masonry schools did not address community at large.

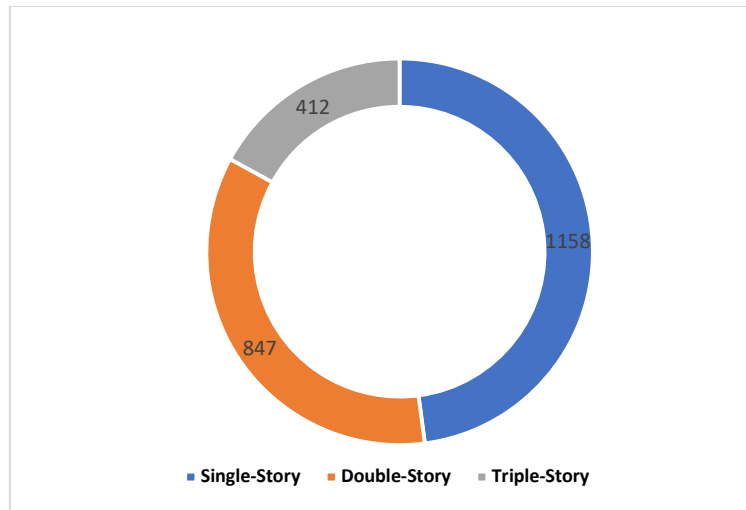


Figure 3.1: Story-Wise number of schools visited during data collection

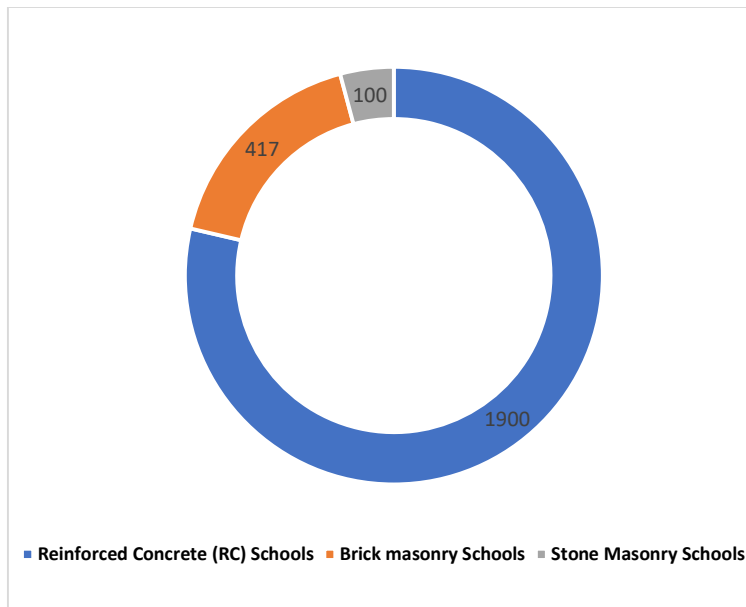


Figure 3.2: No. of schools depending upon the construction material

Table 3.1: No. of Stories of School Buildings depending on material used in construction

No. of Stories	School Building Typology			
	Reinforced Concrete	Brick Masonry	Stone Masonry	<u>Total</u>
Single Story	804	255	99	1158 (48%)
Double Story	684	162	1	847 (35%)
Triple Story	412	0	0	412 (17%)
<u>Total</u>	1900 (79%)	417 (17.25%)	100 (4.14%)	<u>2417 (100%)</u>

3.2.3. Definition of building typologies

During field visits, detailed plans were developed for all types of structural variations. Out of 2417 schools, 1933 schools were thoroughly inspected, and domestic users, and people extended ample cooperation while describing the structural performance of the buildings after the 2005 earthquake. For remaining 484 school buildings, exterior was available from which the external columns, beams, and bays were observed. It had been observed from the collected data that 48% of the building stock comprised single story school buildings, with variations in their story heights and number of bays, 35% and 17% comprised double and triple story school buildings respectively, as indicated in table 3.1. In the present work, the building typologies have been defined by considering the material used in their construction. Thus, based on the material, three school buildings typology have been identified:

1. RC Frame Schools
2. Brick Masonry Schools
3. Stone Masonry Schools

Under each typology, different structural configurations were identified and noted. Public RC schools had set modules for construction. It had been found that ERRA established typical structural and architectural designs that were subsequently replicated throughout the considered areas for the construction of schools. During data collection process, it was observed that ERRA focused on perpetually removing the stone masonry schools in

considered region due to their ability to attract more earthquake forces that eventually result in the collapse of buildings, threatening the lives of pupils, and other users.

3.2.3.1. RC Frame School Buildings

Through the professional interviews and field surveys, 19 types of RC school buildings' configurations were identified. Table 3.2 shows the related information of the schools including their number of bays, story height, and the slab opening areas. All names start from BLR that denotes the nomenclature of "Building-Low Rise", for all 19 RC school configurations.

Table 3.2: General properties of buildings in developed database

Building ID	No. of Stories	No. of Bays X direction	No. of Bays Y direction	Total Building Height (m)	Typical Floor Area (m²)	Area of Slab opening (m²)
BLR-1	1	6	3	3.8	328.6	-
BLR-2	1	3	3	3.0	101.5	-
BLR-3	1	4	2	3.8	143.1	-
BLR-4	1	4	2	3.8	146.6	-
BLR-5	1	5	2	3.6	197.0	-
BLR-6	1	6	3	3.6	328	-
BLR-7	1	6	3	3.0	306.6	-
BLR-8	1	3	2	3.8	80.8	-
BLR-9	2	4	2	7.6	145.2	9.3
BLR-10	2	4	2	7.6	125.5	9.3

BLR-11	2	11	2	6.1	344.5	21.6
BLR-12	2	2	2	6.1	66.4	6.8
BLR-13	2	5	2	6.7	192.7	16.3
BLR-14	2	8	3	6.7	253.6	23.5
BLR-15	2	3	2	6.1	58	5.7
BLR-16	2	5	2	6.1	223	7.7
BLR-17	3	4	2	11	390.2	24.8
BLR-18	3	5	2	11	209.2	15.3
BLR-19	3	12	2	9.1	377.6	21.4

Figure 3.3 provides the number of schools under each of the 19 school building categories.

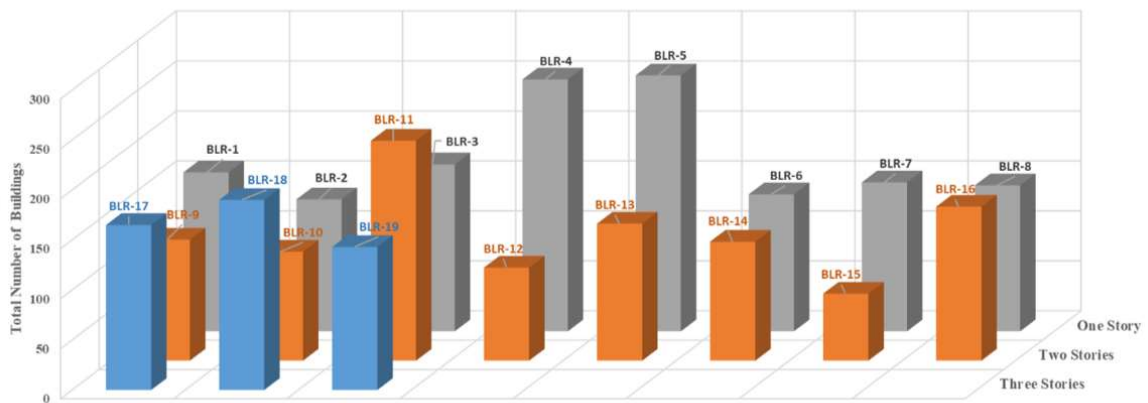


Figure 3.3: Number of schools under each of 19 RC School building categories

For the structural details about all the mentioned configurations, the reader is referred to the attached CD-Rom that contains all the drawings of plans, elevations, X-sections, detailing,

design information and other relevant information. During data collection, BLR-5 was found to be the most frequently constructed school building in a single-story category, whereas, BLR-11 was found to be the same in the two-story schools. On the other hand, in three-story schools, BLR-18 was the most frequently constructed school building. In current work, BLR-11 has been taken as the case study as this configuration accommodated maximum number of students in accordance with the information of the authors. Three-story schools mostly accommodated allied facilities, such as the laboratories, libraries, etc. Therefore, BLR-11 was found to be the most suitable one for demonstration the proposed framework in this study.

3.2.3.1.1 Field observations of structural system and damages for RC Schools

During data collection process, generic observations were made about the structural system and the failure mechanisms of RC schools. For RC schools, structural system comprised moment resisting frames and rigid diaphragms. During field surveys, different types of damages were observed. Some were mechanised, while some were found to be quite random in their nature. Columns were observed under subsection to shear forces, more than their capacity. Obtrusive in-plane and out-of-plane failures were visible for infill panels at numerous places. Figure 3.4 shows a photograph exhibiting the disintegration of infill panels from an RC frame that may eventually result in out-of-plane failure, jeopardizing the life of students, and other users of the school building.

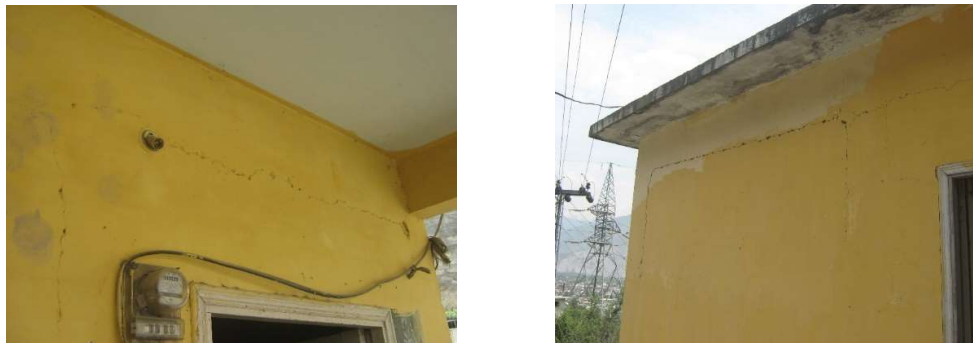


Figure 3.4: Photograph of a school in Muzaffarabad district, showing disintegration of infill wall panels from RC Frame.

Another figure 3.5 shows the photograph of column and beam, cracked after the Kashmir earthquake of 2005. The photograph was taken from a school situated in Neelam District. Figure 3.5 (a) shows the isometric view of visited school, while figure 3.5 (b) and 3.5 (c)

shows the structural cracks propagating through beam and a column respectively. The cracks propagated throughout the structural depth of members, and thus can be further widened in subsequent seismic events.

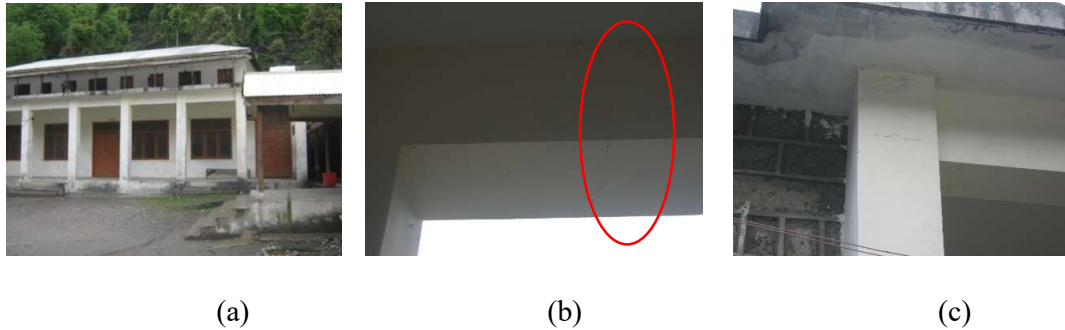


Figure 3.5: Photographs of a school having cracked structural members: a) Isometric view of school in Neelam District; b) Cracked beam; c) cracked column

The formation of cracks identify false practices of design at domestic level that could not explicitly incorporate true seismic forces. Since cracks could be seen near ends or edges of structural members, therefore, it is apprehended that structural detailing was not up to established standards that are conventionally practiced to reduce structural vulnerability, and thus earthquake forces produced cracking near edges of members. Some other observations revealed the shear cracking due to stress concentration during seismic events near the windows. Figure 3.6 shows photographs of a school in Pangran District that was subjected to cracking due to stress being concentrated near the openings. Along with its isometric view.



Figure 3.6: Diagonal adjoining cracks due to stress concentration near openings: (a) isometric view of school; (b) Shear cracking due to stress concentration near openings

Cracks in figure 3.6 (b) manifests the propagation, and subsequently, the adjoining of cracks near wall joints. The photograph of cracks shows that a crack initiated from an opening while propagated to other wall because of weaker wall joints, and thus eventually joined the crack from the other wall that was also initiated due to stress concentration near the openings. Cracks having some slighter thickness near the ceiling can also be observed from figure 3.6 (b); however, it is worthy to mention that formation of plastic hinges was not observed in the slabs itself. Therefore, it can be concluded that diaphragms performed well during the seismic events of varying intensities.

There were some other minor damages that were observed during the field observations. It was revealed that poor structural performance had primarily been attributed to inadequate construction practices (as presented in figure 3.6), lower concrete strengths, inadequate lateral strength and stiffness in weaker directions of school buildings, strong beam and weaker column phenomenon (as shown in figure 3.5 (c)), and insufficient confinement of reinforcing steel near connections, as observed in figure 3.5 (b). Furthermore, infill panels created a sophisticated degree of problems because of an inappropriate connection between the masonry panels and concrete frame. Thus, it has been imperative for domestic authorities to assess the prevailing vulnerability and structurally intervene for improving the structural performance of RC school buildings to safeguard the life of students and other users of building.

3.2.3.2. Stone Masonry Building Typology

As stated previously, ERRA Pakistan had been removing all stone masonry schools in seismic zones due to the brittle behavior of stone masonry during earthquakes. It was also observed that most of the existing stone masonry schools were abandoned. During field visits and data collection process, prominent corner stone displacement was observed along with other in-plane and out-of-plane failures, along with. For the purpose of assessing structural vulnerability and developing generic guidelines for seismic retrofitting, the current study considers most frequently constructed layout of existing stone masonry school structures. Figure 3.7 portrays the general layout of stone masonry schools in an area. Generally, stone masonry schools were found to be constructed in 42' X 18' blocks, with principal and staff room situated separately at some distance. Such blocks contained two classrooms for teaching activities up to primary educational level only. In 18' breadth of a typical stone masonry school, 8' was typically dedicated for pedestrian walkway so that

pupils, teachers, and other users can walk through the building and classrooms. Figure 3.8 shows the typical plan view of the stone masonry schools observed in the region, while figure 3.9 depicts a typical illustration of stone masonry buildings in considered region. Stone masonry school buildings also had a bathroom attached directly to classroom blocks.

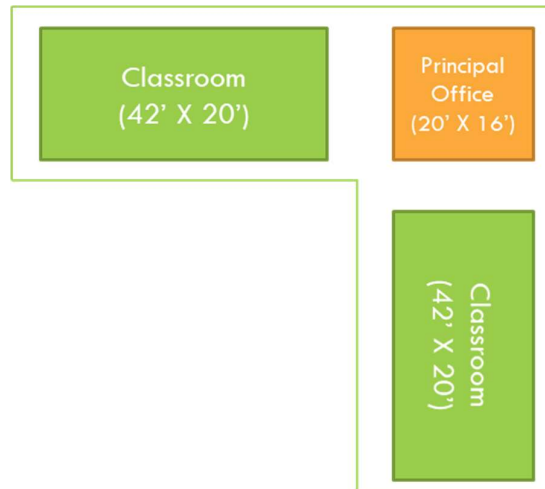


Figure 3.7: General layout of the construction of stone masonry schools

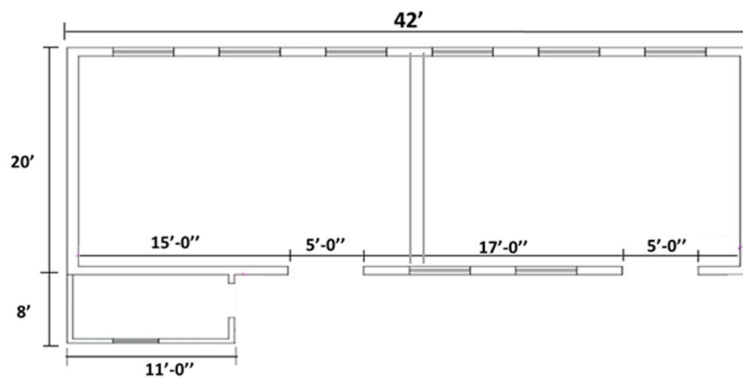


Figure 3.8: Plan view of a single unit of stone masonry schools, comprising two classrooms

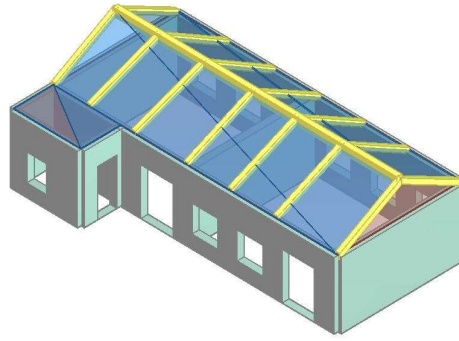


Figure 3.9: Illustrative diagram of stone masonry classroom blocks in considered region

As described earlier, there were a total of 100 stone masonry schools. Out of these 100 schools, only one school was a double story stone masonry structure, while rest of them were single-story buildings with some variations in number of bays. In the present study, only two bay stone masonry structure has been selected for vulnerability assessment and for the development of retrofitting guideline as such variant has been the mostly constructed configuration in considered area.

3.2.3.2.1. Field observations for structural damages in stone masonry schools

As described earlier, stone buildings were found to be highly damaged during field surveys in post-earthquake scenario. Most of the stone masonry buildings were found to be abandoned, while a few were subjected to use after minor repairs instead of full scale retrofitting or strengthening. Most critical damage observed was the out-of-plane damage to walls; however, out-of-plane failure was not a common failure rather only existed in a handful of schools. Figure 3.10 shows different photographs and views of a damaged 5-bay, 1-story stone masonry school in Muzaffarabad District. The school was damaged during 2005 Kashmir earthquake; however, no specific structural intervention was done to retrofit or strengthen the school before it was again subjected to use by the students, teachers, and other staff for educational activities.



(a)

(b)

(c)

Figure 3.10: Photographs of a 5-bay 1-story stone masonry building: (a) isometric view of school (b) Damaged corner wall, susceptible to out-of-plane failure (c) disintegration of corridor in front of the classrooms.

The school shown in figure 3.10 was severely damaged due to earthquake. Many structural cracks were observed and spalling of cement was visible all around the school. The corner walls were found to be critically damages and disintegrated from the adjoining walls. Similarly, figure 3.11 shows photographs of a 1-story 3-bay stone masonry school from Neelam Valley. The mentioned school was also heavily damaged during 2005 earthquake, but was again subjected to use after minor and surficial repairs.



(a)

(b)

(c)

Figure 3.11: photographs of a 1-story, 3-bay stone masonry school: (a) isometric view (b) fallen wooden planks because of earthquake (c) crack propagating from the roof to the window

In figure 3.11, the school in consideration had fallen wooden planks inside the classrooms. The openings (windows) behaved in a typical manner because of the stress concentration around the corners. Similarly, for the purpose of portraying information out of the collected

data, another damaged stone masonry school example has been taken from the Poonch District. Figure 3.12 shows 1-classroom, abandoned stone masonry school structure. Different photographs of the school has been shown in the same figure. The school was damaged to an extent where it could be retrofitted; however, due to unavailability of technical services in the domestic area, the school was abandoned.



(a)

(b)

(c)

Figure 3.12: photograph of an abandoned 1-story school in Poonch District; (a) isometric view, showing out-of-plane failure of wall (b) falling out of stones from the school's corner (c) inside view showing fallen roof planks and cracks in wall.

Figure 3.12 (b) shows the susceptibility of stone masonry schools towards earthquakes. From the presented photograph, it can be easily apprehended that bulging out of stones from the lower corner could trigger progressive collapse of the school, which would had been devastating. With little effort by improving the wall connections, the school could be re-subjected to use. The unavailability prevailing vulnerability information to domestic authorities render it difficult for strengthening and retrofitting of stone masonry structures that make the lives of students, teachers, staff, and other people nearby, endangered due to poor structural behaviour.

3.2.3.3 Brick Masonry Structures

Brick masonry in considered area were largely owned by small scale private investors who opened up the schools in house-buildings with very little or almost no purpose-built environment. Therefore, principal emphasis has been given on the RC frames and stone masonry structures. For incorporating the vulnerability assessment of brick masonry structures and to propose rational retrofitting methodologies and guidelines for brick masonry schools, the current study considers a sample two- story brick masonry school

building representative of the particular stock in considered high intensity seismic zones. The plan view of the considered representative brick masonry school structure is presented in figure 3.13. The presented building is considered as representative of brick masonry stock as it has the typical thickness of brick walls i.e. 13 inches, used as structural components in houses being used as schools. Furthermore, a typical slab thickness of 6 inches has been observed in all such structures. Totally 417 brick masonry schools were visited in the present study. Out of which 255 were single-story and 162 were double-story, as describer earlier. One-story schools have not been considered as such schools had very limited classrooms and were mostly had few pupils up to elementary level of education only.

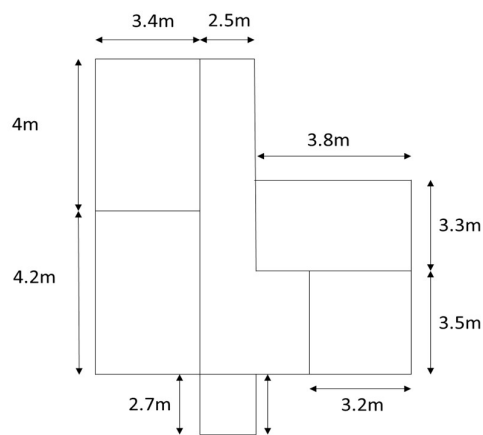


Figure 3.13: Plan view of a typical brick masonry school in considered region

Figure 3.14 shows the 3D analytical model of considered brick masonry school. The model has been developed in 3Muri software package.

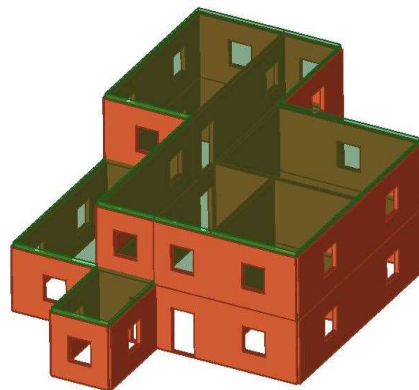


Figure 3.14: 3-Dimensional analytical model of brick masonry school structure

3.2.3.3.1. Field observations for brick masonry schools

As stated earlier, brick masonry schools were observed to be owned by private investors. During field observations, it was noticed that brick masonry schools were built in residential structures and houses, missing the true essence of a purpose-built environment for educational activities. Thus, this study primarily proposes a generic guideline for retrofitting brick masonry walls and structures. During field survey, no significant damage could be observed to brick masonry schools. This was mainly because of two facts; firstly, most of the brick masonry schools were established after 2005 Kashmir earthquake, and secondly, brick masonry schools were subjected to change of use from time to time i.e. from an educational facility to a residential facility and vice versa with minor modifications and repair works.

CHAPTER 4 : VULNERABILITY ASSESSMENT OF SCHOOL BUILDINGS

4.1. Overview

During 2005 earthquake, seismically vulnerable school buildings suffered extreme damages, resulting in deaths of children and unprecedented social loss.

Thus, the safety of children and the continuation of educational activities are primarily important for an eventual societal growth in every possible manner. Therefore, it is imperative to have a lucid insight about structural performance during earthquakes to execute necessary structural interventions. In the current chapter, the vulnerability has been assessed for all three typologies i.e. RC frames, stone-masonry schools, and brick-masonry schools. A new framework has been proposed to assess the structural vulnerability of RC school buildings as such typology has been the most frequently constructed and is currently the prevailing practice for schools' constructions. The validation of proposed methodology has been conducted by applying it over a Pacific Earthquake Engineering Research (PEER) Institute's benchmark structure [38] so that the efficacy and adequacy of proposed methodology can be assessed. Subsequently, the proposed methodology has also been applied over a high-rise structure to check its applicability to other types of building structures.

For stone and brick masonry structures, conventional methodology to assess structural vulnerability has been adopted.

Despite of the fact that numerous research studies have been carried out to evaluate structural vulnerabilities, there is a clear lack of such studies for under developing countries, especially Pakistan. Until today, no specific studies have been conducted to assess potential seismic vulnerability of school buildings in Pakistan. This work particularly addresses the seismic vulnerabilities of school buildings in seismic zone 4 of Pakistan.

Proceeding sections provide the detailed modelling and analyses procedures with which the structural vulnerabilities have been assessed for all three typologies. In the current study, a separate chapter for the discussion of results has not been produced and the obtained results are therefore, presented and discussed inside the respective sections for better reading connection between the analysis methodology and the attained results.

4.2. Vulnerability Assessment of Reinforced Concrete (RC) Schools

This work proposed a new methodology to evaluate vulnerability information in terms of fragility curves for RC school buildings in considered area. Proposed methodology can also be used to assess the seismic vulnerability of other reinforced concrete buildings, subjected to any use, due to its generic applicability. The methodology presented herein essentially differs from other methodologies currently being used to develop fragility curves as it separately considers the contribution of higher vibrational modes while producing fragility relationships, and do not predominantly focused on first mode only. Proposed methodology relies upon Uncoupled Modal Response History Analysis (UMRHA), originally proposed by Chopra and Goel [39]. A brief of UMRHA procedure has been provided in the proceeding section.

The proposed methodology is presented immediately after the proceeding section. For demonstrating the application of proposed procedure, BLR-11 has been taken as a case study and considering a cumulative 90% of modal mass participation ratio, initial two vibrational modes have been considered for developing fragility curves.

4.2.1. Uncoupled Modal Response History Analysis (UMRHA) for elastic and inelastic systems (Conversion of 3D structure to SDOF Systems)

The present study utilizes the Uncoupled Modal Response History Analysis (UMRHA) to explicitly cover the impact of higher modes and the frequency features of an EQ through its dependence on nonlinear dynamic responses of a defined set of SDOF structures. The higher structural vibrational modes are decoupled from each other, according to the use of the following procedure and equations. Afterwards, the nonlinear analysis is then performed separately on each of the mode which is represented by an equivalent SDOF system. Since the present study is specifically targeted to develop the fragility relationships, the analyses results are obtained in terms of global deformation-based response. The maximum drift values are determined for each of the ground motion, for each of its intensity during IDA process, for all the considered modes to check whether the structure attains a predefined DM in any of the mode or not.

For a building with more than a single story, subjected to an earthquake, the linear-elastic response can be obtained through;

$$\mathbf{m}\ddot{\mathbf{u}} + \mathbf{c}\dot{\mathbf{u}} + \mathbf{k}\mathbf{u} = -s_n\ddot{u}_g(t) \quad (4.1)$$

The resulting deformation-based response can be calculated by using equation 4.2:

$$\mathbf{u}_n(t) = \Phi_n q_n(t) \quad (4.2)$$

Where Φ_n is eigen value of the corresponding floor. With the substitution of equation 4.2 in the equation 4.1, and subsequently, multiplying it with Φ_n^T , the transpose of Φ_n , leads to the development of governing equation in terms of the modal coordinate q_n :

$$\ddot{q}_n + 2\zeta_n\omega_n\dot{q}_n + \omega_n^2q_n = -\Gamma_n\ddot{u}_g(t) \quad (4.3)$$

Where ω_n and ζ_n are the natural frequency and the damping ratio for the n^{th} mode. The Γ_n is defined as:

$$\Gamma_n = \frac{L_n}{M_n} \quad \text{Where,} \quad L_n = \Phi_n^T \mathbf{m} \mathbf{l} \quad M_n = \Phi_n^T \mathbf{m} \Phi_n$$

L_n is the modal force distribution, while M_n is the modal participation factor.

Equation (4.3) can essentially be used to represent the governing equation, employed for a SDOF structure. The solution of $q_n(t)$ is:

$$q_n(t) = \Gamma_n D_n(t) \quad (4.4)$$

In above equation 4.4, the deformational response is represented by $D_n(t)$ for the SDOF system, representative of n th mode, with analogous natural frequency ω_n and damping ratio ζ_n , and other vibrational properties of the n th mode, subjected to $\ddot{u}_g(t)$. This is governed by:

$$\ddot{D}_n + 2\zeta_n\omega_n\dot{D}_n + \omega_n^2D_n = -\ddot{u}_g(t) \quad (4.5)$$

The lateral displacements of the floors can essentially be obtained through the substitution of equation 4.4 into equation 4.5, thus:

$$\mathbf{u}_n(t) = \Gamma_n \Phi_n D_n(t) \quad (4.6)$$

Equation 4.6 characterizes the deformation-based response of a building system, with more than one story, earthquake forces. With the superimposition of all the responses, obtained from all the considered modes, the cumulative response of the full system can be evaluated using:

$$r(t) = \sum_{n=1}^N r_n(t) \quad (4.7)$$

In the inelastic range, the governing equation shall become:

$$\mathbf{m}\ddot{\mathbf{u}} + \mathbf{c}\dot{\mathbf{u}} + \mathbf{k}\mathbf{u} = -s_n\ddot{u}_g(t) \quad (4.8)$$

Equation 4.2 shall not be further able to render the solution of equation 4.8, as other modes shall be contributing towards the overall structural response, indicating that the modes are now coupled. Consequently, the first portion of following equation shall characterize the floor displacements:

$$\mathbf{u}_n(t) = \sum_{r=1}^N \Phi_r q_r(t) \cong \Phi_n q_n(t) \quad (4.9)$$

$q_t(t) = 0$ for linear-elastic systems, for modes other than n th mode. It is quite rational to anticipate that $q_r(t)$ may be small for inelastic systems, which implies that there exists a weak coupling of the elastic modes. Due to this feeble coupling, the second portion of equation 4.9 can be used to obtain the structural response because of the seismic excitation. Thus, for inelastic systems, the second portion of equation 4.9 can be substituted in equation 4.8. With the multiplication of the Φ_n^T with the then-equation, the following expression can be produced:

$$\ddot{q}_n + 2\zeta_n\omega_n\dot{q}_n + \frac{F_{sn}}{M_n} = -\Gamma_n\ddot{u}_g(t) \quad (4.10)$$

Where F_{sn} in the above equation portrays the nonlinear F-D relationship function for the n th mode, with the modal coordinate q_n . Analogously, with resemblance of equation 4.10 and equation 4.3, $D_n(t)$ is governed by:

$$\ddot{D}_n + 2\zeta_n\omega_n\dot{D}_n + \frac{F_{sn}}{L_n} = -\ddot{u}_g(t) \quad (4.11)$$

Where the deformational response of the inelastic SDOF system, representative of n th mode with identical modal properties and F-D relationship of n th mode in the actual structure, is interpreted in terms of the $D_n(t)$. To obtain the floor displacements through inelastic SDOF systems, the $D_n(t)$ obtained through equation 4.11 is further substituted in the equation 4.6. In accordance with the described procedure, the current study decouples the structural modes before proceeding with the Incremental Dynamic Analysis (IDA), while the probabilities of exceedances for different limit states have been evaluated in decoupled state of structural modes. The detailed process of evaluation has been demonstrated and discussed during the application of methodology.

4.2.2. Proposed methodology for seismic vulnerability assessment of RC schools

As mentioned earlier, the specific objective of this study is to establish a framework of analytical fragility assessment that can effectively capture the involvement of higher modes. To validate the effectiveness of the established framework, it is imperative that the results obtained from proposed framework must be compared with results from an already existing study that can serve as a benchmark, and also with a structure with more number of stories so that significant modal contribution of higher modes towards seismic vulnerability can be discreetly incorporated and evaluated. For a benchmark structure, the current study considers Pacific Earthquake Engineering Research (PEER) Institute's benchmark RC structure.

While demonstrating the established methodology in the current work, each of the individual mode is represented by a respective Single Degree of Freedom (SDOF) system. For deciding the number of modes to be included, UMRHA procedure emphasizes upon considering that much number of total modes that cumulatively constitutes more than 90 percent of modal mass participation ratio. The proposed methodology depends upon the IDA, while both, monotonic and reversed nonlinear static analyses, are also required before the actual execution of the IDA. The steps of presented methodology are as follows:

1. In step no. 1, the selection is made for the building typology, or the building category, to be assessed.
2. Nonlinear inelastic model is developed in step 2, and modal properties are evaluated which include the modal time periods and other relevant properties.
3. In step no. 3, Both of the orthogonal directions of the structure are subjected to monotonic pushover analysis (POA) to determine the weaker and more susceptible direction.
4. In step no. 4, the higher modes of the weak direction are subjected to static POA.
5. The hysteretic relationships are established in step no. 5 for each considered mode separately. For such purpose, the nonlinear cyclic pushover analysis is conducted. The developed hysteretic behaviors are then employed in the analysis of SDOF structures to satisfy the UMRHA requirements.
6. Subsequently, in step no. 6, the SDOF systems are developed in alignment with the procedure of UMRHA. A separate SDOF system is produced for every considered mode. Each developed SDOF system is characterized by the corresponding mode's hysteretic F-D behavior, developed in the preceding step no. 5.

7. In step no. 7, the SDOF systems are subjected to NLRHA by using a nonlinear ground motion history, and afterwards, the cumulative or the amalgamated response from the SDOF structures is obtained. Such response can be obtained by using equation 3.7.
8. In step no. 8, the nonlinear 3D model is subjected to the same earthquake which excited the SDOF systems in step no. 7. The attained responses in step no. 7 and step no. 8 are then compared. If responses from the 3D nonlinear model and SDOF systems match closely without any substantial loss of accuracy, the subsequent analyses would remain continued by employing the SDOF systems in place of the nonlinear 3D model. Consequently, consecutive analyses would not be computationally demanding, even by considering the contributions from the higher structural modes.
9. Different Limit States (LS), often known as Damage States of the structure, are defined in step no. 9. After defining, the theoretical definitions of the limit states remain same for every considered mode; nevertheless, the mathematical values, corresponding with each qualitative definition of LSs, may vary substantially in each of the considered mode. It is also essential to select a damage measure (DM) upon which the qualitative and quantitative definitions of versatile limit states can be applied to discretely obtain a specific LS of the structure, therefore, the DM, also known as Engineering Demand Parameter (EDP) is also defined or selected in the step no. 9. The mathematical threshold limits of DM relate the structural damage with different qualitative definitions of limit states. The seismic ground motion Intensity Measures (IMs) are also defined in the step no. 9. IMs are used to define discrete intensities of seismic excitations during the analysis. A discrete interval can be set to incrementally scale the IMs, for consecutive reiterations of analyses.
10. Step no. 10 involves the treatment of uncertainty involved in the capacity and seismic demand of the considered building typology. Thus, the vast concept of “uncertainty” involves not only the uncertainties in the structural capacity, but in the seismic demand as well.
11. In step no. 11, the IDA is performed on the SDOF systems by setting a discrete interval for enhancing the intensity of seismic excitation in successive iteration of analysis. The IDA is conducted separately on each of the SDOF structure, representative of different modes of the considered structure.
12. The mathematical definitions of limit states are applied on the obtained results from each SDOF system analysis against every ground motion in this step. The discrete or

- separate contribution rendered by each of the mode towards structural vulnerability can be conveniently obtained in this step.
13. In step no. 13, the probabilities for every limit or damage state, in every mode, are calculated by post-processing the results. The probabilities are calculated collectively i.e. when any of the mode indicates the reaching of an established threshold value of the DM for any limit state, an event is counted in the sample to calculate the probability. For each of the limit state, the probabilities are evaluated against each discrete level of seismic intensity.
 14. Step no. 14 marks the development of analytical fragility functions for each of the limit state. Lognormal cumulative distribution function (CDF) is conventionally used to fit the evaluated probabilities, and to graphically represent the fragility function. The lognormal distribution parameters, i.e. the slope and the median of the CDF, are obtained by using the Maximum Likelihood Method (MLM).

4.2.2.1 Comparison between conventional and proposed methodology and its limitations

This subsection provides a brief comparison between a conventional methodology used by Chaulagain et al. [40] and proposed procedure. The methodology by Chaulagain et al. [40] is dependent upon nonlinear pushover analysis to IDA (SPO2IDA) tool. The tool establishes a nexus of results attained from POA and IDA. For details of SPO2IDA, the reader of this work is referred to Bakalis and Vamvatsikos [33] and Chaulagain et al. [40]. Proposed and conventional, both procedures commence with the development of an analytical model in a software package that can handle the nonlinearity. Subsequently, POA in both orthogonal directions is conducted for establishing frailer direction for further analysis, nevertheless; successive monotonic and cyclic POA are not conducted in higher modes when a conventional methodology is used. Successive monotonic and cyclic POAs help in establishing separate quantitative limit states and overall force-deformation (F-D) relationships in proposed approach, and therefore, results in better insight to individual mode's contribution in seismic vulnerability. In a conventional methodology IDA is conducted for a full nonlinear 3D model, consuming erroneous time and computational power. On the other hand, the computational effort in proposed methodology is significantly diminished by developing the nonlinear SDOF systems for each mode whereupon the IDA is conducted.

In another difference, conventional methodology definitions of limit states on first mode only, whereas, presented procedure applies qualitative and quantitative definitions of limit states separately on all considered modes in accordance with their own nonlinear behavior. The subjection of higher modes towards the application of qualitative and quantitative limit states separately is a novel feature of presented work. Conventionally, only the first mode's response is considered for evaluating the analytical fragility relationships, while by the virtue of current methodology, modal fragility curves can be developed by evaluating the modal SDOF systems. Therefore, a practitioner of this methodology can develop the fragility curves in two different ways; by combining all the results, including higher modes, resulting in cumulative fragility, and also by evaluating the probabilities separately for individual mode, resulting in modal fragilities.

In its limitation, the proposed methodology cannot be adopted for the stone or brick masonry structures as the development of their cyclic or hysteretic behavior is not possible due to their brittle nature of failure. The hysteretic behavior can only be developed if structures could undergo cyclic loadings, strength and stiffness degradation after the yielding, which is not possible for unreinforced masonry, i.e. brick and stone masonry, structures. Therefore, the proposed methodology can only be employed for the RC buildings, and not for the unreinforced masonry buildings. The systematic application of proposed procedure is herein discussed in proceeding section.

4.2.3. Application of proposed methodology

For elucidation purpose, the school building typology BLR-11 is selected. The BLR-11 is particularly taken as the case study for the application of proposed methodology as this specific typology has been found to be the most prevalent type, constructed in the considered region. The configuration of BLR-11 existed even before the 2005 Kashmir Earthquake, and afterwards, it was replicated in the subsequent construction of schools in considered region. Any of the school building with three stories has not been selected as such school buildings housed the allied facilities such as the laboratories, library, computer labs, etc. The produced results can be readily adopted by the relevant stakeholders, and the application of the proposed methodology can be extended by the relevant authorities in order to evaluate the fragility of other school building typologies.

4.2.3.1. Configuration of considered school building

The selected two-story school building typology consists of 11 bays in the x-direction, and 2 bays in the y direction in which one serves as the pedestrian walkway for the students and have somewhat smaller dimensions, while the other bay, with larger dimensions, in the y-direction serves as the classroom for the pupils. The structural system comprises different sizes of columns and beams. The plan of the BLR-11 has been shown in the following figure 4.1.

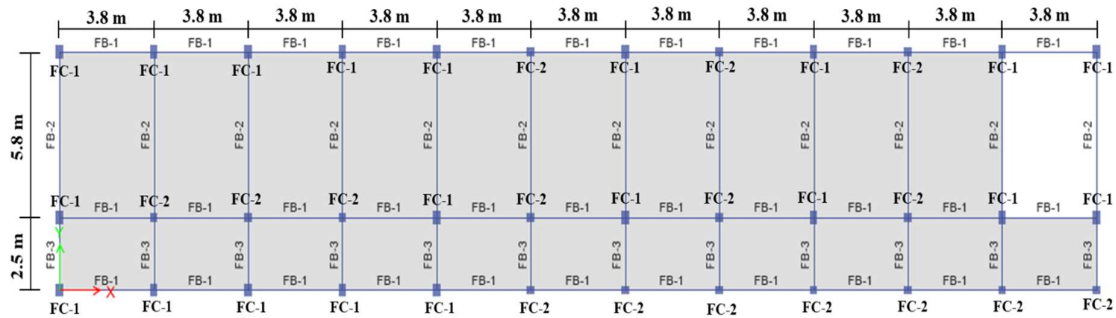


Figure 4.1: Plan view of BLR-11

FC and FB in figure 4.1 are the nomenclature of “Floor Beams (FB)” and “Floor Columns (FC)” respectively. In y-direction, the shorter bay marks the pedestrian walkway for entering and leaving classrooms. Relatively stiff soil was observed at the actual sites of construction, while during the interviews with the design professionals, it was revealed that most of the designers have assumed the Soft Soil type, S_d , according to the BCP SP-2007 [41]. The typical floor area for the selected building is 344.5 m^2 (3,709 sq. ft.). Figure 4.2 presents the elevation of the selected building typology, indicating the story height as well as the total height of the structure.

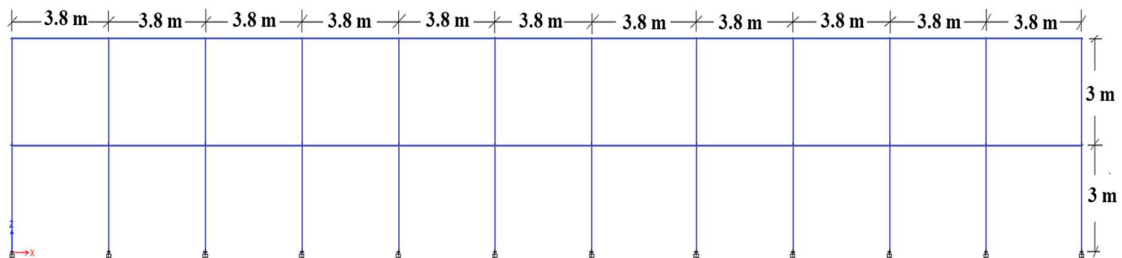
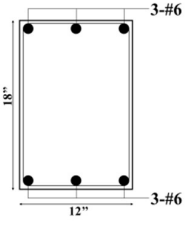
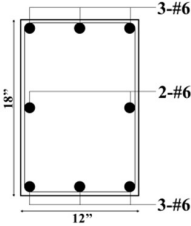
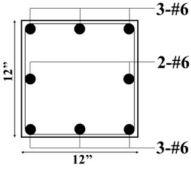


Figure 4.2: Elevation view of BLR-11, indicating the bay widths, story heights, and total height

Table 4.1 depicts the structural details i.e. X-sectional dimensions and steel reinforcements of axial and flexural structural members, FCs and FBs. The X-Sectional dimensions have been validated through the field observations, while the amount of reinforcement has been directly taken from the drawings.

Table 4.1: Reinforcement details of structural members

Structural Component Type	Name	X-Section
Beams	FB-1, FB-2, FB-3	
Columns	FC-1	
	FC-2	

4.2.3.2. Nonlinear structural modelling

The proposed methodology requires the creation of 3D nonlinear structural analytical model for establishing overall hysteretic behavior of the structure as well as to verify the responses from the SDOF systems so that further analyses may be executed using the established SDOF systems, in accordance with UMRHA, instead of the 3D nonlinear model that can pose tremendous computational effort. The development of a nonlinear model was carried out

using software CSI Perform 3D v 7.0 as it has adequate library of analytical tools to effectively capture the nonlinear structural performance by means of hinge rotations or by monitoring the strains that may arise in the structural members as a repercussion of seismic demands. For capturing the region specific construction practices, it was imperative to incorporate the conventional materials' strengths that are normally available domestically. For such a purpose, results obtained by Rafi and Nasir [42] were employed for 28 days mean strength value of concrete. Afterwards, the commendations of American Society of Civil Engineers (ASCE) 41 [43] were extensively followed to establish the expected strengths during the analyses. Moreover, Grade 40 reinforcing bars have been used for the creation of analytical model as most of the professional interviews confirmed easy availability of Grade 40 steel in the domestic market.

For the considered typology, a layer-by-layer fiber-based modelling approach has been adopted to model the reinforcing bars and the concrete for structural members except slabs. The slabs were kept as elastic elements. The F-D relationships of structural elements can be conveniently transformed into the stress-strain relationship of materials by employing the fiber-based models. Fiber-based modelling allows the discrete division for unconfined and confined concrete and as a result, the composite properties of any x-section can be conveniently account for in the structural modelling. The typical sections for the fiber-based approach can be observed in the following figure 4.3. The illustration has been rendered by Xuewei et al. [44].

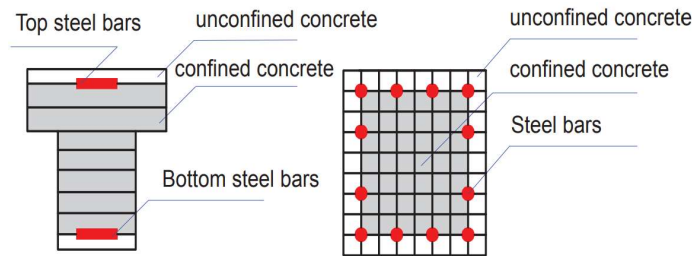


Figure 4.3: Typical representation of Fibers for beams and columns [44]

The analytical model has been developed by employing nonlinear inelastic fiber sections. The strain limits have been established according to ASCE 41 [43]. By the virtue of fiber modelling, the force-deformation relationship of columns and beams is transformed into the stress-strain relationship of construction materials, i.e., concrete and reinforcement. By

employing fibers, an appropriate division may be introduced for confined and unconfined concrete fibers and consequently, a composite section can easily be taken into account. In layered elements, nonlinearity was essentially introduced at, and near the ends of members where plastic hinges can form. In all such nonlinear regions, the nonlinear material strains have been monitored to observe the structural damage.

In the current study, the Mander model, provided by Mander et al. [45] was used for concrete. Complete confinement effect and strength loss were considered in accordance with the reinforcement pattern of beams and columns, during the analysis. Steel models that can capture the buckling and non-buckling behavior of the reinforcements are available within the Perform 3D. For this case, the non-buckling steel model was utilized as ductility design is mainly based on the fact that reinforcement cannot be abruptly brittle. The numerical modelling of strength degradation at high ductility levels was also considered by modelling the strengths of the materials in a nonlinear range. The shear-flexure interaction has been achieved at fiber level, which subsequently permits the coupling shear & flexural interaction at elemental level. The strength and stiffness degradation, as depicted by figure 4.5 shows the shear-flexural interaction. The current study does not consider the infill interaction for the considered structure in this study. The strong beam and weak column mechanism wasn't observed during field visits for the considered structure, therefore, this specific phenomenon hasn't been added to the structural model. Table 4.2 summarizes all the material strengths, live loads, and infill-partitioning loads that were used during the analysis in accordance with the professional interviews conducted during the field surveys.

Table 4.2: Loading values and material strengths for analytical structural model

Loads		Material Characteristics	
Live Load	2.6 KN/m ² (55 psf)	Concrete's strength (fc')	21 MPa (3000 psi)
Infill Partitioning	4.3 KN/m (0.3 K/ft)	Reinforcing steels yielding stress (fy)	275 MPa (40000 psi)

4.2.3.3. Monotonic and cyclic pushover analysis

After structural modelling, modal analysis was performed to obtain modal mass participation ratio. Thus, initial two modes, constituting 90 percent of cumulative modal mass participation ratio in X-direction were considered for subsequent analysis. 83% participation ratio was provided by the 1st mode, while 8% was provided by the 2nd mode in the same direction.

Afterwards, monotonic pushover analyses were performed in both orthogonal directions for establishing weaker axis. X-direction was found to be more vulnerable. Therefore, subsequent analyses were conducted in X-direction. Figure 4.4 shows the monotonic pushover curves in first two modes as presented methodology required the monotonic pushover analysis in all the considered modes.

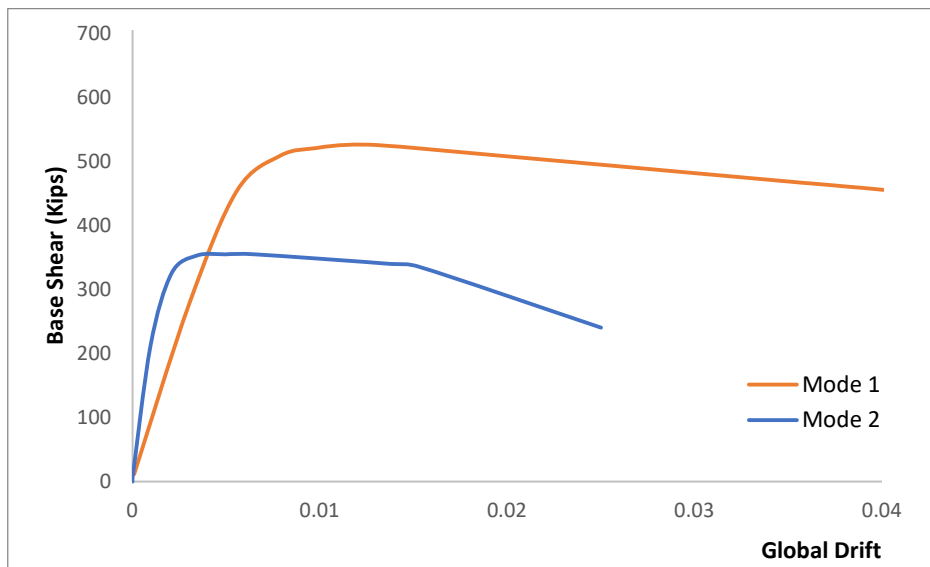


Figure 4.4: Nonlinear static pushover analyses curves for first two modes in the weaker direction

For developing hysteretic loop, cyclic POA was conducted on 3D nonlinear model. A cyclic POA as it identifies the function, $F_{si}(\dot{D}_i, D_i)$. Figure 4.5 shows the results of cyclic POA of 1st mode. Consequently, each F-D relationship was assigned to individual SDOF as required by UMRHA.

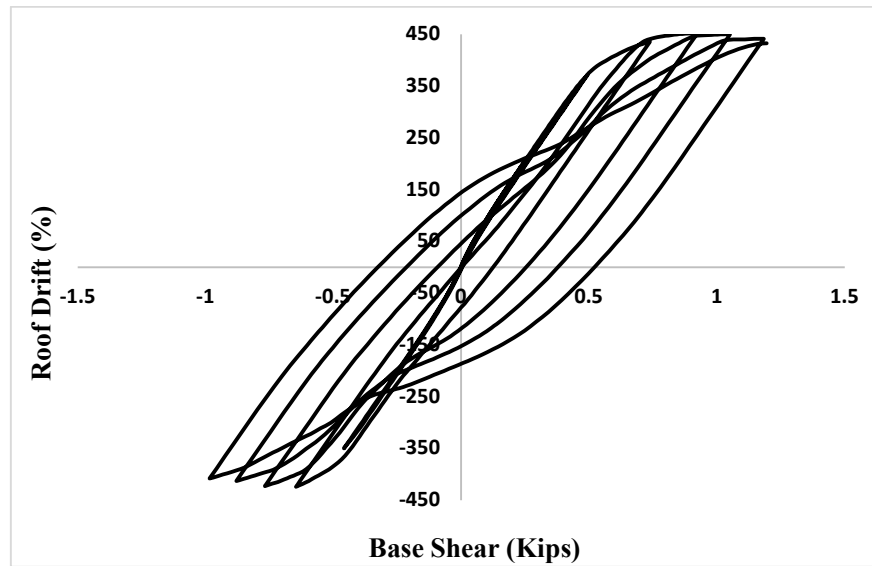


Figure 4.5: Cyclic pushover behavior of considered school building

After cyclic pushover analysis, nonlinear SDOF systems had been developed, and their cumulative response had been evaluated to establish their adequacy in predicting the structural response against ground motion.

4.2.3.4. Establishment of SDOF structures for uncoupled analyses

To develop the two SDOF systems, the Incremental Dynamic Analysis Procedure (IIDAP) V 1.2, [46], has been utilized. All of the modelling parameters have been evaluated in accordance with the UMRHA, and with the recommendations of technical manual of IIDAP. Each SDOF system contains the F-D nexus of its respective mode.

IIDAP provides excellent analytical tools to assess the SDOF systems' response. It contains the deteriorative and non-deteriorative hysteretic behaviors that can be tuned according to the requirements of the user. The hysteretic behaviors have been initially proposed by Ibarra et al. [47] and been subsequently elaborated by Lignos [48] and, Lignos & Krawinkler [49] for capturing the versatile structural behavior with and without the strength and stiffness deteriorating effects. The software directly handles the execution of IDA, and it also contains a predefined set of ground motion histories. However, it softens the SDOF systems when custom hysteretic behaviors are used instead of the predefined ones to counter the effect for the deteriorating stiffness, and same has been projected in the fragility curves developed using the results of SDOF systems analyzed in IIDAP, as the probabilities are marginally on the upper side of those developed using 3D structure; however, it depends on the

discretion of the engineering practitioner as to what level of compromise in the results deems acceptable. In the current study, the predefined ground motion histories had not been utilized, instead, separate ground motion time histories were selected in order to capture the domestic seismo-tectonic conditions of the considered region.

Two distinctive SDOF systems had been developed in IIDAP, and each of them contained hysteretic behavior of first two structural modes respectively according to UMRHA procedure. Before executing the IDA, the responses obtained from the SDOF systems and full nonlinear 3D model have been verified. The SDOF systems and nonlinear 3D model, both were subjected to history of Tabas, Iran (taken from PEER NGA West2 Database). The ground motion held the analogous originating characteristics as that of Kashmir Earthquake 2005, and was scaled to have a PGA of 1.0g, sufficient to trigger inelastic behavior of the considered school building typology. The responses obtained from individual SDOF systems were eventually amalgamated in order to establish the cumulative structural response against the applied seismic motion in the considered direction. The obtained results were interpreted in terms of the global displacement history, and a graph was plotted by superimposing the results obtained from the SDOF systems and the 3D model for a sophisticated graphical comparison. The obtained results from SDOF systems effectively matched with the results attained from the analysis of full nonlinear 3D model, and they depict that developed SDOF systems can adequately be utilized for further analyses. Figure 4.6 shows the well matched response of SDOF systems with the nonlinear 3D model.

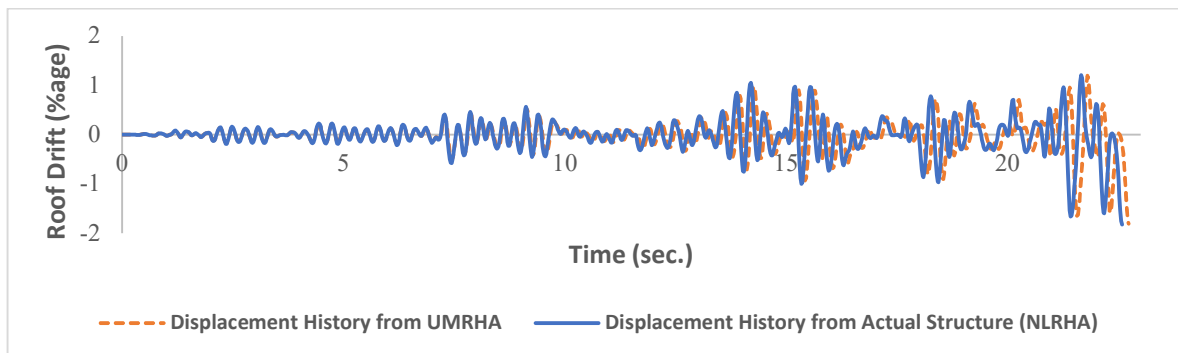


Figure 4.6: Comparison of roof drift, obtained from UMRHA and 3D model subjected to NLRHA

The comparison of NLRHA and UMRHA responses from 3D model and SDOF systems establishes the efficacy of UMRHA for vulnerability assessment. The response history of

considered building from both analyses methods matches well with each other and observed disagreements are insufficient and trivial.

4.2.3.5. Uncertainty treatment and selection of ground motions

Uncertainties are conventional categorized into two categories i.e. epistemic and aleatory [50]. Former characterizes the uncertainties involved because of the inherent deficiencies in the knowledge of inherent structural properties, while latter represents the uncertainties in seismic demands which can only be recognized by the virtue of stochastic processes only.

Epistemic uncertainties relate with the undesirable disparities of in the strength of materials. Literature suggests that strengths can be taken as random variables to tackle such uncertainties; however, Frankie et al. [51], elaborated that even with the incorporation of epistemic uncertainties, the fragility relationships are not significantly different. Frankie et al. [51] had further suggested that vulnerability assessment, carried out by assuming structural parameters as deterministic, and essentially equal to their respective mean or median values, were sufficiently useful for estimating damages and losses resulting from earthquakes. Thus most substantial source of uncertainty is the seismic demand, needed to be tackled during fragility development as stochastically intrinsic disparities in ground motions can induce devastating effects.

Thus, because of the inability of variations in the materials' strengths to instigate any significant uncertain structural response, the current study considers the materials' properties as discrete and deterministic instead of their modelling as random variables. The essential values i.e. strength, modulus of elasticity, etc. have been taken from the design reports as mentioned earlier in this work.

For covering the aleatory uncertainties, associated with record-to-record variability, 20 ground motions are selected to cover the intrinsic variation in seismic demand. The criterion developed for ground motion selection, selected natural time histories, incremental scaling of ground motions for IDA, and other relevant information are given hereafter.

As discussed earlier, record-to-record variability poses significant uncertainty during vulnerability assessment because of the highly erratic seismic demands. Soil conditions, originative source, and path attenuations, all have their substantial part in uncertainties. It is convenient to incorporate a wide-ranging variation of seismic demands during the ground motions selection so that significantly adequate structural dynamic response can be captured.

The current research attempts to consider a broad range of seismic energy levels through scrupulous selection of natural ground motion histories. Pacific Earthquake Engineering Research (PEER) Ground Motion Database, NGA-West2 has been used to select the ground motions. The database provides splendid control over the parameters for selection of earthquake time histories, ranging from shear wave velocity to fault-type. In presented study, the ground motions are selected by considering the geological and soil conditions of the Muzaffarabad District in Pakistan. Special emphasis has been given to the characteristics of 2005 Kashmir Earthquake while selecting the ground motions as it resulted in the most catastrophic and fatally devastation of the region throughout the history, and most of the parameters, during selection, have been kept in strong alignment with those matching with the 2005 Kashmir Earthquake. The fault, which resulted in 2005 Kashmir Earthquake, is reverse-oblique in its character, and as observed, it produced a large magnitude earthquake of 7.6 Mw, with its epicenter at 19 KMs northeast of Muzaffarabad.

In this research, the mechanism of fault, shear wave velocity V_s , magnitude, source-to-site distance, have been taken into account for the selection of ground motions. Therefore, earthquakes having magnitude in range of 6.0 to 8.0, initiated from reverse and revers-oblique faults are used, while 0 to 30 KMs range has been taken into account for covering variations in source-to-site distances, considering uncertainties in path attenuation and soils strata effects. The V_{s30} , shear wave velocity, in the upper 100 feet (or 30 m) of soil strata, is taken between 175 m/sec (575 ft/sec) to 350 m/sec (1150 ft/sec) for selection process, in accordance with the soil type S_d of BCP – 2007. Selected ground motions are shown in table 4.3. The magnitude, source mechanism, distance-to-rupture, V_{s30} , and magnitudes are also mentioned in the same table.

Table 4.3: Selected natural ground motion histories

Sr. No.	Earthquake Name	Year	Rrup (km)	Mag.	PGA (g)	Vs30 (m/sec)
1	Chi-Chi Taiwan	1999	24.96	7.62	0.137	235.13
2	Chi-Chi Taiwan	1999	16.04	7.62	0.273	233.14

3	Chi-Chi Taiwan	1999	25.43	7.62	0.1448	297.86
4	Chi-Chi Taiwan	1999	17.11	7.62	0.165	272.67
5	Chi-Chi Taiwan	1999	11.57	7.62	0.1918	212.72
6	Chuetsu-oki Japan	2007	29.45	6.8	0.176	334.0
7	Gazli USSR	1976	5.47	6.8	0.864	259.58
8	Iwate_ Japan	2008	8.43	6.9	0.2194	279.36
9	Iwate_ Japan	2008	16.67	6.9	0.2057	349.0
10	Kashmir Earthquake	2005	26.00	7.60	0.2517	223.04
11	Loma Prieta	1989	24.57	6.93	0.1695	239.69
12	Loma Prieta	1989	9.30	6.93	0.331	347.9
13	Montenegro Yugoslavia	1979	5.76	7.1	0.2928	318.73
14	Niigata Japan	2004	12.81	6.63	0.4764	274.17
15	Northridge-01	1994	8.65	6.69	0.345	297.71
16	Northridge-01	1994	12.50	6.69	0.309	326.47
17	San Fernando	1971	22.77	6.61	0.225	316.46
18	Spitak Armenia	1988	23.99	6.77	0.20	343.53
19	St Elias Alaska	1979	26.45	7.54	0.1759	306.37
20	Tabas Iran	1978	28.79	7.35	0.106	324.57

By selecting numerous number of natural ground motion time histories with variable source to site distances, magnitudes, and V_{s30} , it can be conveniently apprehended that aleatory uncertainties are adequately dealt in this study.

4.2.3.6. Selection and scaling of intensity measure

Intensity measures (IMs) portray the correlation of intensity of seismic excitation with structural damage, therefore, it is vital that a good correlation should exist between the structural damages and the selected or defined IMs.

In the present study, IDA has been conducted by considering the Sa and PGA as IMs. Since the 2nd mode is also involved, the Sa has been scaled separately for all considered modes. For scaling of IMs, USGS suggests four methods: (i) spectral matching of GMs, (ii) geometric scaling of GMS, (iii) as per the spectral demands' distributions, and (iv) scaling on the time period of fundamental mode to suggested or targeted values of spectral acceleration. In the presented work, no (ii) has been employed when PGA has been used as IM, while no. (iv) has been employed when Sa has been used as the IM. IMs are scaled over a discreet range, from 0.2g, and culminating at 1.40g. A discrete increment of 0.2g has been made for every successive iteration of analysis.

For representative SDOF system for the fundamental mode, Sa has been scaled on the corresponding modal period. Analogously, for the analysis of SDOF system, representative of the 2nd mode, the scaling of Sa has been done on the time period of the 2nd mode itself. Because of the smaller time period of structural vibrations in the 2nd mode, it is believed that the structural response towards high frequency seismic motion shall be adequately accounted for.

For the purpose of developing analytical fragility curves, the cumulative/amalgamated response of both of the considered modes has been used against all levels of spectral acceleration Sa(T1,T2).

4.2.3.7. Definition of limit states (LS) and damage indicator

Limit States (LS), often termed as damage states (DS), are one of the essential ingredients of any process for vulnerability assessment, so that varying levels of discrete structural damage can be identified against the earthquakes with different intensities. In a broader sense, qualitative definitions can be developed for all considered limit or damage states,

which can be further complimented through the quantitative values of Engineering-Demand Parameter (EDP) or the structural damage-indicator.

As stated earlier, the descriptive damage of a structure can be dealt under the qualitative definitions, without any mathematical characterization, while numerical/mathematical values of some EDP can further correlate with the descriptive damage state of the structure.

Thus, it is vital to select or propose a damage indicator in order to physically relate the structural damage with the defined limit states. After the selection of an EDP, different threshold values for the EDP can be conveniently defined to discretely distinguish different limit states or the damage states of the structure or the stock of structures.

EDP or the damage indicator, can be defined at both levels i.e. local and/or global. Strains in construction materials, members' flexural strength, inter-story drifts, and global drifts are some of the typical examples of EDPs which can be found in the literature to correlate with the structural limit states. Three distinctive limit states, defined by Federal Emergency Management Agency (FEMA) 356, i.e. Immediate Occupancy (IO), Life Safety (LS), and Collapse Prevention (CP), correlates the damage with inter-story drift ratio of 1%, 2% and 4% respectively, as the damage-indicator or EDPs.

Since the current study is targeted to assess the vulnerability of a generic building stock in Pakistan's seismic zone 4, the definition of limit states considering the global response shall be more practical instead of basing the definition upon the local responses. Hence, depending upon the versatile literature, global drift ratio is used as the EDP in presented study for interacting with the defined limit states for considered case study.

Serviceability Limit State (LS1), Damage Control Limit State (LS2), and Collapse Prevention Limit State (LS3) have been defined in this study for developing the analytical fragility curves. Since the presented methodology includes the influence of second mode, it is relevant to state that the same qualitative definitions for the established limit states have been maintained for both of the structural modes. The LS1 is characterized by the first yielding of the longitudinal steel reinforcement in the considered building typology. Conventionally, the LS1 is indicated by the formation of first plastic hinge, but as described earlier, the present study employs nonlinear fiber elements in place of the plastic hinges, thus the attainment of the yielding strain in a structural component symbolizes advent of LS1.

LS2, is governed simultaneously by the structural strength and the deformational features of the considered school building typology. It is characterized as the 75% of the third limit state, the Collapse Prevention Limit State, LS3.

Erberik [52] defined Collapse Prevention Limit State as the smaller of the 75% of ultimate deformation or the value for which structural strength drops by more than 20% relative to its maximum strength.

The mathematical limiting values for the considered limit states cannot be directly adopted from the past literature as no specific research for the school buildings in seismic zone 4 of Pakistan has been conducted. Apart from that, conventional researches have been remained focused upon the response of the fundamental mode only, while the presented research emphasizes upon considering the higher structural modes in the vulnerability assessment process. For establishing the numerical thresholds limits for each of the limit state in both of the modes, in terms of the global response i.e. global drift, the separate capacity curves, developed for each mode, have been employed. The qualitative definitions of all the limit states have been applied upon each capacity curve, and consequently, the correlating global drifts have been chosen. The numerical threshold values for all three limit states in the considered modes have been given in table 4.4.

Table 4.4: Numerical threshold values of global drifts for limit states in first two modes

Mode No.	Limit State		
	Serviceability Limit State (LS1)	Damage Control Limit State (LS2)	Collapse Prevention Limit State (LS3)
1	0.35	0.66	0.89
2	0.096	0.26	0.348

4.2.3.8. Incremental Dynamic Analysis

Incremental Dynamic Analysis (IDA) is considered to be the most effective method for assessing the structural behavior against seismic excitations. Several researchers, i.e., ; Kostinakis and Athanatopoulou; Fereshtehnejad et al., Zarfam and Mofid [53]-[55] have

employed IDA for establishing fragility relationships of different structures. Despite of the colossal computational effort, IDA has been a tremendous analysis procedure for probabilistic evaluations of structural seismic vulnerabilities. While executing the IDA, the ground motions are discretely scaled to achieve a larger value of acceleration in each successive iteration during the analysis. The scaling interval can be linear i.e. a fixed acceleration value to be augmented in the acceleration in the preceding iteration of dynamic analysis, or it may lie at the discretion of the analyst as how to increase the accelerations of the ground motions for subsequent iterations.

In the current study, a fixed increment of 0.2g has been used to enhance the PGA and the S_a of the selected ground motions. All the ground motions have been scaled with 0.2g increment, starting from the base value of 0.2g to 1.4g in the IDA. The results in terms of the plots between scaled PGAs, from 0.2g to 1.4g, and the global drift are shown in figure 4.7. The figure shows the results obtained by incrementally scaling and applying the all twenty ground motions. The results are also produced and presented in the same figure by scaling the spectral acceleration at the fundamental period of the structure for the same intensity levels.

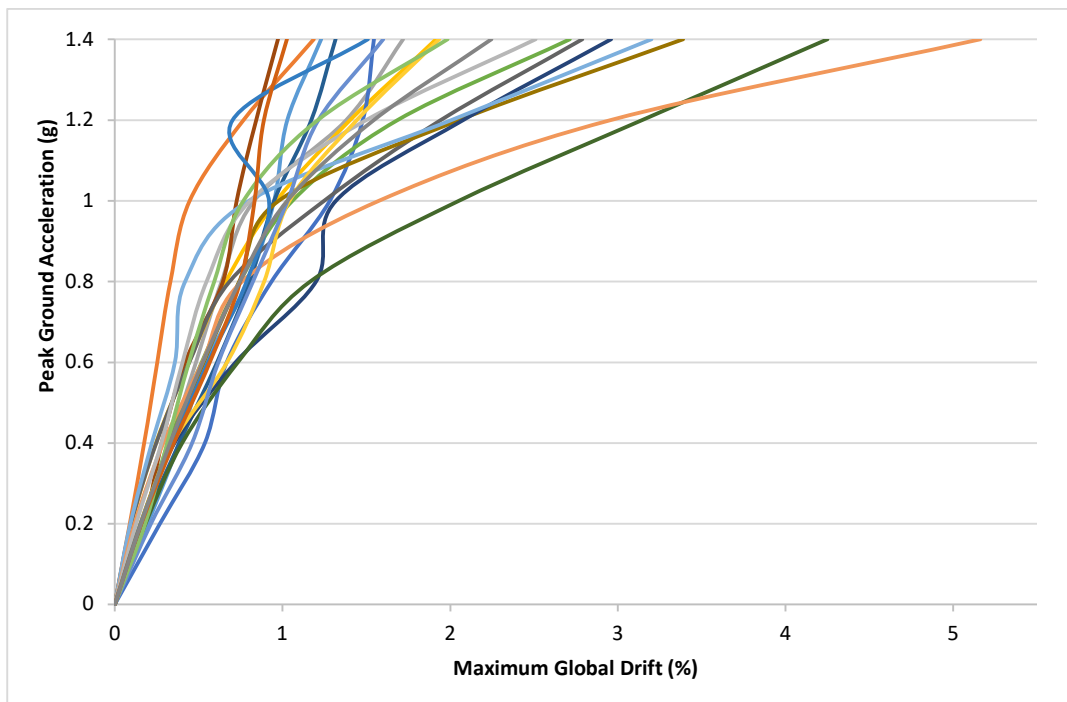


Figure 4.7: IDA Curves for maximum global drift v/s PGA (g)

The same category of results has also been produced by using the S_a , scaled separately at 1st mode's time period, as well as on the second mode's time period. After analyzing both of the structural modes using UMRHA procedure, the obtained results from each of the structural mode were eventually combined, and maximum roof drifts were evaluated from the combined results. Figure 4.8 shows the results as follows:

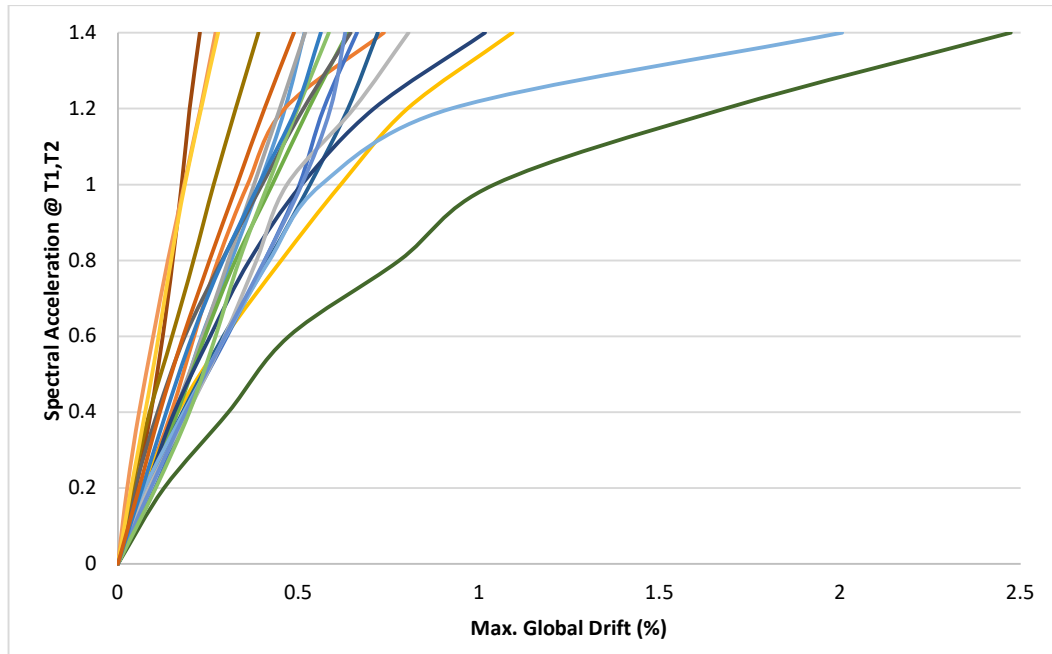


Figure 4.8: IDA Curves for maximum global drift v/s Spectral Acceleration scaled at the time periods of first two modes ($S_a @ T1,T2$)

In figure 4.7, IDA curves portray the maximum global drift remained at between a minimum of 0.20% and a maximum of 5.13% when PGA had been used as an IM. Whereas figure 4.8 presented the IDA results when S_a had been used as an IM. When S_a was employed as IM, the maximum global drift reached 2.47% at 1.4g.

It is essentially clear from the figures 4.7 and 4.8 that inherently variable and versatile properties of separate ground motions pose significant disparities in the overall structural response. These disparities can be substantially attributed to the differences in the natural frequency contents of the ground motions as they vary significantly over the duration of the ground motions.

Hazard-damage (H-D) relationships were also developed after IDA to evaluate the influence of aleatory uncertainty. H-D relationships are useful for presenting the structural behaviour for varying levels of excitations. A direct nexus between structural damage and seismic intensities is presented in figures 4.9 and 4.10.

The damage had been quantified by employing global drift, while the seismic intensities are provided as per the selected IMs where spectral acceleration has been scaled at T1 and T2.

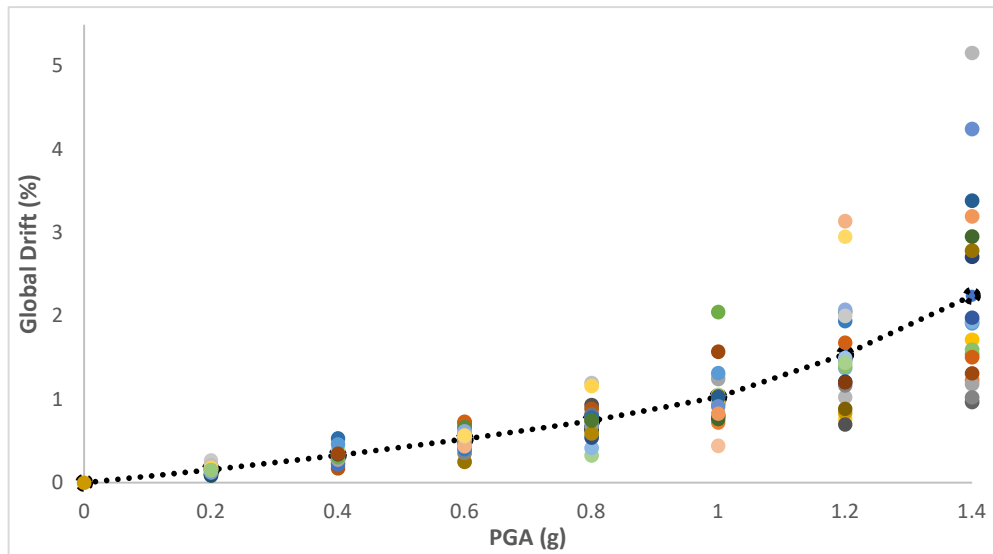


Figure 4.9: Hazard-Damage Relationship: PGA v/s Global Drift

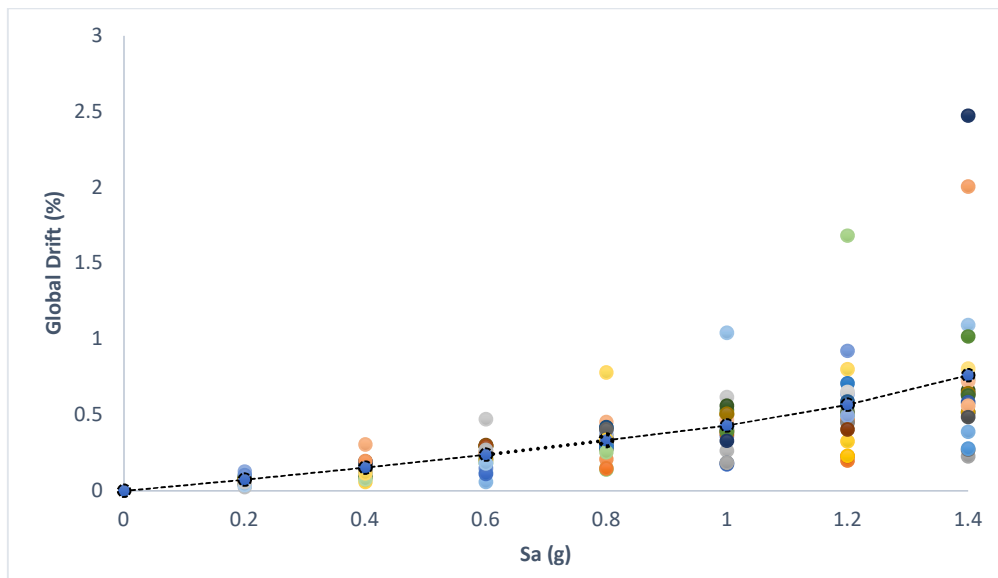


Figure 4.10: Hazard-Damage Relationship: Sa v/s Global Drift

In both figures (4.9 and 4.10), at any single seismic intensity, there are 20 dots for considered 20 ground motions. This specific behaviour indicates the uncertainty in structural response, attributed to intrinsic variability and uncertainties involved in natural ground motions. Therefore, at a single seismic intensity of 1.4g, when PGA has been used as IM, one ground motion produced global drift of less than 1%, while at the other hand, at the same seismic intensity of 1.4g, some other ground motion could produce global drift of more than 5%. Similar behaviour could be observed when S_a had been used for representing seismic intensity. The connecting dotted line in figure 4.9 and figure 4.10. manifests the mean structural response in H-D relationships.

4.2.3.9. Fragility derivation

Fragility curves portray the probabilistic information for the correlation between limit states and the seismic demands. Thus, fragility curves are the graphical representation of the probability exceeding or attaining different limit states against a discrete value of seismic demand, represented by an IM. The qualitative and quantitative definitions of limit states are applied upon the obtained results, and eventually, calculations are made to evaluate the probabilities to reach a limit state against a specific value of IM. Once a threshold value has been crossed by an EDP for a specific limit state, an event is considered as counted within the whole sample of all ground motions at a considered value of excitation.

Since effect of second mode has been taken into account, cumulative probability has been evaluated, once a threshold value of an EDP exceeds in any mode, such as 1st or 2nd. This process has been repeated for all seismic intensity levels to obtain probability values. Considering available literature on fragility curves, it is a conventional practice to portray the graphical information of obtained probabilities by using a lognormal cumulative distribution function, separately for each limit state. Therefore, for generic comprehension and of the fragility curves by the technical community, this study also deems it feasible to employ lognormal distributions for presenting vulnerability information of considered school typology, as depicted by following equation;

$$P(LS|IM) = \phi\left(\frac{\ln IM - \lambda_c}{\beta_c}\right) \quad (4.1)$$

The first part of equation (4.1), $P(LS|IM)$, designates the conditional probability of exceeding a specific limit state, against a discrete value of an IM. ϕ represents standard

cumulative distribution function (CDF). Controlling parameters for the curves are represented by λ_c and β_c . Maximum Likelihood Method (MLM) has been employed to obtain a optimized values for the controlling parameters i.e. slope of the curve, β_c and the median, λ_c . MLM is considered as one of the widely acceptable and most suitable methods for obtaining optimized values of λ_c and β_c (Baker and Eeri; Dang et al. [56]-[57]). The optimization of controlling parameters is described by the following equation;

$$\{\lambda_c, \beta_c\} = \arg \max_{\lambda_c, \beta_c} \sum_{j=1}^m \left\{ \ln \binom{n_j}{z_j} + z_j \ln \phi \left(\frac{\ln (IM_i/\lambda_c)}{\beta_c} \right) + (n_j - z_j) \ln \left(1 - \phi \left(\frac{\ln (IM_i/\lambda_c)}{\beta_c} \right) \right) \right\} \quad (4.2)$$

Where number of IM levels are denoted by m , total number of earthquakes at any given intensity is represented by n_j , while the number of achieving a limit state is specified by z_j .

4.2.3.9.1 Fragility curves – developed using fundamental mode only

The developed analytical fragility curves by employing the nonlinear 3D model that relies on the analysis of fundamental mode only are shown in figure 4.11 for PGA as an IM.

Since the current study also employs Sa as an IM, the fragility curves have also been developed for Sa as well. For the purpose of analyzing the structure in its fundamental mode, the Sa of the ground motions was scaled at the fundamental time period of the considered school building typology. Figure 4.12 depicts the established fragility relationships for all the limit states using the Sa @ T1 as an IM.

Fragility curves, developed by using the fundamental mode only, are presented in figure 4.11 and 4.12 with PGA and Sa@T1,T2 as IMs respectively.

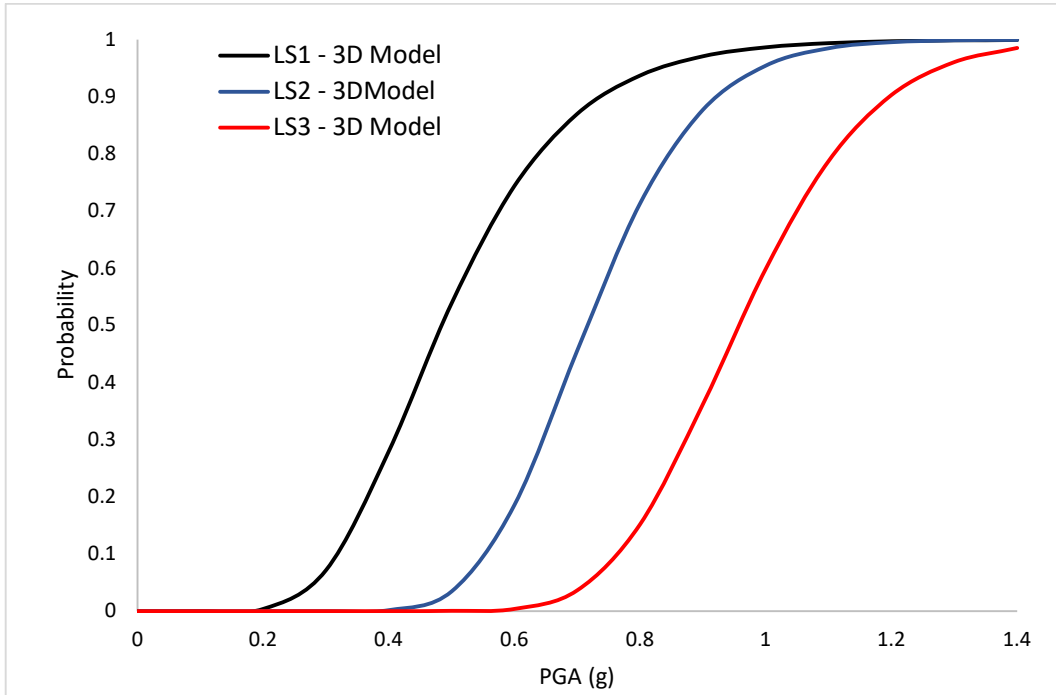


Figure 4.11: Derived fragility curve using fundamental mode only against PGA as an IM

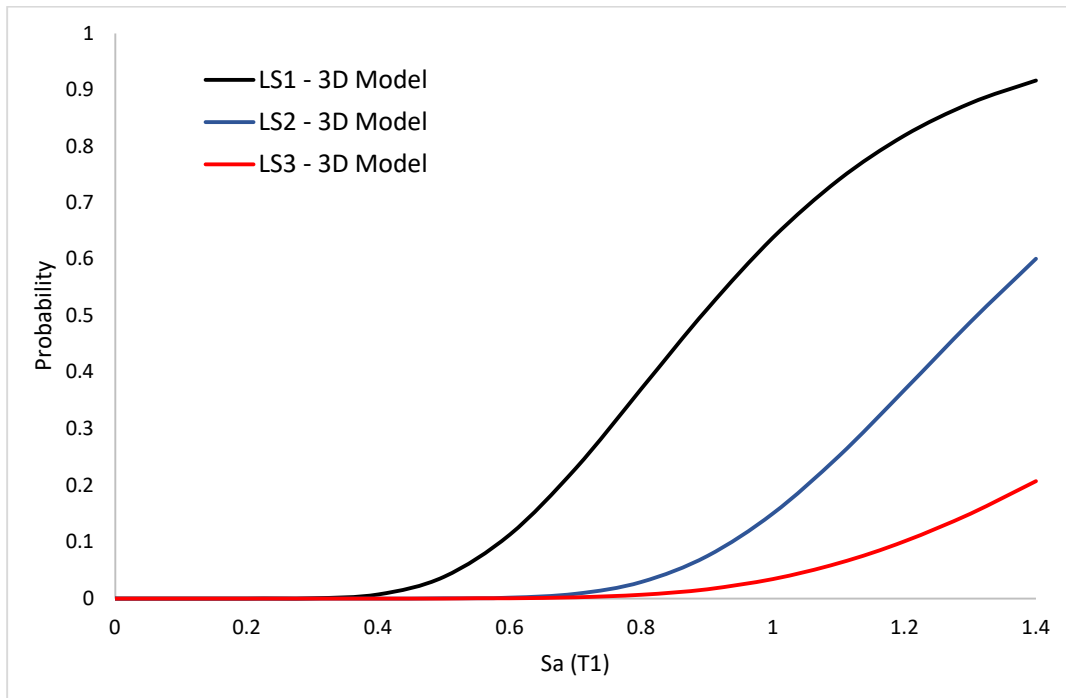


Figure 4.12: Derived fragility curve using fundamental mode only against Sa@T1 as an IM

It can be clearly observed that higher values of probabilities of exceedances are achieved when PGA is used as an IM for each of the LS for the presented case study; nevertheless, lower probabilities were observed for the same building typology when scaled Sa at the fundamental mode's time period was used as an IM.

This particular disparity is primarily related with the incorporation of specific structural characteristics i.e. time period, stiffness and deformation capacity, during the analyses when Sa was scaled at the fundamental mode's time period.

Thus, it is viable to state that Sa @ T1 portrays a better contemporary state of vulnerability, relative to PGA. Table 4.5 shows the developed values of the controlling parameters i.e. λ_c and β_c for the developed fragility relationships against each limit state against and for each of the IM.

Table 4.5: Lognormal distribution parameters for fragility curves against PGA and Sa@T1

Fragility Parameter	Serviceability (LS1)		Damage Control (LS2)		Collapse Prevention (LS3)	
	PGA	Sa @ T1	PGA	Sa @ T1	PGA	Sa @ T1
λ_c	0.4842	0.8908	0.7156	1.3094	0.957	1.8399
β_c	0.327	0.3266	0.1974	0.2606	0.1742	0.3353

4.2.3.9.2. Development of fragility curves using proposed methodology

The development of analytical fragility curves by using UMRHA procedure requires the interpretation of the obtained results separately for each of the considered mode. This separate interpretation allows to obtain an articulate insight to observe the contribution of each structural mode towards the seismic vulnerability. As stated earlier, the probabilities in the case of proposed procedure have been calculated in such a way that whenever the EDP crosses a threshold value for a specific limit state, an event is counted regardless of the mode number in which it passes the threshold value. Figure 4.13 shows the developed fragility relationship by considering the contribution of the 2nd mode against PGA as an IM.

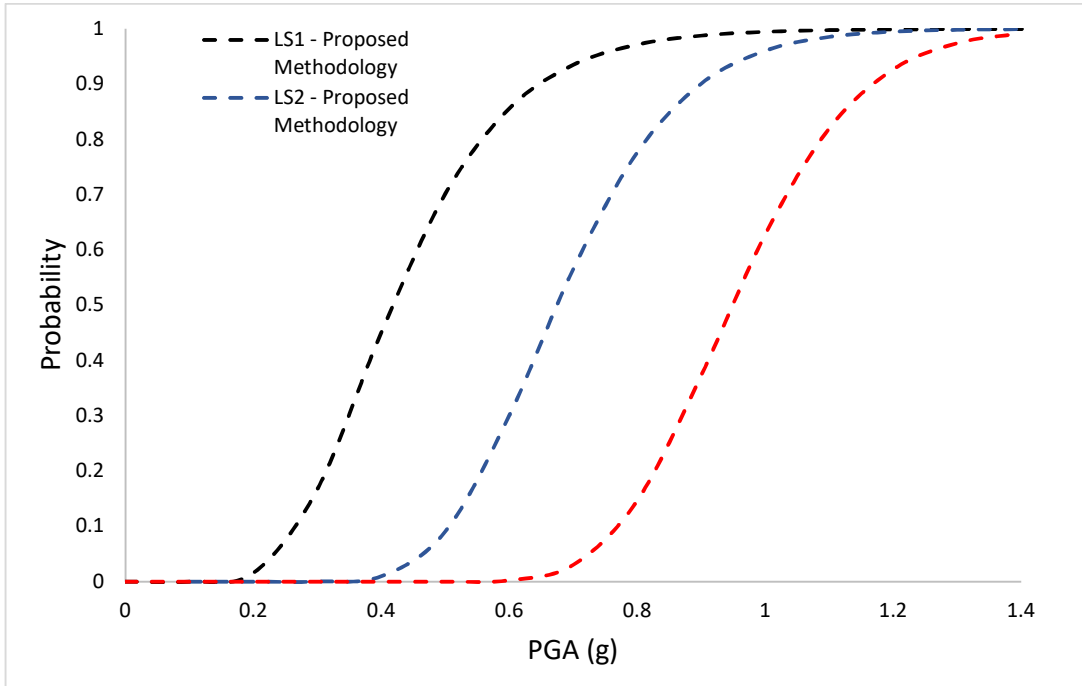


Figure 4.13: Fragility curves with 2nd mode's contribution (UMRHA framework) using PGA as an IM

Figure 4.14 depicts the fragility relationships, developed by incorporating 2nd mode's contribution, along with fundamental mode, when Sa has been used as an IM. In this case, as described earlier, the Sa has been scaled at two different time periods i.e. at the fundamental mode's time period for the analysis of SDOF system characterizing the first mode, and at the 2nd mode's time period for the analysis of SDOF system characterizing the 2nd mode of the considered building typology.

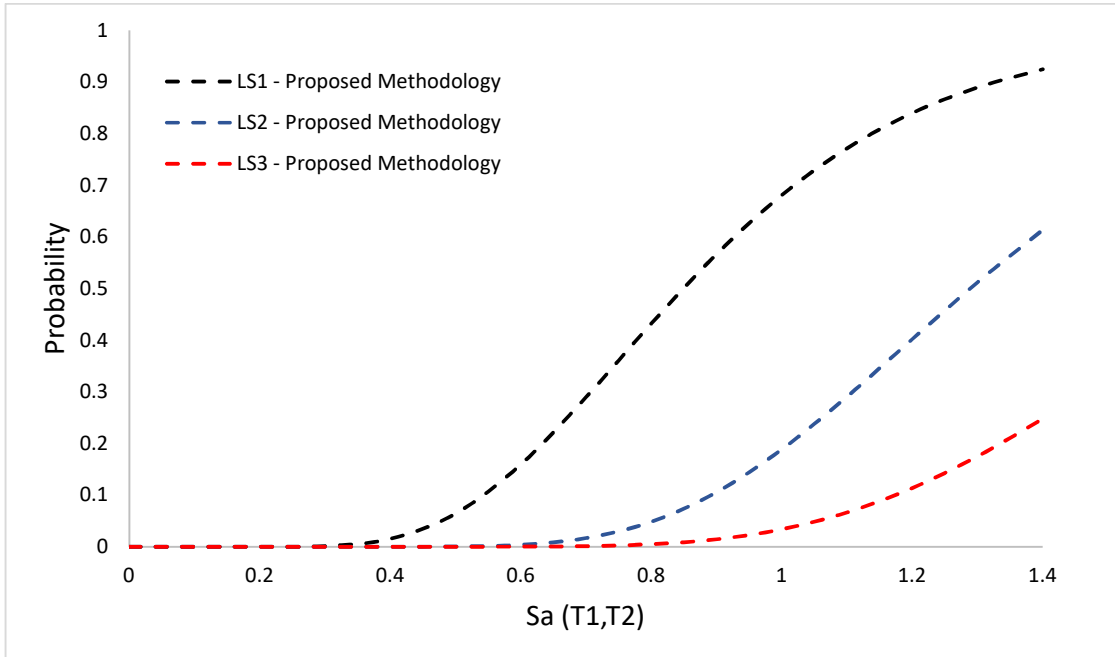


Figure 4.14: Fragility curves with 2nd mode's contribution (UMRHA framework) using Sa @ T1, T2 as an IM

Table 4.6 shows the values of the controlling parameters obtained for the development of fragility relationships using the presented methodology.

Table 4.6: Controlling parameters for fragility curves, developed using presented methodology

Fragility Parameter	Serviceability (LS1)		Damage Control (LS2)		Collapse Prevention (LS3)	
	PGA	Sa @ T1	PGA	Sa @ T1	PGA	Sa @ T1
λ_c	0.4171	0.8489	0.6744	1.2886	0.9483	1.7102
β_c	0.3419	0.34801	0.2242	0.28705	0.1620	0.2936

Following subsection provides a comparison of results obtained through the analysis, conducted considering the fundamental only, with the analysis conducted considering the 2nd mode's influence as well.

4.2.3.9.3. Comparison of obtained results in terms of analytical fragility relationships

A rational comparison of the obtained fragility curves, using the fundamental mode and the presented framework which considers the effect of 2nd mode, has been made to validate the efficacy of newly established methodology. The comparison is made in order to observe the effect of 2nd mode in the overall seismic vulnerability of the considered school building typology. Figures 4.15 and 4.16 show the comparison of newly developed fragility relationships against the PGA and Sa respectively.

The plots in figures 4.15 and 4.16 do not show the discrete probability values as shown previously because of depicting better graphical representation. The dotted lines in figures 4.15 and 4.16 are showing the fragility curves, established using proposed method in this study and contains the effect of 2nd mode of vibration. Such curves are already presented in the figures 4.13 and 4.14 against PGA and Sa (scaled at T1 and T2) as IMs. Solid lines in figures 4.15 and 4.16 are the fragility curves developed by analyzing the structure in fundamental mode only. These curves have also been shown separately in figures 4.11 and 4.12 against PGA and Sa (scaled at T1 only) as IMs.

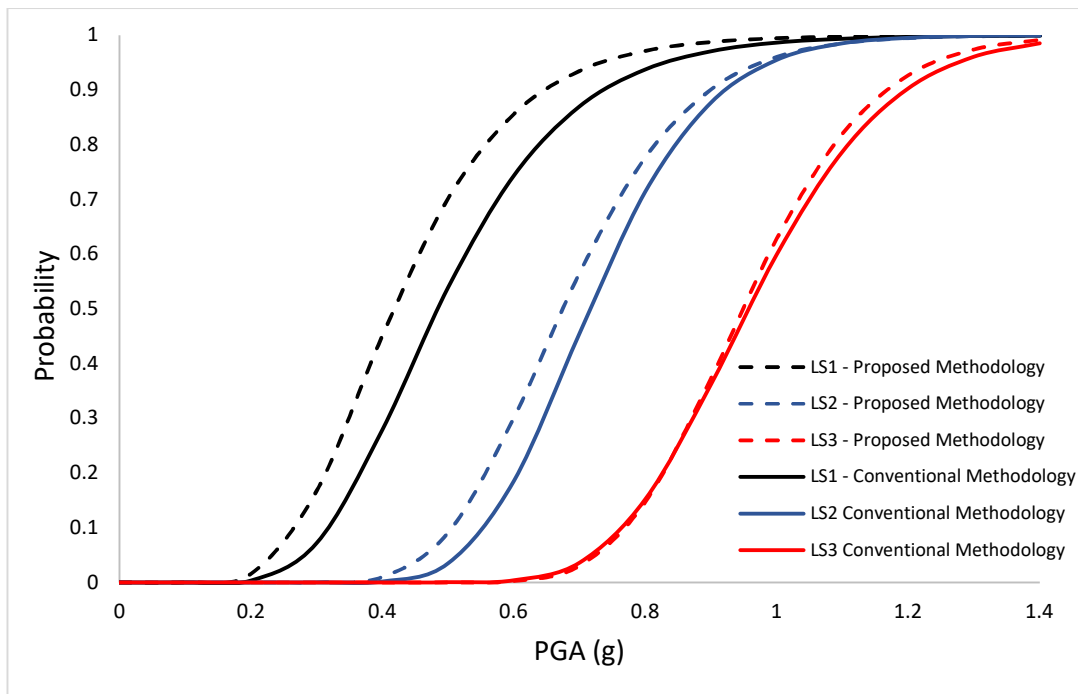


Figure 4.15: Comparison of fragility curves developed through analyses in fundamental mode only with the curves developed using presented methodology, considering two modes, against PGA as an IM.

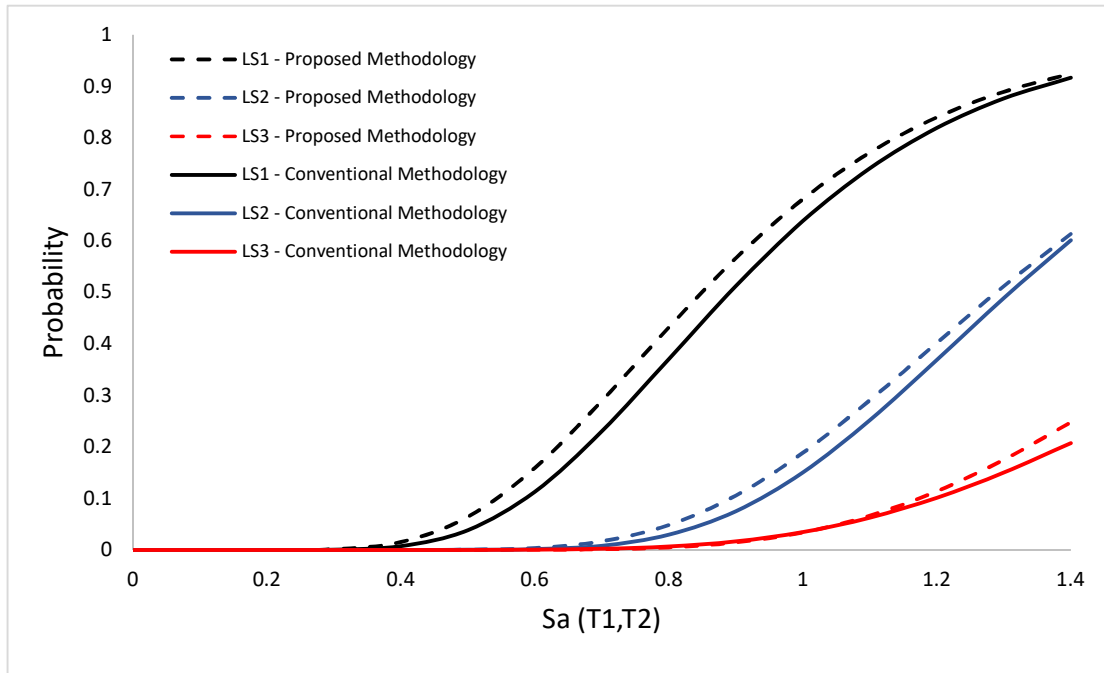


Figure 4.16: Comparison of fragility curves developed through analyses in fundamental mode only with the curves developed using presented methodology, considering two modes, against $S_a @ T_1, T_2$ as an IM

The contribution of the second mode is clearly visible in the figures 4.15 and 4.16. It is manifested by the comparison that the consideration of 2nd mode (or even other higher modes) shall result in enhancing the structural vulnerability. As indicated by the obtained results, LS1 has received the most substantial effect of the incorporation of 2nd mode in vulnerability assessment process, while Collapse Prevention limit state, the LS3 has received not so significant contribution even with the inclusion of the 2nd mode, and has remained mainly dependent upon the 1st mode for the considered school building typology. This insignificant change in the LS3 is mainly attributed to the relatively low modal mass participation ratio of 2nd mode, and consequently, a substantial increase in the evaluated probabilities, particularly for LS3, could not be observed. However; the obtained results through the newly established methodology provided an articulated comprehension for evaluating the contribution of each structural mode towards the structural seismic vulnerability.

The established methodology has been verified and validated by applying it to two different case studies; first one is a benchmark structure, developed by Pacific Earthquake Engineering Research (PEER) Institute, second one is a high-rise building structure so that efficacy of presented methodology can be established against discreet consideration of higher vibrational modes.

4.3. Validation of Proposed Methodology

Validation of proposed methodology for RC schools has been conducted by applying it to two different structures and the subsections have been arranged accordingly. Initially, the proposed procedure for vulnerability assessment has been applied over a benchmark low-rise RC structure, developed by Pacific Earthquake Engineering Research (PEER) Institute, and eventually, the proposed methodology has been applied to a 55 story high-rise structure with an intention to obtain a clear insight of the contribution of higher modes towards seismic vulnerability as the 55 story structure would have substantial contribution of higher modal mass participation ratio in comparison with a two-story and a four-story structure. Following subsection i.e. 4.3.1 provides all the description, modelling, analyses, results, and discussions through analysing the PEER's benchmark structure and comparing its original fragility (developed by PEER) with the fragility developed using proposed methodology. Afterwards, the subsection 4.3.2 provides the details of high-rise building case study, used to validate the broader application of proposed methodology, and all pertinent details about the structural modelling, analysis, and fragility development have been discussed accordingly.

4.3.1. Validation of proposed methodology through PEER's benchmark building

All steps of proposed procedure, as elaborated previously, have been employed to develop the fragility information of PEER's benchmark structure. Subsequently, the fragility curves, developed by PEER have been compared with the fragility curves that have been developed using proposed procedure for the considered benchmark structure. PEER had developed the structural model in PEER's Open System for Earthquake Engineering Simulation, OpenSees, and used two different models i.e. fiber-based model for low intensity levels and lumped plasticity model for structural collapse. The reader of this work is referred to PEER's report, An Assessment to Benchmark the Seismic Performance of a Code-Conforming Reinforced Concrete Moment-Frame Building, for detailed modelling and analysis

parameters used by PEER. The report also indicated that IDA had been used to develop the collapse level fragility relationship for the considered code-conforming benchmark structure.

In the present work, CSI Perform 3D has been used to establish the analytical model. The details pertaining to modelling parameters, analytical details, and simulation results are presented in the proceeding subsections.

4.3.1.1. PEER's benchmark site and building description

PEER's benchmark building consists of a four-story building, which had been designed in accordance with International Building Code (IBC) of 2003 [58]. The Los Angeles basin characterizes the location of the building. The selected location by PEER specifically represents high-intensity seismic zone in California. However, it is pertinent to mention that the selected site by PEER did not had any localized near-fault effects. In geotechnical perspective, the site had been characterized by deep-seated alluvial deposits with upper 30m comprising sands and silts. The shear wave velocity in the upper 30 meters had been indicated as 285 m/sec.

Figure 4.17 presents the layout of benchmark building, while figure 4.18 exhibits the elevation of the frame with a 14 ft. (4.3 m) first-story height and three 13 ft. (3.9 m) upper floors. The benchmark building has been designed as an office building.

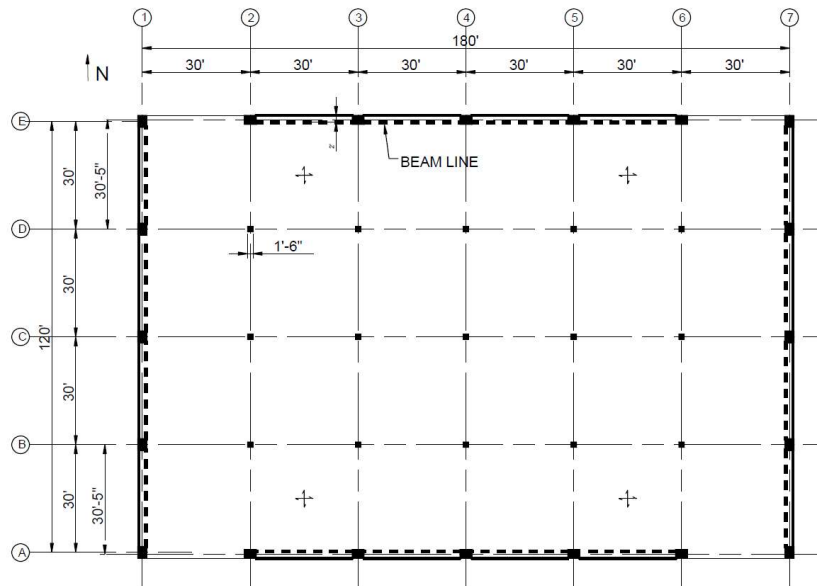


Figure 4.17: Plan view of PEER's benchmark building

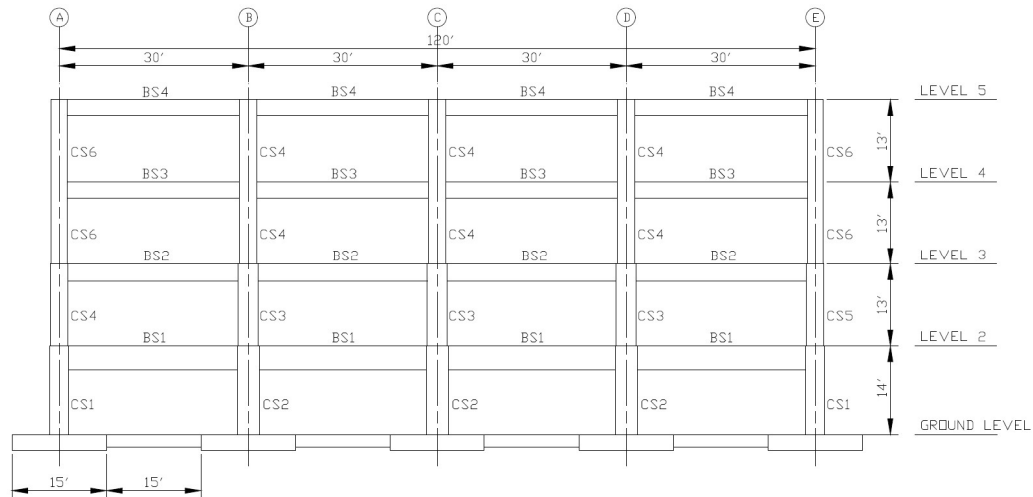


Figure 4.18: Elevation view of PEER's benchmark building

PEER had employed two-dimensional nonlinear dynamic response history analyses for assessing seismic performance of benchmark building. PEER's work considered the architectural features i.e. non-structural components such as wallboard partitions, exterior glazing, elevators, sprinklers, and ceilings for assessing the damage and loss calculations; however, this work specifically uses their structural information and PEER's benchmark results for structural damages and collapse only.

4.3.1.2. PEER's Intensity Measure selection and Ground Motion characterization

PEER employed spectral acceleration at fundamental mode's time period, $S_a @ T_1$, as the *IM* for benchmark building, and subsequently stated that $S_a @ T_1$ had been an effective and superior *IM*, in comparison with PGA that could not discreetly take into account the structural characteristics. During research study, PEER also conducted Probabilistic Seismic Hazard Assessment (PSHA) for characterizing the seismic Hazard; however, since the contemporary work is specifically related with the vulnerability analysis instead of the hazard analysis, therefore, only the selection and ground motions characterization by PEER has been discussed here. PEER, in total, developed 7 different hazard levels, ranging from a 7-years return period to 2475-years return period (2% probability of exceedance in 50 years), and selected ground motions for each of the hazard level. For an ornate elaboration over PSHA, the reader is referred to the PEER's report. Table 4.7 provides the summarization of criteria followed by PEER to select the ground motion records.

Table 4.7: PEER’s criterion for GM selection for benchmark structure

Sr. No.	Criterion	Restriction	Parameter of interest
1	Magnitude	Hazard-level dependent	Frequency content and duration of earthquakes
2	Source-to-site distance	PSHA results	Frequency content and near-fault characteristics
3	Fault Mechanism	Strike-slip fault and reverse-oblique fault	Amplitude of ground motion and attenuation

PEER has considered the earthquakes having magnitude between 5.9 and 8.0 with $S_a(T1)$ values ranging from a minimum of 0.10g to 0.82g. For the benchmark building, ground motions were selected from the PEER database, and records were selected by depending upon the mean of two horizontal components. Table 4.8 shows the earthquake events employed by PEER for benchmark RC building.

Table 4.8: Selected ground motions for PEER benchmark building

Sr. No.	Earthquake	Magnitude (M)	Day/Month/Year
1	ChiChi Taiwan	7.62	20/09/1999
2	Duzce	7.2	12/11/1999
3	Izmit	7.51	17/08/1999
4	Hector Mine	7.1	16/10/1999
5	Kobe	6.9	16/01/1995
6	Northridge	6.7	17/01/1994
7	Northridge Aftershock	5.9	17/01/1994

8	Big Bear	6.4	28/06/1992
9	Landers	7.3	28/06/1992
10	Loma Prieta	6.9	18/10/1989
11	Cape Mendocino	7.1	25/04/1992
12	Superstintn Hills (A)	6.3	24/11/1987
13	Superstintn Hills (B)	6.7	24/11/1987
14	Whittier Narrows	6	01/10/1987
15	Chalfant Valley	5.8	31/07/1986
16	Chalfant Valley	5.6	21/07/1986
17	Chalfant Valley	6.2	21/07/1986
18	Chalfant Valley	5.9	20/07/1986
19	N. Palm Springs	6	08/07/1986
20	Taiwan Smart1 (40)	6.4	20/05/1986
21	Hollister	5.4	26/01/1986
22	Bishop	5.8	23/11/1984
23	Morgan Hill	6.2	24/04/1984
24	Coalinga	5.8	22/07/1983
25	Coalinga	6.4	02/05/1983
26	Westmorland	5.8	26/04/1981
27	Taiwan Smart1 (50)	6	29/01/1981
28	Livermore	5.4	27/01/1980
29	Livermore	5.8	24/01/1980
30	Imperial Valley	5.5	16/10/1979
31	Imperial Valley	6.5	15/10/1979

32	Coyote Lake	5.7	06/08/1979
33	Tabas, Iran	7.4	16/09/1978
34	Santa Barbara	6	13/08/1978
35	Point Mugu	5.8	21/02/1973
36	San Fernando	6.6	09/02/1971
37	Lytle Creek	5.4	12/09/1970
38	Borrego Mtn	6.8	09/04/1968
39	Parkfield	6.1	28/06/1966
40	Kern County	7.4	21/07/1952
41	Imperial Valley	7	19/05/1940

4.3.1.3. Application of proposed methodology

Proposed methodology has been adopted for structural analysis and fragility development of benchmark structure in order to compare the newly developed fragility curves with those, developed by PEER.

4.3.1.3.1 Structural modelling

The structural modelling of the benchmark building in this work has been done in accordance with the details provided in section 4.2.3.2. Same concrete and reinforcing steel material models have been employed that had been used by PEER. Figure 4.19 shows the backbone and hysteretic behaviour of concrete as employed by PEER. Further details of the concrete model can be obtained from Fenves and Filippou [59].

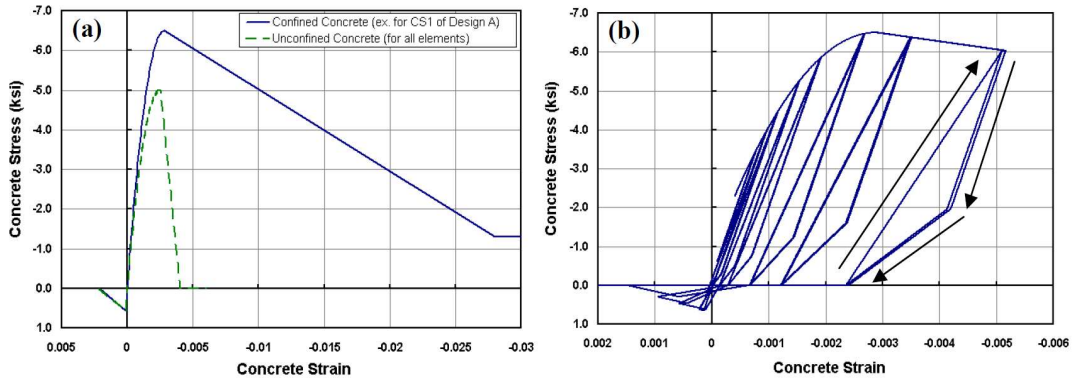


Figure 4.19: Concrete model (a) unconfined and confined backbone curve (b) hysteretic behavior

Similarly, figure 4.20 shows the material model for reinforcing steel. PEER’s study employed Guiffre-Menegotto-Pinto’s model for steel’s hysteretic stress-strain relationship.

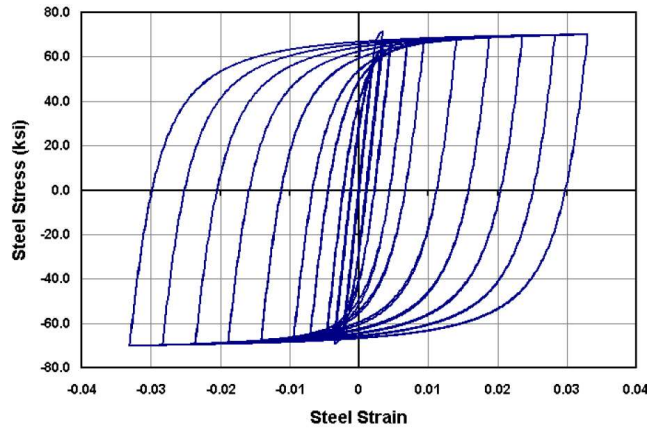


Figure 4.20: Hysteresis loop for steel by Guiffre-Menegotto-Pinto, used by PEER

It is pertinent to mention that PEER has specifically stated that incorporation of soil-structure interaction in the analytical model did not induce any significant change in the results, given the long period of fundamental mode. For all other details about the dimensions and reinforcement details of structural components, the reader of this work are referred to PEER’s report.

4.3.1.4. Comparison of results

Since there exists some differences in the modelling approach by PEER and the presented work, the comparison of results has been made in terms of collapse level seismic fragility

curves as PEER has only developed the collapse level fragility curve for the benchmark structure; while other levels of damages have not been considered by PEER. All other analyses results have not been compared as all other analyses conducted by PEER have been in accordance with conventional procedures, already discussed in section 4.2.3.

Furthermore, PEER has also thrived to establish fragility information for architectural and non-structural components of the building i.e. paint works, elevators, sprinklers, etc. by correlating them with roof drifts. However, since the presented work herein is discretely related with the structural damages, hence the results are compared only for the structural damage (collapse level fragility curves). Figure 4.21 presents the original collapse level fragility curve developed by PEER. For developing collapse level fragility, PEER has considered 6% of global drift as an EDP to correlate with $S_a @ T1$.

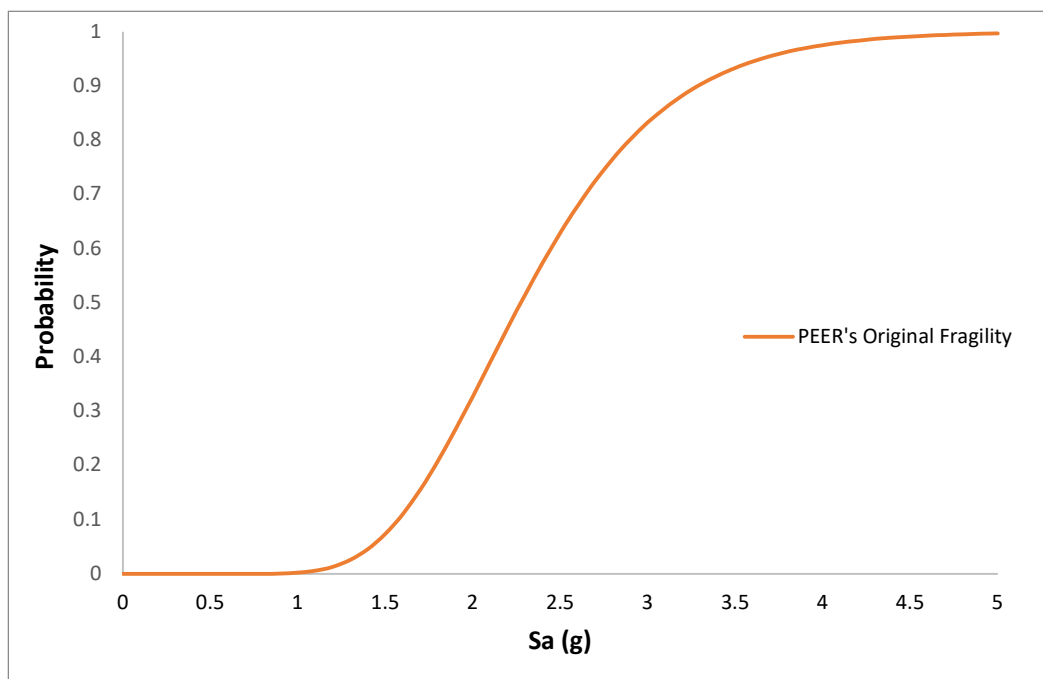


Figure 4.21: Fragility curve developed by PEER against collapse level LS

The subsequent figure 4.22 exhibits the comparison of fragility curves (seismic vulnerability information) developed by PEER and herein presented methodology.

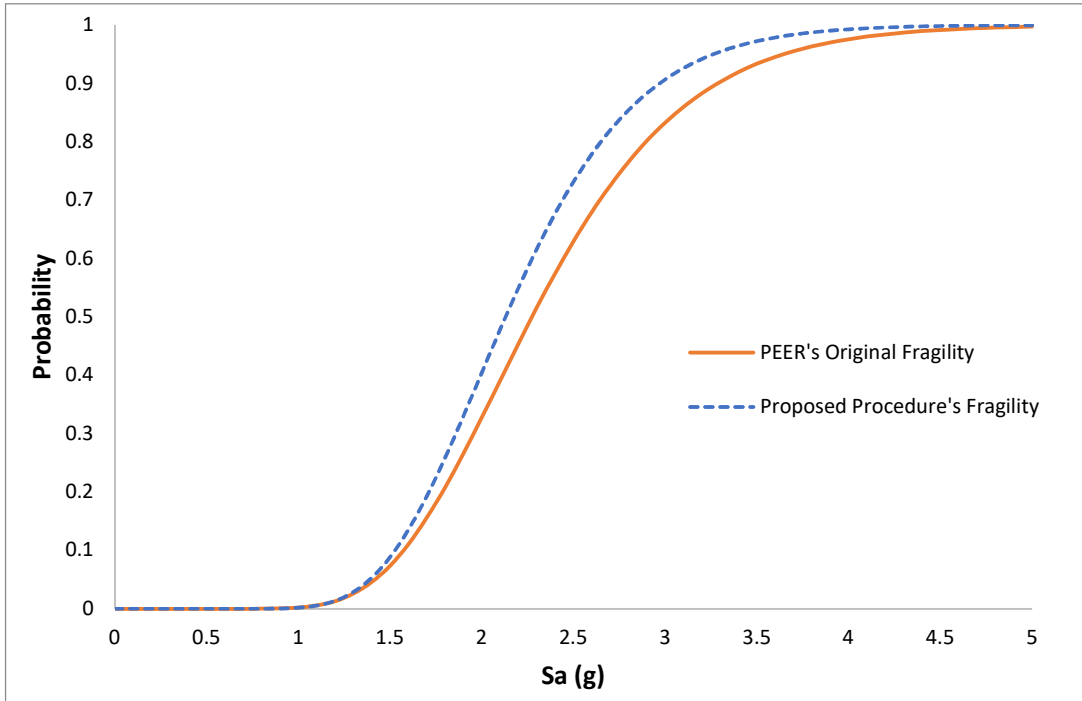


Figure 4.22: Comparison of Fragility curves developed by PEER and proposed methodology

The increase in the seismic fragility values by using established methodology can be clearly observed at each value of seismic intensity measure. The increase is primarily attributed to the difference in modelling approaches. PEER has employed lumped-plasticity approach that consolidates the masses at story levels with two-dimensional analysis, and primarily targets only the near collapse response with a fundamental focus on 1st mode only, while the presented methodology incorporates complete 3D structural cyclic force-deformation relationship at global level in place of material level only. The second prominent reason for the increase in probability values is the discreet consideration of 2nd mode during analysis. The wholesome incorporation of 2nd mode in accordance with UMRHA procedure has directly influenced the probability and resulted in its increase.

After validation with the PEER's benchmark structure, the current methodology has been applied on a high-rise structure so that efficacy of the proposed methodology can be checked for a structure with significantly higher modal mass participation ratio from higher vibrational modes. Following section contains all the pertinent details of the application of

presented methodology to a 55 story high-rise building structure in which first four modes have been considered that constitute more than 90% of modal mass participation ratio.

4.3.2. Validation of proposed methodology through a high-rise structure

4.3.2.1. Reference building description and structural modelling

The considered case study comprises of 55 story tall, core-wall building, located in Manila, Philippines. CSI Perform 3D was used to develop the 3D nonlinear model. The software package consists of excellent nonlinear modelling elements to adequately capture the nonlinear structural response. The shear wall was modelled completely nonlinear by using fibre elements to monitor the strains arising in shear wall. The link beams were also modelled as nonlinear, however fibre elements were not used, instead, nonlinear plastic hinges have been eventually employed to capture the behaviour of link beams. Hysteretic behaviours were explicitly modelled for construction materials, i.e. concrete and steel for considering the hysteretic damping and stiffness degradation mechanism. Table 4.9 describes the geometrical features of the considered building, while table 4.10 shows the concrete’s strength, which has been considered in nonlinear modelling, for flexural and axial components along with the shear wall. Figure 4.23 shows the graphical view of developed nonlinear 3D model in CSI Perform 3D.

Table 4.9: Geometrical features of considered high-rise building

Total height	163 m
Number of stories	55
Podium plan area	92 m X 54 m
Tower plan area	40 m X 39 m
First story height	4.7 m
Typical story height	2.9 m

Table 4.10: Material characteristics for structural components

Structural Member		Concrete Strength (MPa)
Slabs, Beams & Girders	Base to 40 th Story	41
	40 th Story to Roof	34
Shear Walls & Columns	Base to 11 th floor	69
	12 th to 21 st floor	59
	21 st floor to roof	48

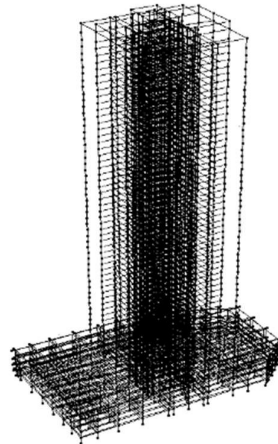


Figure 4.23: Isometric view of 3-Dimensional nonlinear analytical model

4.3.2.2. Application of proposed methodology

4.3.2.2.1. Hysteretic behaviour and development & response verification of SDOF systems

First four structural modes along weaker axis of building have been considered in the analysis as they cumulatively comprise more than 90 percent of modal mass participation ratio. Table 4.11 portrays the modal mass participation ratio of all four modes.

Table 4.11: Modal mass participation ratios

Mode No.	Modal mass participation ratio (%)
1	60
2	17
3	8
4	5

The time periods for first four modes are 4.67, 1.12, 0.51, and 0.30 seconds, respectively. Since presented methodology requires SDOF systems that can represent the individual mode in its decoupled state, four SDOF systems have been developed for considered four modes, and each SDOF system contains the respective modal force-deformation behavior. Figure 4.24 shows the F-D relationship of the considered structure.

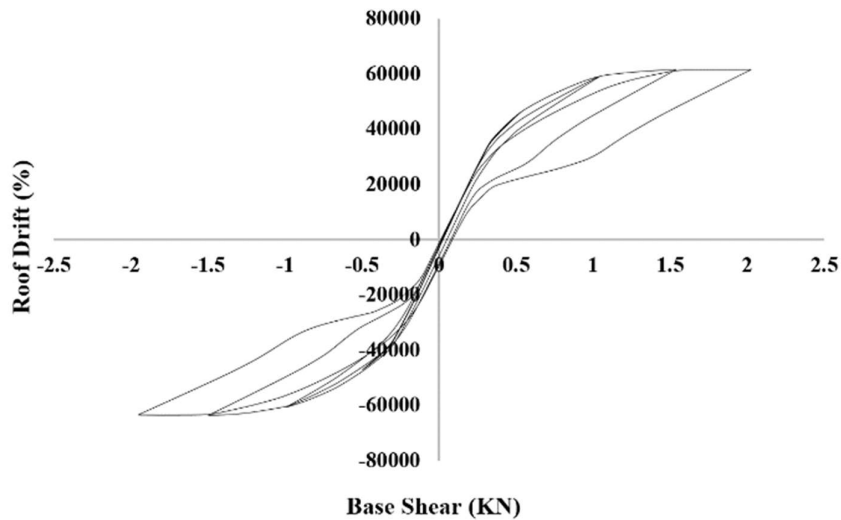


Figure 4.24: Hysteretic behavior of considered building (Cyclic POA)

The analysis of SDOF systems have been conducted by using IIIDAP. For verifying the cumulative response obtained from SDOF systems analysis with the response attained from 3 dimensional nonlinear model, a single ground motion with a similar scaled intensity has

been employed for analysis. Figure 4.25 shows the comparison of deformation based response obtained through analysis of 3 dimensional model and UMRHA procedure.

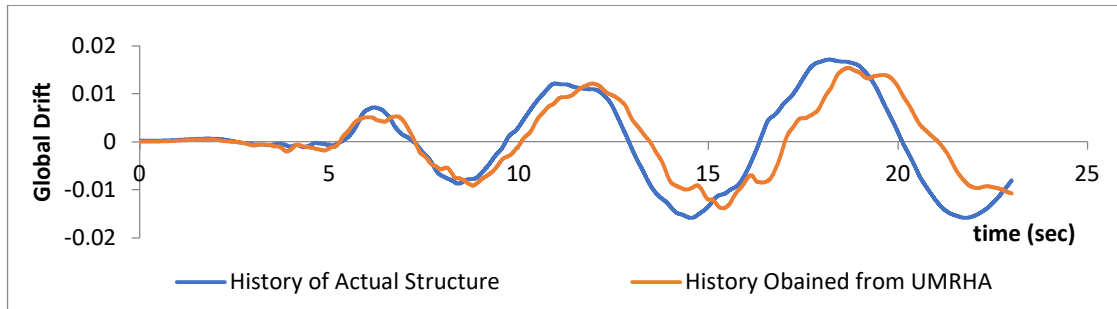


Figure 4.25: Roof drifts obtained through 3D model and UMRHA procedure (Proposed methodology)

4.3.2.2.2. Uncertainty treatment

As described earlier, the current work vehemently considers the aleatory uncertainties, primarily attributed to the intrinsic variability in the nature of ground motions. The aleatory uncertainties cover the record-to-record variability of seismic ground motions by incorporating a wider range of ground motions with varying intrinsic characteristics i.e. PGA, attenuation path, source-to-site distance, etc. Present study, for high-rise structure, takes into account 15 ground motions with varying features as given in table 4.12. The ground motions have been selected by considering the earthquake magnitude, source to site distance, and soil conditions at which the records were made available. This selection criteria has been discussed in detail under section 4.2.3.5.

Table 4.12: Selected ground motions for high-rise building

Earthquake	Magnitude	PGA (g)	Distance to rupture (KM)	Soil condition at site
Aftershock of Friuli EQ	5.7	0.2305	10	Soft
Alkion, Greece	6.1	0.1199	25	Soft
Anza (Horse Cany)	4.9	0.097	20.6	Soft

Caolinga	5.0	0.673	12.6	Stiff
Chi-Chi, Taiwan	7.6	0.821	7.31	Stiff
Chi-Chi, Taiwan	7.6	0.088	39.34	Soft
Dinar, Turkey	6.0	0.3193	1.0	Soft
Imperial Valley	6.5	0.775	2.5	Soft
Kobe, Japan	6.9	0.694	1.2	Soft
Kobe, Japan	6.9	0.081	89.3	Stiff
Kocaeli, Turkey	7.4	0.179	76.1	Stiff
Kocaeli, Turkey	7.4	0.249	78.9	Soft
Loma Prieta, USA	6.9	0.644	5.1	Stiff
Northridge	6.7	1.779	17.5	Stiff
Northridge	6.7	0.139	64.6	Soft

4.3.2.2.3. Definition of limit states and engineering demand parameter (EDP)

Limit states serve the purpose of defining discrete levels of damage to any structure. Limit states are correlated with mathematical values of an Engineering Demand Parameter (EDP). The present study considers three limit states, namely Immediate Occupancy (LS1), Damage Control (LS2), and Collapse Prevention (LS3). The formation of first plastic hinge or the reaching of plastic strain in any of the fiber characterizes LS1. Strength and deformational features control the LS2, and it is taken as 75 percent of LS3. LS3 is taken as the maximum deformational capacity of primary load resisting system, after which the complete collapse is imminent. Table 4.13 provides quantitative values for all limit states. The qualitative definitions for all limit states have been kept same, while the quantitative definitions have

been different for all four modes of considered structure due to their own individualistic decoupled behavior.

Table 4.13: Quantitative thresholds for considered limit states for considered modes

Mode No.	Limit State (%age Global Drift)		
	Immediate Occupancy (LS1)	Damage Control (LS2)	Collapse Prevention (LS3)
1	0.68	2.8	3.7
2	0.11	0.28	0.38
3	0.045	0.135	0.18
4	0.043	0.13	0.17

4.3.2.2.4. Seismic intensity indicator

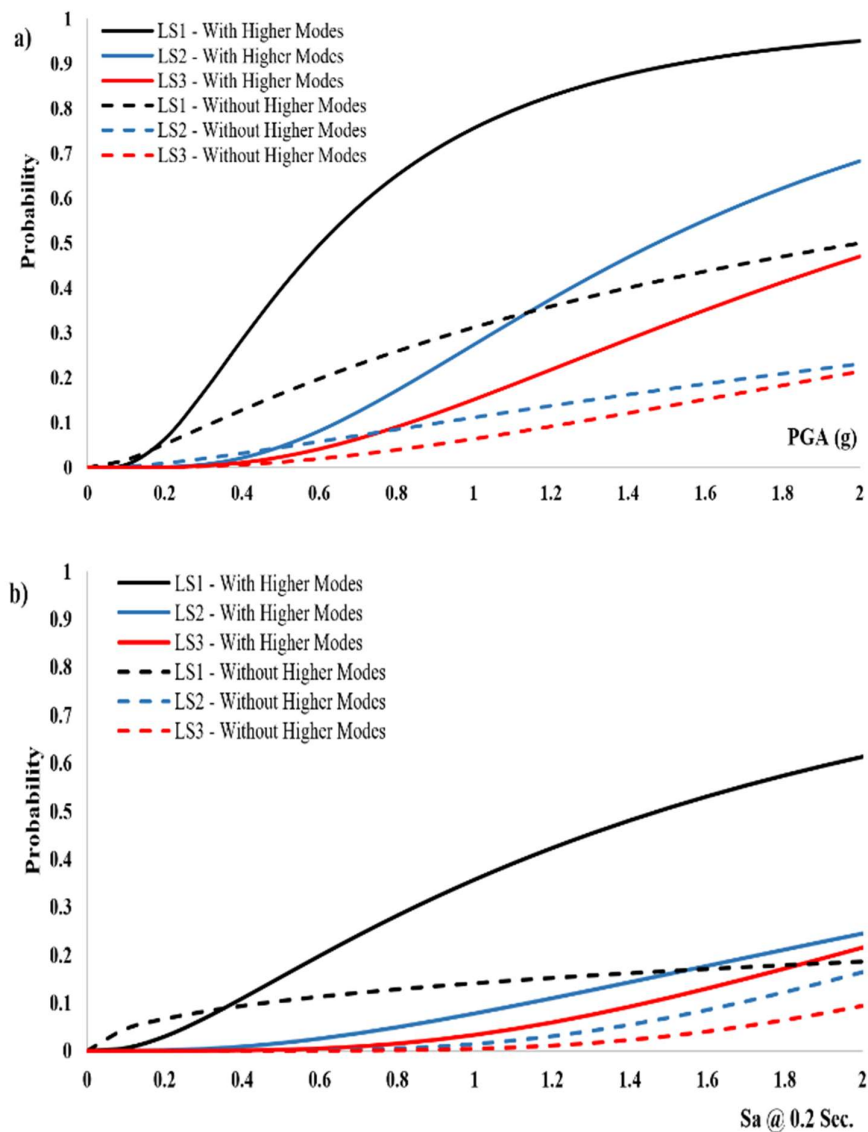
For assessing seismic vulnerability, it is imperative to take into account the wider frequency content of seismic ground motions as it may induce highly convoluted structural response by exciting lower and higher modes simultaneously. For representation of seismic intensity, PGA and Sa as IMs. The spectral accelerations have been considered at two periods; 0.2 sec. and 1.0 sec. so that lower and higher frequency responses can be adequately captured.

4.3.2.2.5 Incremental dynamic analysis and fragility derivation

Incremental Dynamic Analysis (IDA) has been used to determine the vulnerability of considered case study against seismic motions. All ground motions had been initially scaled to match their intensities, and subsequently, each SDOF system is subjected to seismic loading for obtaining cumulative responses. For conducting the analysis, a set interval of 0.25g had been used to augment the seismic intensity for each successive iteration, and ground motion intensities varied from 0.25g to 2.0g. Since this work is primarily related with the fragility assessment, so the final results of considered high-rise buildings have been reported in terms of fragility curves instead of IDA curves. For comprehending all the

process about IDA, the reader of this work is referred to sections 4.2.3.5 and 4.2.3.8 as same process has been repeated for high-rise structure, considering PGA, Sa @ 1.0 sec, and Sa @ 0.2 sec as IMs.

For developing fragility curves and determining controlling parameters, Maximum Likelihood Method (MLM) has been used. The developed fragility relationships for all three considered limit states, with and without considering the higher modes, are shown in figure 4.26 against PGA, Sa @ 0.2 Sec., and Sa @ 1.0 Sec. as IMs. Solid lines describe the fragility by considering the influence of higher modes along with the 1st mode, while dotted lines are depicting structural vulnerability by taking into account the fundamental mode only.



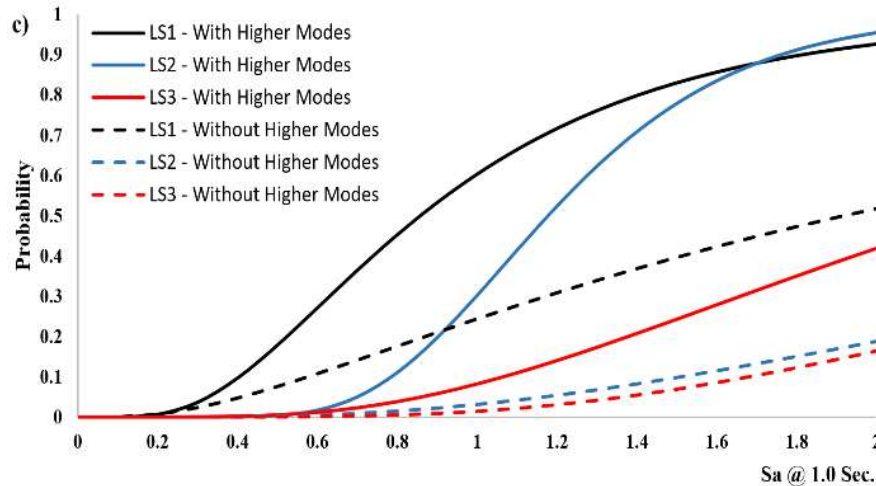
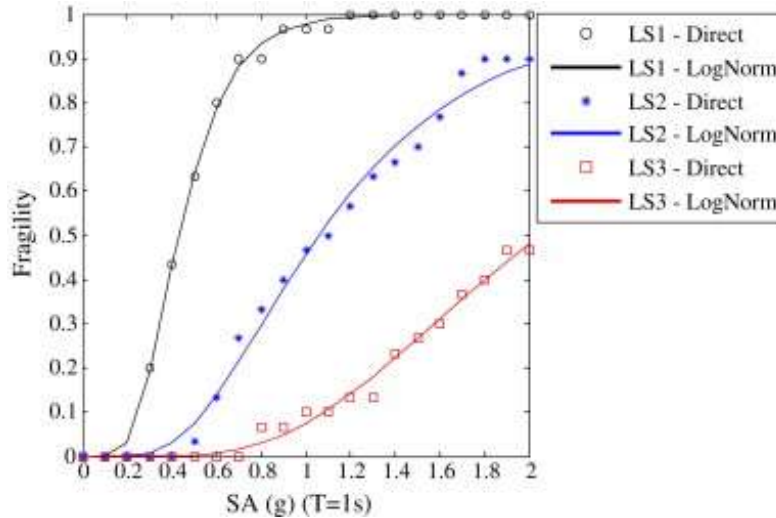


Figure 4.26: Comparison of fragility relationships, developed with and without the contribution from higher modes: a) Fragility curves against PGA b) Fragility curves against Sa @ 0.2 sec. c) Fragility curves against Sa @ 1.0 sec.

Analytical fragility curves for a specific class of tall buildings i.e. core-wall buildings, are developed in the current study. Fragility relationships for considered high-rise buildings had been developed considering the response of each individual mode towards structural vulnerability. In the presented work, a set of fragility curves for high-rise building is presented with and without the consideration of higher modes to evaluate the significance of proposed methodology. It is imperative to mention that higher modes play substantial role in seismic vulnerability. For instance, the probability of exceeding LS1 against Sa @ 1.0 sec., with seismic intensity of 1.0g, is about 60 percent when the higher modes are considered, in comparison with the probability of 24 percent when only the response of fundamental mode is taken into account. The presented results have been compared with another study conducted by Jun ji et. al. (2009), where the fragility curves of a 54 stories were developed using a simplified model, developed through genetic algorithms. The below picture shows the fragility curves developed by Jun ji et. al. and it has the same criteria of defining limit states as used in the presented work. The IM used by them is Sa @ 1 sec.



While comparing the results of the figure with the presented work, it can be observed that at the Sa of 1.8g of the curve developed by Jun Ji et. al., the probability of exceeding LS1 is almost 100%, while in the presented work, the probability of exceeding LS1 at the exact same intensity is 91% as depicted by figure 4.26. Similarly, if LS3, the Collapse Limit State, is compared, the fragility developed by Jun Ji et. al. [34] depicted the probability value of approximately 48% for the similar category of structure, while the probability of exceeding LS3 for the high-rise structure, employed in the presented work, is 41%. The difference is obtrusively due to the differences in the sizes and configuration of the structural members that develop the stiffness discretely for each structure. However, the values experienced by both of the structures are quite in the similar range, and this similarity sufficiently presents the adequacy and the efficacy of the proposed methodology.

Unlike conventional procedures of IDA, that render almost impossible to develop fragility curves for this class of buildings (high-rise) using IDA of a 3D nonlinear model because of highly extensive computational effort, the presented methodology did not consume several days to assess structural vulnerability; rather it rendered the computational effort way less expensive. Along with that, as evident by the obtained results, the proposed methodology did not depend only upon the response of fundamental mode, rather it portrayed the potential to incorporate the contribution of as many higher modes as desirable.

Subsequent sections of this chapter present the fragility analysis of stone and brick masonry schools. However, for determining the fragility relationships for stone and brick masonry schools, conventional methodology has been used as the proposed methodology is

specifically related with the RC buildings as RC buildings, unlike brick and stone masonry buildings, can be subjected to cyclic loading, which is an inherent requisite for the proposed procedure.

4.3. Vulnerability Assessment of Stone Masonry Schools

The current study also presents the vulnerability assessment of a typical, representative school building, made up of domestically available limestone. A typical layout of stone masonry structures has been provided in preceding chapter that depicts the construction of single story stone masonry school in blocks of 12.8mX5.5m (42'X18') (figure 3.7). In these dimensions of stone masonry school blocks, two classrooms are constructed, along with adjoining washroom. The load bearing wall thickness is 0.65m. Figure 4.27 presents a photograph of a typical stone masonry school block.



Figure 4.27: A photograph of typical stone masonry block, showing the adjoining toilet, repaired door, and flexible diaphragm

4.3.1. Structural modelling of a representative stone masonry school building

A representative stone masonry building model was initially developed in 3Muri software commercial version. The license was specifically obtained through an official request to 3Muri. The nonlinear model was developed in 3Muri (*3Muri*) [60] analytical software.

To develop a rational strength criterion by considering the structural properties of stones, experimental investigation was made to determine the properties of stone masonry. Figure 4.28 provides photographs of lab testing to determine the material characteristics of stone and mortar's properties.



(a)



(b)

Figure 4.28: Experimental investigation to determine material characteristics of stone: (a) Core extraction for testing; (b) Core testing

It is pertinent to mention that BCP 2007 design strength criterion has been used to evaluate the in-plane behaviour of spandrels and piers. Beam theory has been employed to evaluate the combined bending and compressive behaviour, while the tensile strength has been neglected during analysis. Table 4.14 shows the obtained material properties of stone. The mortar characteristics are also provided in the same table.

Table 4.14: Material characteristics of stone and mortar

Stone			Mortar		
Compressive strength	f_m'	66 MPa	Compressive Strength	f_c'	15 MPa
Elasticity Modulus	E	50 GPa	Tensile Strength	$0.1f_c'$	1.5 MPa
Shear Modulus	Γ	23 MPa	Shear Strength	$0.15f_c'$	2.25 MPa

Figure 4.29 shows the plan view of considered school building. It represents the typical construction of stone masonry schools in considered region. The building consists of two classrooms, each having plan of 6.4m X 3.3m as depicted by figure 4.29. The walkway, in front of the classrooms has a plan area of 12.8m X 2.1m. The geometry of the arrangements are presented in figure 4.29.

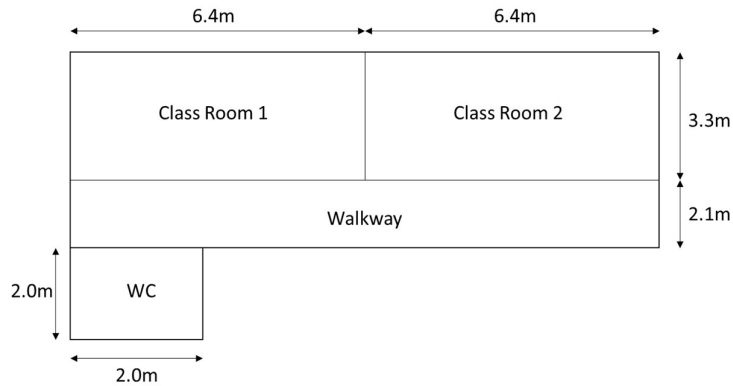


Figure 4.29: Plan view of considered stone masonry school building

For analytical structural modelling, Equivalent Frame Model (EFM) approach was employed. Flexible diaphragm was modelled because of the timber roofing. Almost all the stone masonry schools in considered region had timber roofs. For developing ample analytical model, it was necessary to incorporate the material characteristics of timber; however, due to experimental limitations, the experimental investigation had not been conducted to determine the structural properties of timber joists. To account for this shortcoming, research conducted by Giongo et al. [61] and New Zealand Society for Earthquake Engineering (NZSEE) [62] were employed. During field visits, timber joists were found in poor condition. The joists were observed to be poorly connected to the perimeter walls and membrane. For analytical modelling, following values were adopted.

Shear modulus = 6.8 MPa

Young's modulus = 7 GPa

Load = 1 KN/m²

For capturing the in-plane response of masonry walls, including openings, macroelements were used. The illustration of macroelements for considered school building is shown in figure 4.30.

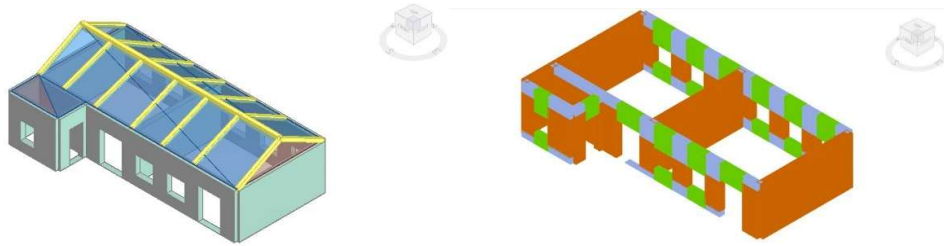


Figure 4.30: 3-Dimensional view of the stone masonry school and corresponding macroelements

In figure 4.30, orange colour characterizes the piers that bolster the live and dead loads, while spandrels are horizontal elements, characterized by green colour, placed between openings. Spandrels and piers act collectively to resist lateral loads.

4.3.2. Structural analysis, performance assessment, and fragility development

4.3.2.1. Nonlinear static analysis

The literature contains numerous options for mathematical modelling and the kind of analysis to assess the structural performance of contemporary structures. The uncertainties involved in all such methods are directly related with the level of accuracy and adequacy required to establish the fragility information of an infrastructural facility. In the presented study, it was quite essential to obtain the in-plane capacity of considered building typologies. POA was conducted to obtain the in-plane characteristics by subjecting the school building to a static loading. The nonlinear analyses were conducted in both directions (U_x and U_y). The eccentricity had also been taken into account to acutely observe the structural performance when centre of mass could not coincide with centre of rigidity. The previous versions of 3Muri program did not offer to select a control node or to produce a fictional node at roof level for pushing the structure. However, the current version of the software amply allows to conduct the pushover analysis by selecting a control node at roof level.

Pushover analyses curves had been plotted for both primary directions. Figure 4.31 depicts the obtained pushover curves for the considered stone masonry school building. From the figure, it can be inferred that both, base shear capacity (V_b) and stiffness, are lower in U_x direction, motivated by a lower resistant area and cross-section in this specific direction. Moreover, unlike what was observed in the U_y direction, the available ductility in the U_x direction is lower in the curve.

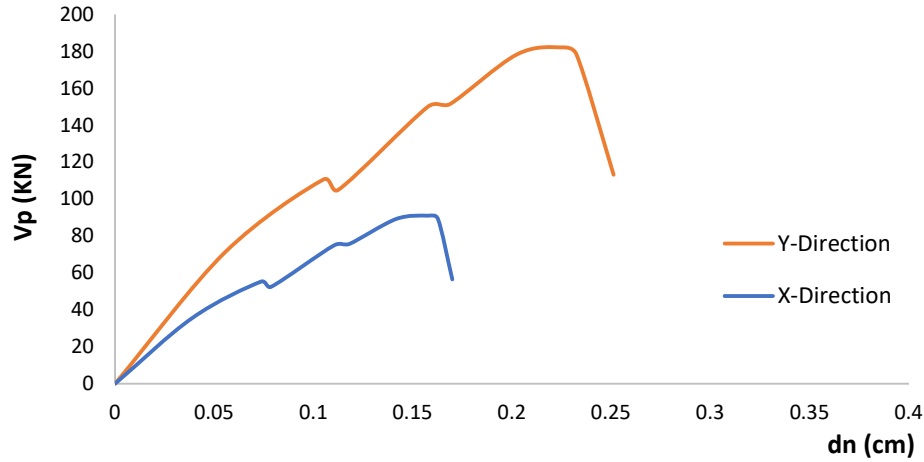


Figure 4.31: Pushover curves of a typical stone masonry school building structure in seismic zone 4 of Pakistan, representing structural capacity in terms of base shear, V_b , v/s global displacement

By the virtue of pushover analysis, the limit states have been defined in this study as described in section 4.2.3.7. The performance based assessment was conducted in terms of the ratio of ultimate displacement v/s target displacement (du/dt). The required safety condition is fulfilled when du/dt becomes equal to 1 or more than 1. The respective values of yield, target, and ultimate displacements were achieved by means of pushover analysis in accordance with ASCE 41-13. ASCE 41 determines the displacements by means of Displacement Coefficient Method (DCM). In DCM, A monotonically increasing lateral load pattern (representative of inertial forces developed during an earthquake) is applied on the nonlinear model, until a target displacement is achieved at a control node. This target displacement is intended to represent the maximum displacement likely to be experienced during the design earthquake and is calculated using the following expression.

$$\delta_t = C_0 C_1 C_2 S_a \frac{T_e^2}{4\pi^2} g \quad (4.3)$$

In the above equation,

$$T_e = T_i \sqrt{\frac{K_e}{K_i}} \text{ (where } K_e \text{ is the effective lateral stiffness)}$$

$$C_1 = 1 + \frac{R - 1}{\alpha T_e^2}$$

$$C_2 = 1 + \frac{1}{800} \left(\frac{R - 1}{T_e} \right)^2$$

R is the normalized yield strength factor that is evaluated in accordance with following equation.

$$R_{max} = \frac{\Delta_d}{\Delta_y} + \frac{\alpha_e^h}{4}$$

where Δ_d is lesser of the displacement at maximum base shear or the target displacement. Δ_y represents the displacement at effective yield strength. α_e is the effective negative post-yield slope ratio, while $h = 1 + 0.15 \ln(T)$.

The ASCE 41-13 requires the assessment of building performance under extreme condition i.e. by pushing the structure more than 150% of displacement target.

Subsequently, base obtained shear v/s lateral displacement is converted into an idealized force-deformation relationship to determine effective yield strength (V_y) and effective lateral stiffness (K_e). These parameters are eventually used to evaluate the strength factor and effective time period. All these parameters are then eventually employed to determine the coefficients involved in DCM.

In the present study, the yield displacement turned out to be 0.18 cm, while the ultimate displacement was 0.41 cm in accordance with ASCE. Figure 4.32 depicts the performance based assessment by means of pushover analysis in both directions i.e. X and Y. The value of target displacement, however crossed the ultimate displacement by a difference of 0.74 cm. The target displacement's value of 1.15 cm was greater than that of the ultimate displacement that means the considered typology of school building was unable to withstand the seismic forces during earthquakes.

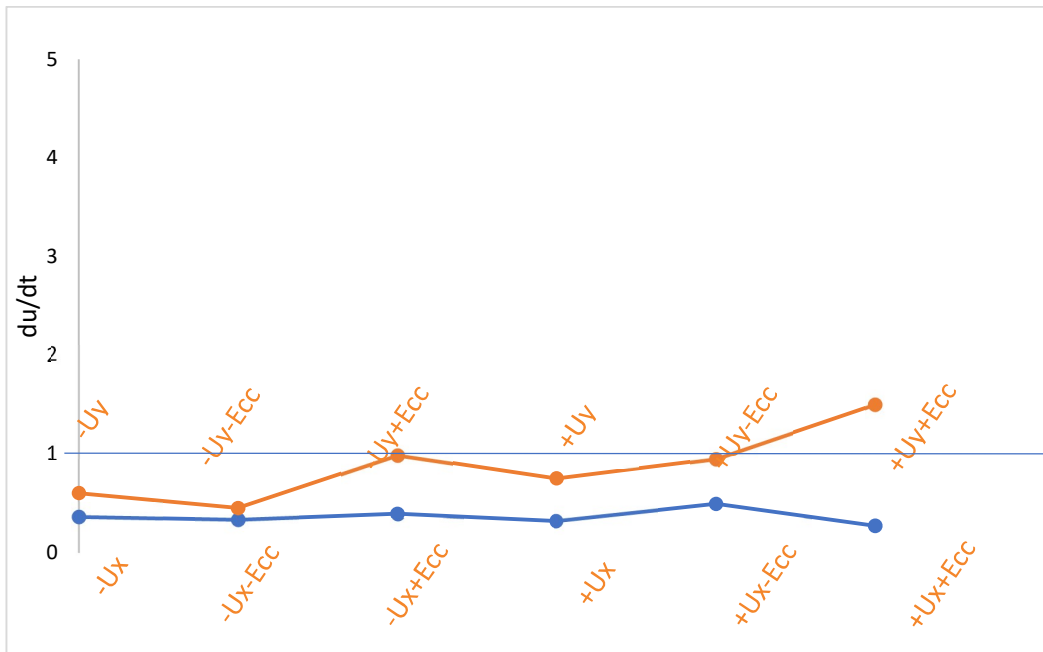


Figure 4.32: Results of seismic performance-based assessment in terms of du/dt

From figure 4.32, it can be inferred that the considered building showed some reasonable performance in Y direction when eccentricity was considered. In only one direction of Y, the structural performance could ensure the safety i.e. +Uy+Ecc. While in rest of the nonlinear static analyses, the structure could not perform well against seismic forces.

4.3.2.2. Nonlinear dynamic analysis

It is vital to assess the structural performance of school buildings against actual earthquakes. For Nonlinear dynamic analysis of stone masonry buildings, 15 ground motions were considered (instead of 20 ground motions that were considered for RC schools).

As described earlier, in this research, the mechanism of fault, source to site distance, magnitude, and the shear wave velocity V_s , in the upper 100 feet of soil strata have been considered as the controlling parameters for selecting the ground motions. It is pertinent to mention that special emphasis has been given to the characteristics of 2005 Kashmir Earthquake while selecting the ground motions as it resulted in the most catastrophic and fatally devastation of the region throughout the history, and most of the parameters, during selection, have been kept in strong alignment with those matching with the 2005 Kashmir Earthquake. The fault, which resulted in 2005 Kashmir Earthquake, is reverse-oblique in its character, and as observed, it produced a large magnitude earthquake of 7.6 Mw, with its

epicenter at 19 KMs northeast of Muzaffarabad. Therefore, only the earthquakes ranging from 6.50 to 8.0 in magnitude, originated from the reverse and revers-oblique faults are selected, and 0 to 30 KMs range has been used for source-to-site distance so any random variation due to path attenuation effects and varying soil characteristics could be effectively considered. Moreover, for selecting the ground motions, shear wave velocity, V_{s30} , has been kept between 170 m/sec (575 ft/sec) to 350 m/sec (1150 ft/sec) in accordance with BCP-2007 for the soil type S_d . Following table 4.15 shows the selected ground motions for vulnerability assessment. Magnitude, distance-to-rupture, V_{s30} , and source mechanism are also mentioned.

Table 4.15: Selected ground motions for stone masonry school buildings in seismic zone 4 of Pakistan

Sr. No.	Earthquake Name	Year	Station Name	Mag.	PGA (g)	Rrup (miles)	Vs30 (ft./sec)
1	San Fernando	1971	LA – Hollywood Stor FF	6.61	0.225	14.15	1038.25
2	Gazli USSR	1976	Karakyr	6.8	0.864	3.40	851.67
3	Tabas Iran	1978	Boshrooyeh	7.35	0.106	17.89	1064.86
4	Spitak Armenia	1988	Gukasian	6.77	0.20	14.91	1127.07
5	Loma Prieta	1989	Agnews State Hospital	6.93	0.1695	15.27	786.38
6	Loma Prieta	1989	Sratoga - W alley Coll.	6.93	0.331	5.78	1141.4
7	Northridge-01	1994	Arleta - Nordhoff Fire Station	6.69	0.345	5.38	976.74

8	Northridge-01	1994	N Hollywood - Coldwater Can	6.69	0.309	7.77	1071.1
9	Chi-Chi Taiwan	1999	CHY002	7.62	0.137	15.51	771.42
10	Chi-Chi Taiwan	1999	CHY036	7.62	0.273	9.97	764.90
11	Chi-Chi Taiwan	1999	TCU038	7.62	0.1448	15.80	977.23
12	Chi-Chi Taiwan	1999	TCU059	7.62	0.165	10.63	894.59
13	Chi-Chi Taiwan	1999	TCU110	7.62	0.1918	7.19	697.90
14	Kashmir Earthquake	2005	ABD-Abbottabad	7.60	0.2517	16.16	731.76
15	St Elias Alaska	1979	Icy Bay	7.54	0.1759	16.44	1005.15

The ground motion spectra for considered accelerograms are shown in figure 4.33. For stone masonry buildings, incremental dynamic analysis has not been used due to complexities and limitations involved in the research version of 3Muri software.

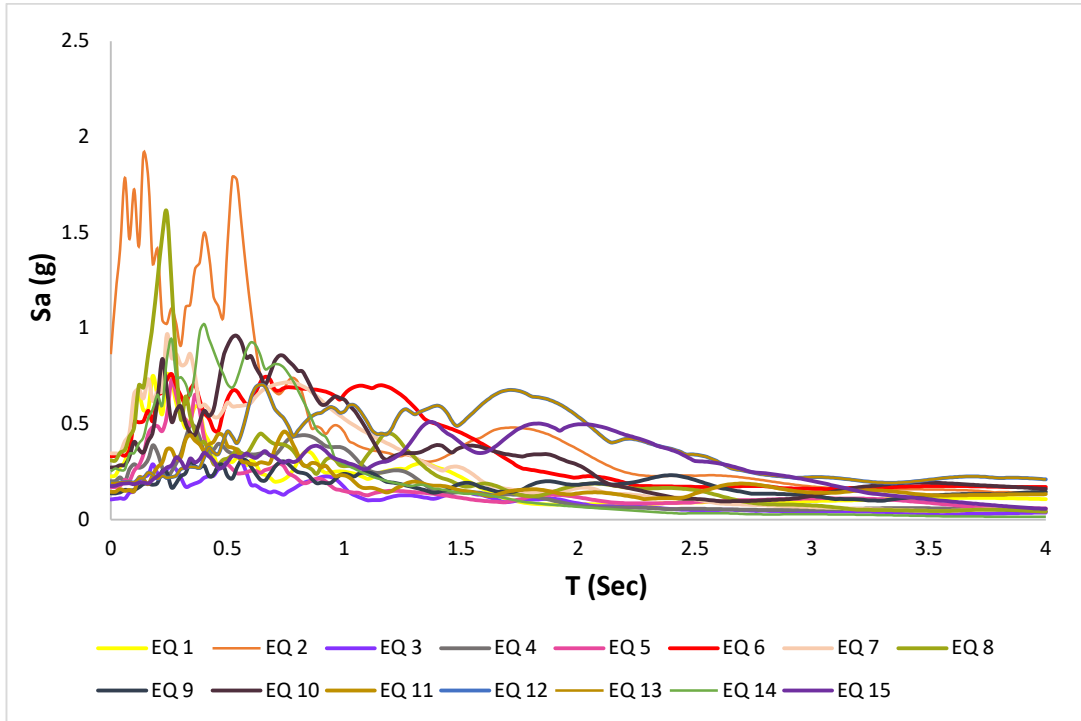


Figure 4.33: Ground motion spectra of considered GM histories in terms of Period (T)

The obtained results by applying ground motions are presented in figure 4.34. The results exhibit the relationship between PGA and Spectral Displacement (S_d).

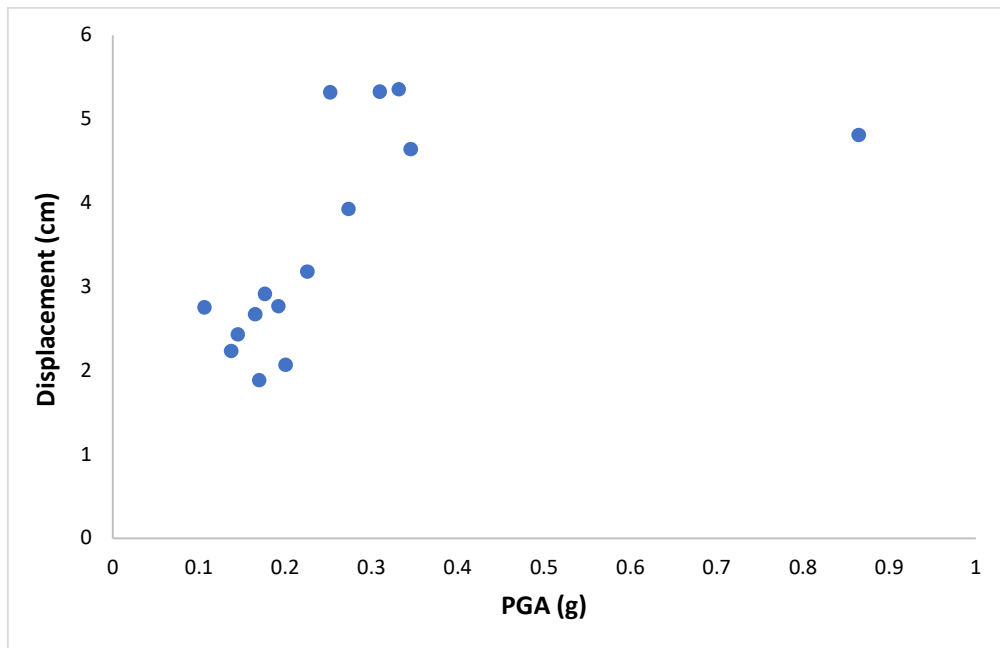


Figure 4.34: Results of GM history analyses

From figure 4.34, it can be observed that every ground motion induces excessive displacement up to 5.4 cms. Against every single ground motion, the spectral displacement is greater than the target displacement value of 1.15 cms. The minimum displacement was observed at PGA of 0.16g where the structure experienced 1.9 cms of displacement. 1.9 cms are still greater than the target displacement value of 1.15 cms, obtained through nonlinear static analysis. It essentially means that stone masonry school buildings could easily collapse under seismic excitations in their contemporary condition.

4.3.2.3. Seismic vulnerability assessment in terms of fragility curves

4.3.2.3.1. Mathematical Definition of damage indicator, limit states, and seismic intensity measure

As described earlier, fragility curves describe the probabilistic information about structural vulnerability against discrete seismic intensities. In the present study, the theoretical background for selection and adoption of different damage indicators and limit states have already been discussed in section 4.2.3.7. For depicting the structural damage, global displacement has been used to characterize the limit states. Three limit states i.e. serviceability limit state (LS1), life safety limit state (LS2), and collapse prevention (LS3) has been used for the considered stone masonry school building. The qualitative description of these limit states has been provided previously, thus, yielding and ultimate displacements, obtained from the capacity curve, have been utilized to establish the quantitative values of limit states. For characterizing the seismic intensity for stone masonry school buildings, spectral acceleration has been employed as seismic intensity measure to derive fragility relations.

Since there were only one-story stone masonry school buildings in the considered region, therefore, the developed methodology for fragility assessment has not been utilized for stone masonry schools as only single/fundamental mode's response has been considered. The quantitative values of all three limit states have been provided in table 4.16. It is worth mentioning that qualitative criterion for limit states for all three typologies of school buildings i.e. RC Schools, stone masonry schools, and brick masonry schools, has been kept consistent.

Table 4.16: Quantitative values of limit states for stone masonry school buildings

Limit State	In terms of global displacement value in centimetres (cms)		
	Serviceability (LS1)	Life Safety (LS2)	Collapse Prevention (LS3)
	0.035	0.11	0.16

4.3.2.3.2. Fragility derivation

As described earlier, fragility relationships portray the probabilistic information about exceeding a specific damage or limit state against discrete intensities of seismic intensity measures. Equation no. 7 manifests the mathematical form of fragility curves. Since it is essential to maximize the values of controlling parameters, Maximum Likelihood Method has again been utilized here to develop optimized slope of the fragility curves. Figure 4.35 presents the obtained fragility curves after executing dynamic analysis.

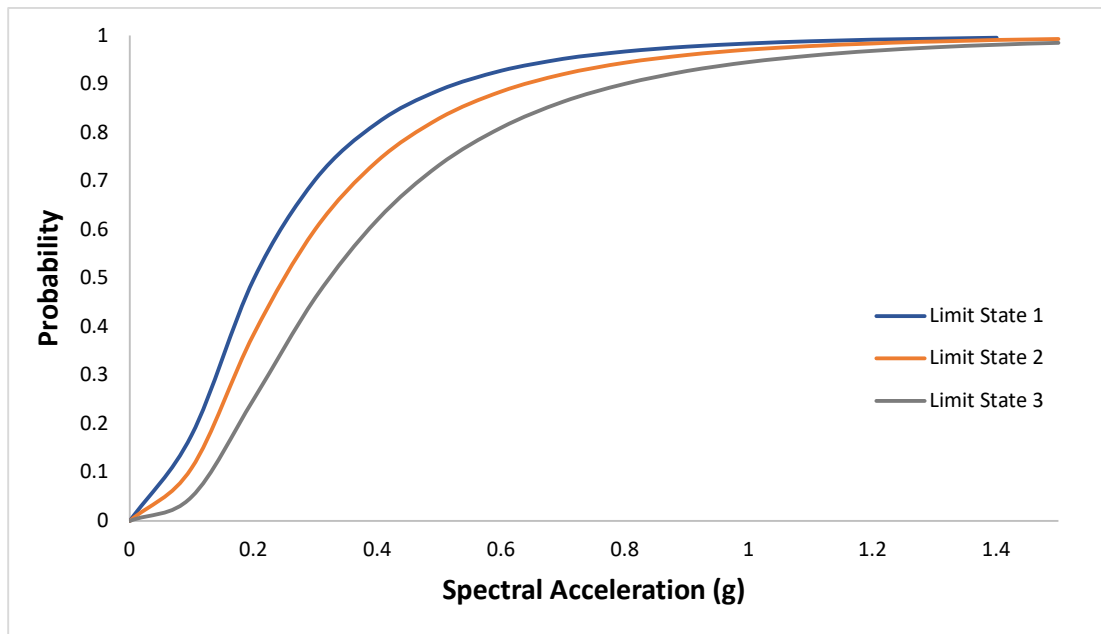


Figure 4.35: Fragility curves for typical stone masonry school buildings in considered region

The fragility relationships depict that contemporary school buildings in the surveyed area are highly vulnerable to earthquakes. At Sa of 0.1g, the probability of being in LS 1 was 18

percent, while with S_a of 0.2g, the probability of exceeding LS1 rapidly increased to 50 percent. Similarly, the probability of being in failure limit state i.e. LS3 was 25 percent at S_a of 0.2g, while it rapidly increased to 46 percent at S_a of 0.3g. These rapid increases indicate the poor structural performance of stone masonry schools in the considered area. Same trend has been observed for the probability values of LS2. In order to decrease the values of probabilities of exceedances, structural intervention is vital.

For the reliability analysis of structural modelling of stone and brick masonry school structures, this work has employed the research outcome provided by Domanski & Matysek (2018). Their work highlights the specifics of computational & diagnostics analysis for masonry structures. Their work presented numerous factors i.e. the configuration of loads, the structural capacity, etc. to be the basics for a reliability analysis that eventually presents the probability of failure in accordance with the following equation:

$$P_f = P[g(X) \leq 0] = \int_{g(x) \leq 0} f_x(x) dx \quad (4.4)$$

Where:

Function for performance is indicated by $g(\mathbf{X})$, and vector of random variables is denoted by \mathbf{x} . While $f_x(\cdot)$ is the function of multidimensionality for \mathbf{x} variables. For a better understanding, the reader of this work is referred to Domanski and Matysek (2018), and the work done by Murtaza (2022) for an elaborative understanding of the results of reliability analysis for the masonry structures considered in this work.

4.4. Vulnerability Assessment of Brick Masonry Schools

Brick masonry schools in considered region were mostly developed by private investors in house buildings, thus, they lack the primary spirit of an educational infrastructure. Brick masonry compose a major stock of residential building in considered area, and thus, these were the residential buildings that were being used as schools by private school owners. Therefore, it is worthy to mention that brick masonry schools did not portray the greater national interest in considered region. However, with the intention to develop a comprehensive document that could contain vulnerability information for all types of school typologies, this work assesses the vulnerability of a two-story brick masonry school so that a reasonable level of information about structural susceptibility can be obtained.

4.4.1. Structural modelling of brick masonry schools

A stone masonry school was selected for analytical modelling from Muzaffarabad District as that district was heavily damaged during 2005 Hazara-Kashmir Earthquake. The selection has been made depending upon the maximum number of students. The plan of selected school is provided in figure 4.36. The considered school has two stories. The plan showed represents the ground floor. Story height is taken as 11 feet.

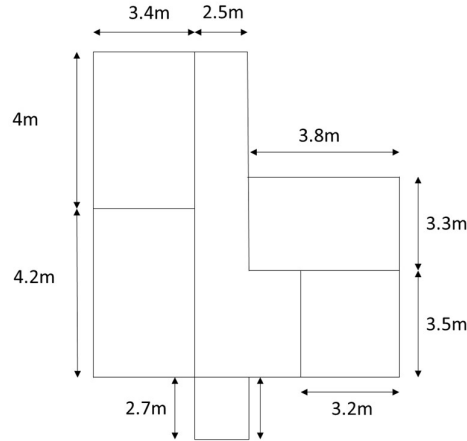


Figure 4.36: Plan view of considered brick masonry school

It is essential to possess ample information about material characteristics of bricks being used at domestic level. Therefore, a research conducted by Shahzada et al. [63] was utilized. In their research, they produced a full scale model of an internal room using locally available bricks. 228 mm thick brick masonry was used to construct the walls by using English bond as such pattern is frequently used in considered region.

228 mm wide and 150 mm high RC lintel beams were provided above all openings. In their research study, they provided 150 mm thick slab with half-inch diameter reinforcing bars, placed at discrete interval of 228 mm in both directions. For producing the effect of vertical precompression, arising from adjacent parts, walls having thickness of 343 mm were provided in all directions of casted slab, while for incorporating the effect of dead load from the finishes, sand layer having thickness of 254 mm was provided on the roof. All the experimental model was constructed by providing a 190 mm thick RC foundation.

Their research contained experimental investigation to determine the material characteristics of Pakistani bricks. The modulus of elasticity and compressive strength were determined in

accordance with ASTM International’s C1314 by conducting experimental investigation on masonry prisms of 400 mm wide and 228 mm thick, being used in construction in seismic zone 4 of Pakistan. The values obtained from their experimental study are given in Table 4.17.

Table 4.17: Material characteristics of brick masonry

Material Property	Symbol	Quantitative value
Masonry unit compressive strength	f_b	12.4 MPa
Compressive strength of mortar	f_{mo}	5 MPa
Masonry compressive strength	f_m	3 MPa
Masonry diagonal tensile strength	f_{tu}	0.05 MPa
Elastic modulus of masonry	E_m	1227 MPa

For structural modelling, Equivalent Frame Method (EFM) [64]-[65] was used. Same software tool, 3Muri, was employed to develop the structural model. As mentioned earlier, the license was specifically obtained from the developers of software. Obtained license allowed for modelling both, stone and brick masonry structures. Figure 4.37 shows developed 3 dimensional model in 3Muri commercial version. For carrying out POA, commercial version of software was used, while for conducting time history analysis, research version was eventually employed to determine seismic performance.

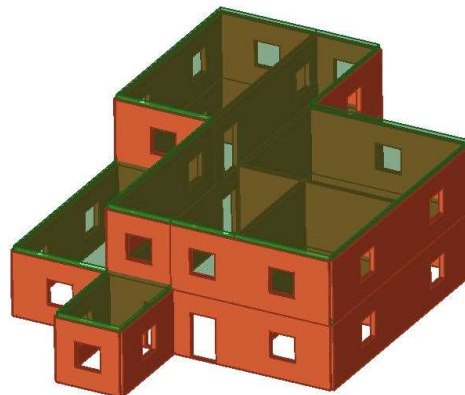


Figure 4.37: 3-Dimensional analytical model of brick masonry school structure in considered area

Figure 4.38 presents the 3-dimensional un-cracked model, providing a view on the macro elements. Modelling of the building is done by insertion of walls which are made into discrete macro elements. These represent deformable masonry piers and spandrel beams on the level. Rigid nodes are indicated in the areas of the masonry that are typically less subject to earthquake damage. Generally, the piers and the spandrel beams are contiguous at the openings, and the rigid nodes are an element that connects the piers and spandrel beams. The mathematical concept behind the use of this element allows the damage mechanism to be found. This is shear damage in the central part, or compression-bending at the edges of the element. In this way, the damage dynamic can be understood in the way that it actually occurs in reality.

The nodes of the model are three-dimensional, with five degrees of liberty. (three displacement components in the overall reference system and the rotation around the X and Y axes) Alternatively, they are two-dimensional nodes with three degrees of liberty (two transfers and the rotation of the level of the wall). The three-dimensional nodes are used to allow transfer of the actions from one wall to a second wall which is located transversally to the first. The two-dimensional nodes only have degrees of liberty on the level where the wall is found, allowing transfer of the force states between the various points of the wall.

The horizontal structures are modelled with the three node floor elements connected to three-dimensional nodes. They can be loaded perpendicularly to their level using accidental or permanent loads. Seismic actions load the floor along the direction of the level. For this reason, the floor finite element is defined with axial rigidity, but without bending rigidity. This is because the main mechanical behavior of interest is that receiving horizontal loads due to the seismic action.

The modal analysis was performed to check the adequacy of established analytical model, and to check the modal time periods. The maximum modal mass participated in the fundamental mode of the structure. The fundamental mode's time period came out to be 0.115 seconds. Table 4.18 provides the obtained modal results for first three modes of the considered brick masonry school building. The first column represents the number of modes, while the corresponding time periods are provided in 2nd column of the table. 3rd column provides the modal mass participation percentage. From the excessive modal mass participation in 1st mode, it can be observed that building would mostly remain in its fundamental mode during seismic excitation.

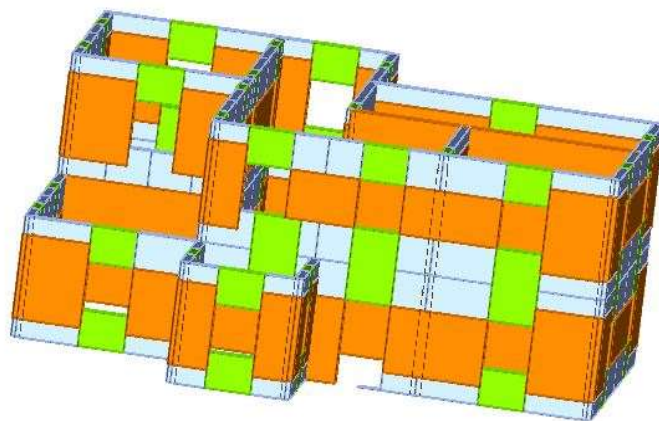


Figure 4.38: 3-Dimensional model of brick masonry school, showing macro elements

Table 4.18: Modal analysis results for brick masonry school building

Mode No.	Time period (sec.)	Modal mass participation (%)
1	0.115	92.41
2	0.085	6.73
3	0.077	0.91

4.4.2. Pushover analysis

Pushover analysis had been performed to establish the fundamental force-deformation relationships of considered brick masonry school building. The current work does not make any idealization to produce capacity curves, rather directly employs the analysis outcome of 3-dimensional analytical model. Figure 4.39 shows the colour legend of results. The legend is imperative to be understood in order to comprehend the results in a better and rational manner. The results are herein presented graphically to depict the bending damage, bending failure, shear failure, and failure during elastic phase.

	Undamaged
	Shear damage
	Bending damage
	Shear failure
	Bending failure
	Compression failure
	Tension failure
	Failure during elastic phase

Figure 4.39: Color legend of brick masonry results

The reader of this work is referred to figure 4.39 for understanding the graphical presentation of results, obtained after executing pushover analysis. Figure 4.40 shows plan view of whole structure, while a wall has been highlighted to display damage, experienced by equivalent frames in that specific wall. Figure also depicts the deformed shape in plan view.

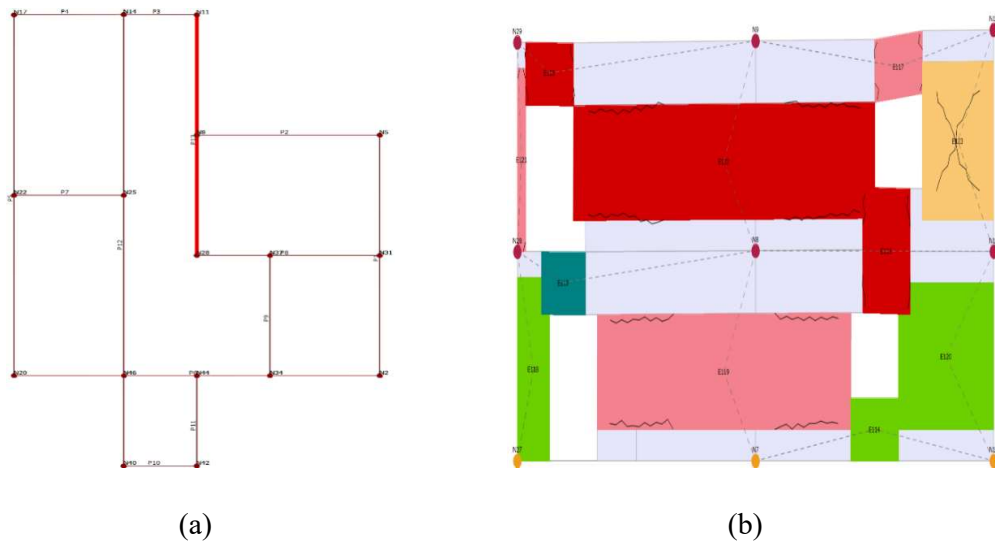


Figure 4.40: (a) Plan view of structure (b) Deformed shape of wall to check damage

In figure 4.40, it is eminent that the equivalent frames are subjected to bending damage, bending failure, shear cracking and failure during elastic phase of structural behaviour. Similar results have been extracted for some other walls. Figure 4.41 shows the plan view again but with different wall highlighted to check the structural damage. The considered wall has gone under shear failure and flexural damage, while some portion has remained undamaged. The pushover analysis results are shown in figure 4.42. The figure portrays the image of pushover curve, directly obtained from 3Muri software. The software package allows for the bilinearization of obtained curve in accordance with specified codes. Thus, the figure also shows the bilinear curve that can be used in conjunction with the original pushover curve.

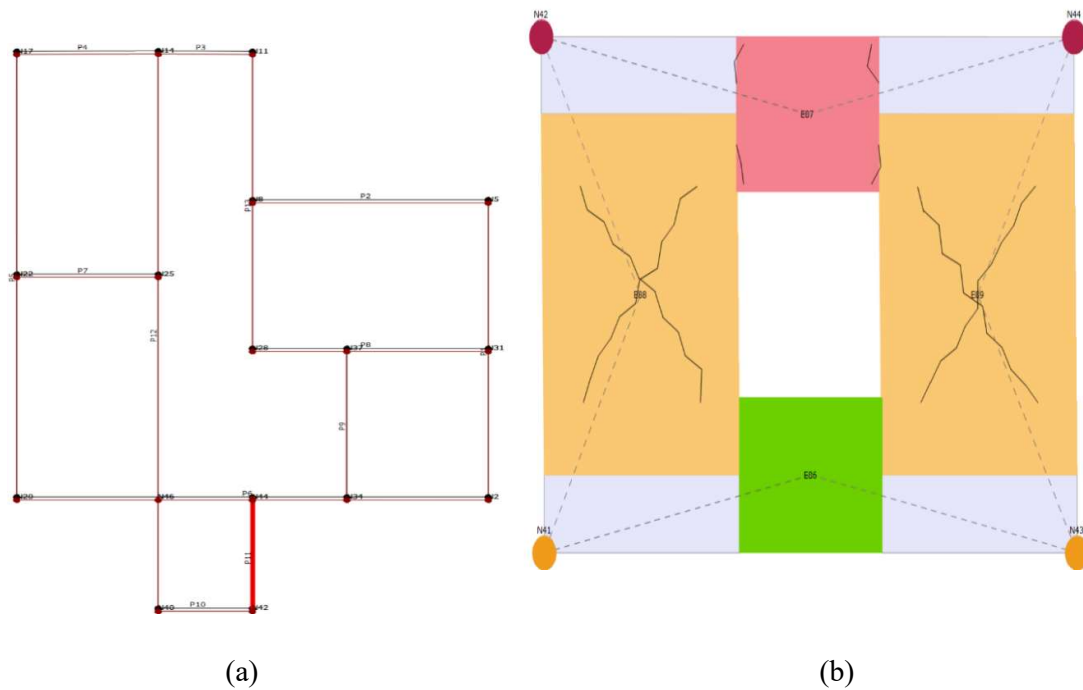


Figure 4.41: (a) Plan view showing considered wall to check damage (b) Deformed shape of considered wall in EFM

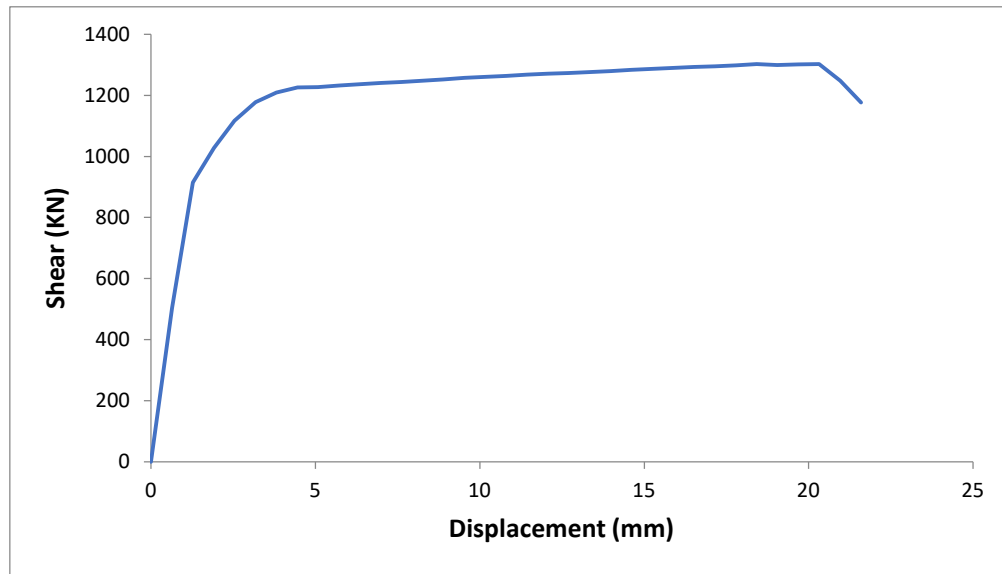


Figure 4.42: Pushover curve of considered brick masonry school building, showing maximum capacity of structure as 21.59 mm (less than 1 inch)

Pushover curve depicted that considered brick masonry school type loses all its structural capacity at the lateral displacement of 21 mm. The ultimate displacement came out to be 20.32 mm. The pushover curve had been used to establish the quantitative definition of limit states for the school building in consideration.

4.4.3. Nonlinear time history analysis and fragility derivation

Nonlinear time history analyses were conducted using the research version of 3Muri software package. Primary purpose was to establish fragility relationships for brick masonry school building. Real ground motion histories were used in order to establish the fragility relationships. Analogous ground motions have been employed to develop fragility curves for typical stone masonry buildings. Herein, table 4.19 shows the ground motions used for conducting the nonlinear time history analysis. All ground motions were scaled in accordance with the Pakistan' seismic zone 4 spectra by conducting spectral matching software package, SeismoMatch. The software has excellent capabilities for the spectral matching.

Table 4.19: Ground motions for brick masonry school building

Sr. No.	Earthquake Name	Year	Station Name	Mag.	PGA(g)	Rrup (miles)	Vs30 (ft./sec)
1	San Fernando	1971	LA - Hollywood Stor FF	6.61	0.225	14.15	1038.25
2	Gazli USSR	1976	Karakyr	6.8	0.864	3.40	851.67
3	Tabas Iran	1978	Boshrooyeh	7.35	0.106	17.89	1064.86
4	Spitak Armenia	1988	Gukasian	6.77	0.20	14.91	1127.07
5	Loma Prieta	1989	Agnews State Hospital	6.93	0.1695	15.27	786.38
6	Loma Prieta	1989	Saratoga - W Valley Coll.	6.93	0.331	5.78	1141.4
7	Northridge-01	1994	Arleta – Nordhoff Fire Station	6.69	0.345	5.38	976.74
8	Northridge-01	1994	N Hollywood – Coldwater Can	6.69	0.309	7.77	1071.1
9	Chi-Chi Taiwan	1999	CHY002	7.62	0.137	15.51	771.42
10	Chi-Chi Taiwan	1999	CHY036	7.62	0.273	9.97	764.90
11	Chi-Chi Taiwan	1999	TCU038	7.62	0.1448	15.80	977.23
12	Chi-Chi Taiwan	1999	TCU059	7.62	0.165	10.63	894.59

13	Chi-Chi Taiwan	1999	TCU110	7.62	0.1918	7.19	697.90
14	Kashmir Earthquake	2005	ABD- Abbottabad	7.60	0.2517	16.16	731.76
15	St Elias Alaska	1979	Icy Bay	7.54	0.1759	16.44	1005.15

Same ground motion selection criteria has been followed as mentioned in section 4.2.3.5. The mechanism of fault, source to site distance, magnitude, and the shear wave velocity V_s , in the upper 30 m (100 feet) of soil strata have been considered as the controlling parameters for selecting the ground motions. It is pertinent to mention that special emphasis has been given to the characteristics of 2005 Kashmir Earthquake while selecting the ground motions as it resulted in the most catastrophic and fatally devastation of the region throughout the history, and most of the parameters, during selection, have been kept in strong alignment with those matching with the 2005 Kashmir Earthquake. The fault, which resulted in 2005 Kashmir Earthquake, is reverse-oblique in its character, and as observed, it produced a large magnitude earthquake of 7.6 Mw, with its epicenter at 19 KMs northeast of Muzaffarabad. Therefore, only the earthquakes ranging from 6.50 to 8.0 in magnitude, originated from the reverse and revers-oblique faults are selected, and 0 to 30 KMs range has been used for source-to-site distance so any random variation due to path attenuation effects and varying soil characteristics could be effectively considered. Moreover, for selecting the ground motions, shear wave velocity, V_{s30} , has been kept between 170 m/sec (575 ft/sec) to 350 m/sec (1150 ft/sec) in accordance with BCP-2007 for the soil type S_d . Table 4.19 also shows the selected ground motions for vulnerability assessment. Magnitude, distance-to-rupture, V_{s30} , and source mechanism are also mentioned.

4.4.3.1. Damage indicator, seismic intensity measure, and limit states

For the presented study, S_a has been employed as seismic intensity measure, while global response has been considered to quantitatively match the qualitative description of limit states. The discrete quantitative value of spectral acceleration against Serviceability Limit

State (LS1) is 1.27 mm. For Collapse prevention Limit State (LS3), the quantitative value of global displacement stands at 18.42 mm, while for Life Safety Limit State (LS2), the discrete mathematical value is in between LS1 and LS2, 13.82 mm. Thus, all limit states are displacement-based that have been derived from yielding and ultimate displacements of the capacity curves.

4.4.3.2. Fragility derivation

Established fragility curves are presented in figure 4.43. Equation (4.1), reiterated herein, have been used to develop the fragility curves.

$$P(LS|IM) = \Phi\left(\frac{\ln IM - \lambda_c}{\beta_c}\right)$$

All parts of the equation have been described earlier. As previously employed, Maximum Likelihood Method (MLM) was again used to develop the optimized values of controlling parameters, λ_c , and β_c .

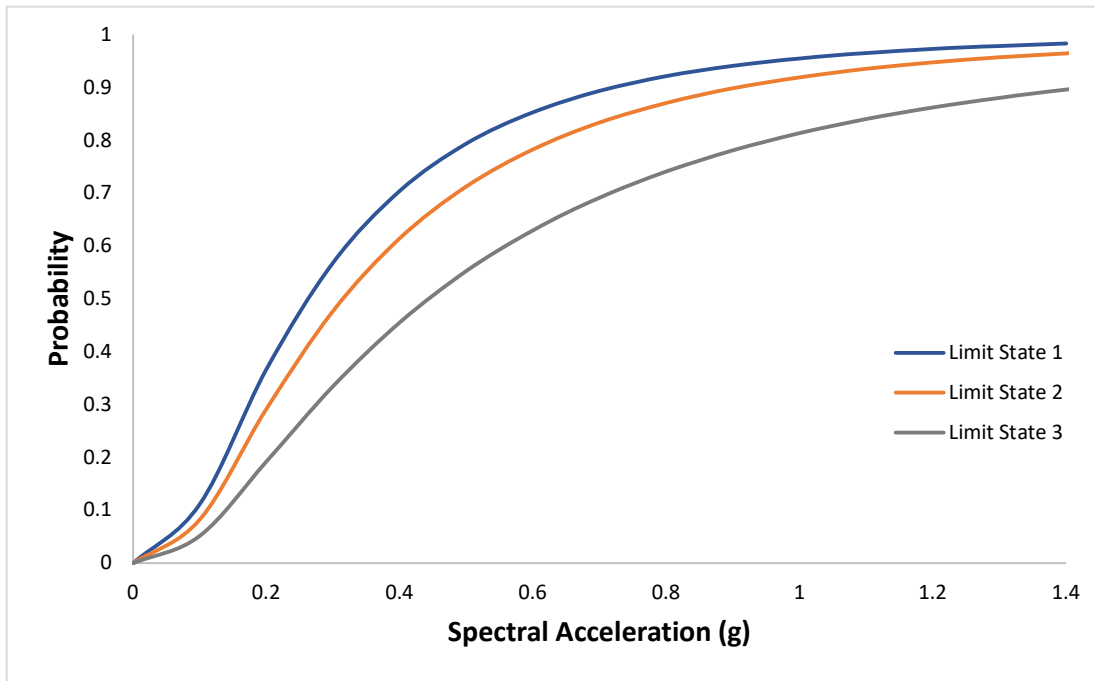


Figure 4.43: Fragility relationships for brick masonry school building

The fragility relationships depicts that contemporary school buildings in the surveyed area are highly vulnerable to earthquakes. It can be observed from the fragility relationships that

discrepancy between LS2 and LS3 is higher in comparison with the discrepancy between LS2 and LS1. The probable reason is that the considered brick masonry structure that has manifested ductile behaviour before reaching the LS 3. At Sa of 0.1g, the probability of being in LS 1 was 11 percent, while with Sa of 0.2g, the probability of exceeding LS1 rapidly increased to 37 percent. Similarly, the probability of being in failure limit state i.e. LS3 was 19 percent at Sa of 0.2g, while it increased to 33 percent at Sa of 0.3g. For intended depletion of these values of probabilities of exceedances, structural intervention is vital.

CHAPTER 5: CONCLUSIONS AND RECOMMENDATIONS

5.1. Conclusions

Current work portrays the architectural and structural configuration of school buildings in Kashmir region by means of collected data. 2417 schools were visited during data collection process. It was noted that Government of Pakistan developed typical design modules for the construction of schools in Muzaffarabad. In the whole process of data collection, numerous field visits were conducted and professional interviews were taken to establish the school buildings typologies in the considered region. The school buildings have been categorized into 3 categories i.e. Reinforced Concrete (RC) Schools, Stone Masonry Schools, and Brick Masonry Schools.

A new procedure for establishing vulnerability information has been developed for RC schools. Presented framework considers higher modes & significantly reduces computational effort for considered school by 68 hours. It took 72 hours on a core i7, 6th generation computer with 8 GBs of RAM for developing the fragility curves of considered RC school building using conventional procedure that primarily focused upon fundamental mode only. However, by employing the presented procedure, the fragility curves for the considered RC school were developed in 4 hours and 50 minutes only, using the same computer. It is pertinent to mention that during analysis, the effect of higher vibrational modes was discreetly considered through their decoupling, and by subjecting them to their own unique nonlinear behaviour by means of SDOF systems.

While developing the fragility curves using a conventional methodology that primarily concentrates at the first-mode response only, the probability of exceedance at 0.60g PGA for LS1 stood at 74%; while with the proposed methodology, where 2nd mode was discreetly incorporated in the IDA and post-processing of results, the probability value for LS1 escalated up to 85%. As indicated by the obtained results, LS1 has received the most substantial influence of the incorporation of 2nd mode in the vulnerability assessment process, while it is pertinent to mention that the Collapse Prevention limit state, the LS3 has received not so significant contribution even with the inclusion of the 2nd mode, and has remained mainly dependent upon the fundamental mode for the considered school building typology. This insignificant change in the LS3 is mainly attributed to the relatively low modal mass participation ratio of 2nd mode, and consequently, a substantial increase in the

evaluated probabilities, particularly for LS3, could not be observed. However; the obtained results through the newly established methodology provided an articulated comprehension for evaluating the contribution of each structural mode towards the structural seismic vulnerability.

The proposed methodology relies upon the nonlinear analysis of representative SDOF structures, and hence, it allows to greatly diminish the colossal computational effort which would be required to conduct the full 3-dimensional nonlinear analyses. For the present work, against twenty ground motions with seven scaling levels, 140 simulations were conducted for a single IM, thus making the total number of simulations equal to 420 i.e. 140 for PGA, 140 for Sa @ T1, and 140 for Sa @ T2. The execution of analysis took less than 5 hours for generating all sets of fragility curves. With insignificant and negligible loss of accuracy in the analyses process, the seismic vulnerability of structures can be assessed in few hours rather than conducting days-long analyses.

The proposed framework has been verified and validated by using it upon two other case studies. First case study was taken from PEER's database for benchmark structures. PEER's benchmark structure was analysed using proposed methodology and obtained fragility was then compared with the fragility developed by PEER. The presented methodology yielded a little higher collapse level probability values, while PEER as a whole presented results with little lower values. The increase is primarily attributed to the difference in modelling approaches. PEER has employed lumped-plasticity approach that consolidates the masses at story levels with two-dimensional analysis, and primarily targets only the near collapse response with a fundamental focus on 1st mode only, while the presented methodology incorporates complete 3D structural cyclic force-deformation relationship at global level in place of material level only. The second prominent reason for the increase in probability values is the discreet consideration of 2nd mode during analysis. The wholesome incorporation of 2nd mode in accordance with UMRHA procedure has directly influenced the results by increasing the probability values.

The second case study was a 55 story high-rise building. The high-rise building was specifically selected as it had significant contribution of higher vibrational modes in comparison with the low-rise buildings, considered in this study. Analytical fragility curves for a specific class of tall buildings i.e. core-wall buildings, were developed in the current

study. Fragility relationships for considered high-rise buildings had been developed considering the response of each individual mode towards structural vulnerability. The fragility curves were developed with and without the consideration of higher modes to evaluate the efficacy of proposed procedure. For high-rise building, three IMs were used i.e. PGA, Sa @ 1.0 sec, and Sa @ 0.2 sec to adequately cover the low and high frequency structural responses.

The probability of exceeding LS1 against Sa @ 1.0 sec, with seismic intensity of 1.0g, was only 24% when only the first mode's response was considered during fragility analysis. With the proposed methodology, when higher modes were taken into account, the probability value rose to 60 percent for the same LS against same seismic intensity. Thus, unlike conventional procedures of IDA, that render almost impossible to develop fragility curves for this class of buildings (high-rise) using IDA of a 3D nonlinear model because of highly extensive computational effort, the presented methodology consumed not only very less amount of time, rather it rendered the computational effort way less expensive. Along with that, as evident by the obtained results, the proposed methodology did not depend only upon the response of fundamental mode, rather it portrayed the potential to incorporate the contribution of as many higher modes as desirable.

5.2. Recommendations

Proposed procedure establishes a baseline for further research in modal fragility analysis, and thus holds potential for integration with other defining factors of structural behaviour. Therefore, subsequent improvement in research may include differential settlements and soil-structure interaction.

This work is particularly focused upon the assessment of seismic vulnerability of school buildings in seismic zone 4 of Pakistan; nevertheless, the established methodology is generic in its fundamental nature, and thus, it can readily be adopted for evaluating the structural vulnerability of other types of RC buildings including the mid-rise and high-rise. It is comprehended that the proposed methodology would even function more elaborately in case of the buildings where the higher modes possess more modal participation ratios and require extensive computational effort. As for the considered region, the application of the presented framework can be extended to other types of the school building typologies to evaluate their structural seismic vulnerability.

Because of the simplicity, the presented framework can be employed by the domestic disaster preparedness and mitigation agencies from the view point of extending the application. For under developing countries, such as Pakistan, such studies are comparatively in their nascent form; with extending the application of presented work to other building types, a specific need for immediate structural intervention can be identified to enhance the dynamic resistance of structure(s) to safeguard the life of users and the inhabitants.

Furthermore, it is recommended that proposed procedure should be extended to evaluate the seismic vulnerability of other types of RC school buildings and a catalogue for vulnerability information of public infrastructure i.e. hospitals, should be developed at national level.

Vulnerability assessment methodology presented herein has been developed considering the ease of application. The proposed procedure should reach to practitioners, working in engineering sector. To ensure better understanding and best use, training programmes for users are recommended. An integrated effort by the concerned authorities like local government, municipalities, NGO's, INGO's and other related organizations towards dissemination is recommended with a consistent effort to conduct continuous research for improving presented methodology and for developing other computationally effective methods.

In the present work, the seismic pounding effects have not been covered. It is recommended that subsequent research may incorporate a separate module in the proposed methodology for evaluating the problems related to seismic pounding in the considered region.

For a better consideration of aleatory uncertainties, the number of ground motions may be increased for the analyses purpose, and moreover, the scaling of the intensity measures can be kept at a more discretized level.

For incorporating different modes of failure in a structure, some other types of limit states can also be defined for observing different modes of structural failures. Such an ornate effort would be helpful in determining the structural resilience more accurately.

The presented work includes only the process to assess the vulnerability and does not specifically address the assessment of the total risk involve in the considered region. Therefore, it is recommended that some probabilistic seismic hazard assessment must be made for the considered region, and the established fragility relationships, for a particular

class of school buildings, can be superimposed on the seismic hazard curve for their integration to finally evaluate the total risk involve. By their integration, the domestic authorities shall be able to devise better disaster preparedness and mitigation strategies for a proactive response instead of adopting the passive measures for minimizing the effects of an earthquake or other disasters after their occurrence.

REFERENCES

- [1] P. by the Applied Technology Council for the Federal Emergency Management Agency, “Rapid Visual Screening of Buildings for Potential Seismic Hazards: A Handbook Third Edition.”
- [2] F. Najam and N. Anwar, “Consequence-based Engineering Approach towards Earthquake Disaster Mitigation Post Earthquake Re-construction Project View project Structural Assessment and Recommendation for Risk Mitigation of Baltit Fort, Pakistan View project”, doi: 10.13140/RG.2.1.3939.1769.
- [3] M. Dolce *et al.*, “Seismic risk assessment of residential buildings in Italy,” *Bull. Earthq. Eng.*, vol. 19, no. 8, pp. 2999–3032, Jun. 2021, doi: 10.1007/s10518-020-01009-5.
- [4] Y. K. Wen, B. R. Ellingwood, and J. Bracci, “Vulnerability Function Framework for Consequence-based Engineering MAE Center Project DS-4 Report,” 2004.
- [5] D. P. Abrams, “Consequence-Based Engineering Approaches for Reducing Loss in Mid-America,” 2002.
- [6] M. Zain, M. Usman, S. H. Farooq, and T. Mehmood, “Seismic Vulnerability Assessment of School Buildings in Seismic Zone 4 of Pakistan,” *Adv. Civ. Eng.*, vol. 2019, 2019, doi: 10.1155/2019/5808256.
- [7] E. M. Güneşisi, “Seismic reliability of steel moment resisting framed buildings retrofitted with buckling restrained braces,” *Earthq. Eng. Struct. Dyn.*, vol. 41, no. 5, Apr. 2012, doi: 10.1002/eqe.1161.
- [8] M. Shinozuka, M. Q. Feng, J. Lee, and T. Naganuma, “Statistical Analysis of Fragility Curves,” *J. Eng. Mech.*, vol. 126, no. 12, Dec. 2000, doi: 10.1061/(ASCE)0733-9399(2000)126:12(1224).
- [9] S.-L. Lin, S. R. Uma, and A. King, “Empirical Fragility Curves for Non-Residential Buildings from the 2010–2011 Canterbury Earthquake Sequence,” *J. Earthq. Eng.*, vol. 22, no. 5, May 2018, doi: 10.1080/13632469.2016.1264322.
- [10] L. Hofer, P. Zampieri, M. A. Zanini, F. Faleschini, and C. Pellegrino, “Seismic damage survey and empirical fragility curves for churches after the August 24, 2016 Central Italy earthquake,” *Soil Dyn. Earthq. Eng.*, vol. 111, Aug. 2018, doi:

- 10.1016/j.soildyn.2018.02.013.
- [11] J. J. Kim, “Development of Empirical Fragility Curves in Earthquake Engineering considering Nonspecific Damage Information,” *Adv. Civ. Eng.*, vol. 2018, Dec. 2018, doi: 10.1155/2018/6209137.
- [12] J.-W. Bai, M. B. D. Hueste, and P. Gardoni, “Probabilistic Assessment of Structural Damage due to Earthquakes for Buildings in Mid-America,” *J. Struct. Eng.*, vol. 135, no. 10, Oct. 2009, doi: 10.1061/(ASCE)0733-9445(2009)135:10(1155).
- [13] I. Ioannou, W. Aspinall, D. Rush, L. Bisby, and T. Rossetto, “Expert judgment-based fragility assessment of reinforced concrete buildings exposed to fire,” *Reliab. Eng. Syst. Saf.*, vol. 167, Nov. 2017, doi: 10.1016/j.ress.2017.05.011.
- [14] D. Forcellini, “Analytical fragility curves of shallow-founded structures subjected to Soil-Structure Interaction (SSI) effects,” *Soil Dyn. Earthq. Eng.*, vol. 141, Feb. 2021, doi: 10.1016/j.soildyn.2020.106487.
- [15] N. Giordano, F. De Luca, and A. Sextos, “Analytical fragility curves for masonry school building portfolios in Nepal,” *Bull. Earthq. Eng.*, vol. 19, no. 2, pp. 1121–1150, Jan. 2021, doi: 10.1007/s10518-020-00989-8.
- [16] D. Forcellini, “Analytical Fragility Curves of Pile Foundations with Soil-Structure Interaction (SSI),” *Geosciences*, vol. 11, no. 2, Feb. 2021, doi: 10.3390/geosciences11020066.
- [17] Sadraddin, “Fragility Assessment of High-Rise Reinforced Concrete Buildings Fragility Assessment of High-Rise Reinforced Concrete Buildings Sadraddin.”
- [18] S. Karimzadeh, K. Kadaş, A. Askan, M. Altuğ Erberik, and A. Yakut, “A study on fragility analyses of masonry buildings in Erzincan (Turkey) utilizing simulated and real ground motion records,” in *Procedia Engineering*, 2017, vol. 199, pp. 188–193. doi: 10.1016/j.proeng.2017.09.237.
- [19] A. Di Cesare and F. C. Ponzo, “Seismic Retrofit of Reinforced Concrete Frame Buildings with Hysteretic Bracing Systems: Design Procedure and Behaviour Factor,” *Shock Vib.*, vol. 2017, 2017, doi: 10.1155/2017/2639361.
- [20] A. J. Kappos, “An overview of the development of the hybrid method for seismic

- vulnerability assessment of buildings,” *Struct. Infrastruct. Eng.*, vol. 12, no. 12, Dec. 2016, doi: 10.1080/15732479.2016.1151448.
- [21] A. Sandoli, G. P. Lignola, B. Calderoni, and A. Prota, “Fragility curves for Italian URM buildings based on a hybrid method,” *Bull. Earthq. Eng.*, Jun. 2021, doi: 10.1007/s10518-021-01155-4.
- [22] M. Serdar Kirçil and Z. Polat, “Fragility analysis of mid-rise R/C frame buildings,” *Eng. Struct.*, vol. 28, no. 9, Jul. 2006, doi: 10.1016/j.engstruct.2006.01.004.
- [23] A. Singhal and A. S. Kiremidjian, “Method for Probabilistic Evaluation of Seismic Structural Damage,” *J. Struct. Eng.*, vol. 122, no. 12, Dec. 1996, doi: 10.1061/(ASCE)0733-9445(1996)122:12(1459).
- [24] P. Zhai, P. Zhao, Y. Lu, C. Ye, and F. Xiong, “Seismic Fragility Analysis of Buildings Based on Double-Parameter Damage Models considering Soil-Structure Interaction,” *Adv. Mater. Sci. Eng.*, vol. 2019, Oct. 2019, doi: 10.1155/2019/4592847.
- [25] M. Ercolino, G. Magliulo, and G. Manfredi, “Seismic Performance of Single-Story Precast Buildings: Effect of Cladding Panels,” *J. Struct. Eng.*, vol. 144, no. 9, Sep. 2018, doi: 10.1061/(ASCE)ST.1943-541X.0002114.
- [26] F. Wu *et al.*, “Performance-Based Seismic Fragility and Risk Assessment of Five-Span Continuous Rigid Frame Bridges,” *Adv. Civ. Eng.*, vol. 2021, Apr. 2021, doi: 10.1155/2021/6657663.
- [27] J. Pejovic and S. Jankovic, “Selection of Ground Motion Intensity Measure for Reinforced Concrete Structure,” *Procedia Eng.*, vol. 117, 2015, doi: 10.1016/j.proeng.2015.08.219.
- [28] E. Abraik and M. Youssef, “SEISMIC FRAGILITY ASSESSMENT OF SUPERELASTIC SHAPE MEMORY ALLOY REINFORCED CONCRETE SHEAR WALLS.”
- [29] D. Wu, S. Tesfamariam, S. F. Stiemer, and D. Qin, “Seismic fragility assessment of RC frame structure designed according to modern Chinese code for seismic design of buildings,” *Earthq. Eng. Eng. Vib.*, vol. 11, no. 3, Sep. 2012, doi: 10.1007/s11803-012-0125-1.
- [30] S. Siva *et al.*, “Seismic fragility analysis of regular and setback RCC frames-A few hypothetical case studies Strength and durability studies on special concretes View project Fragility assessment of composite structures with irregularities View project SEISMIC

FRAGILITY ANALYSIS OF REGULAR AND SETBACK RCC FRAMES-A FEW HYPOTHETICAL CASE STUDIES,” 2016.

- [31] C. Casotto, V. Silva, H. Crowley, R. Nascimbene, and R. Pinho, “Seismic fragility of Italian RC precast industrial structures,” *Eng. Struct.*, vol. 94, pp. 122–136, Jul. 2015, doi: 10.1016/j.engstruct.2015.02.034.
- [32] A. Al Mamun, M. Saatcioglu, A. Al Mamun, and M. Saatcioglu, “FRAGILITY CURVES FOR SEISMIC VULNERABILITY ASSESSMENT OF REINFORCED CONCRETE FRAME BUILDINGS IN CANADA Geotechnical and Structural Health Monitoring View project Seismic Design and Assessment View project FRAGILITY CURVES FOR SEISMIC VULNERABILITY ASSESSMENT OF REINFORCED CONCRETE FRAME BUILDINGS IN CANADA,” 2017.
- [33] K. Bakalis and D. Vamvatsikos, “Seismic Fragility Functions via Nonlinear Response History Analysis,” *J. Struct. Eng.*, vol. 144, no. 10, Oct. 2018, doi: 10.1061/(ASCE)ST.1943-541X.0002141.
- [34] J. Ji, A. S. Elnashai, and D. A. Kuchma, “Seismic fragility relationships of reinforced concrete high-rise buildings,” *Struct. Des. Tall Spec. Build.*, vol. 18, no. 3, Apr. 2009, doi: 10.1002/tal.408.
- [35] M. N. Fardis, A. Papailia, and G. Tsionis, “Seismic fragility of RC framed and wall-frame buildings designed to the EN-Eurocodes,” *Bull. Earthq. Eng.*, vol. 10, no. 6, Dec. 2012, doi: 10.1007/s10518-012-9379-2.
- [36] N. Ghimire and H. Chaulagain, “Seismic Fragility Analysis of Institutional Building of Pokhara University,” *Himal. J. Appl. Sci. Eng.*, vol. 1, no. 1, Dec. 2020, doi: 10.3126/hijase.v1i1.33539.
- [37] B. Khazai, Q. Ali, S. M. Ali, and M. Khan, “EERI Special Earthquake Report-The Kashmir Earthquake of October 8, 2005: Impacts in Pakistan,” 2006.
- [38] C. B. Haselton and G. G. Deierlein, “An Assessment to Benchmark the Seismic Performance of a Code-Conforming Reinforced-Concrete Moment-Frame Building Basin Effects on Earthquake Ground Motion View project Bayesian methods View project,” 2008.
- [39] A. K. Chopra and R. K. Goel, “A modal pushover analysis procedure to estimate seismic

- demands for unsymmetric-plan buildings,” *Earthq. Eng. Struct. Dyn.*, vol. 33, no. 8, pp. 903–927, Jul. 2004, doi: 10.1002/eqe.380.
- [40] H. Chaulagain, V. Silva, H. Rodrigues, E. Spacone, and H. Varum, “EARTHQUAKE LOSS ESTIMATION FOR THE KATHMANDU VALLEY.”
- [41] “BCP SP-2007 Preface.”
- [42] M. M. Rafi and M. M. Nasir, “Experimental Investigation of Chemical and Physical Properties of Cements Manufactured in Pakistan,” *J. Test. Eval.*, vol. 42, no. 3, May 2014, doi: 10.1520/JTE20130158.
- [43] *Seismic Evaluation and Retrofit of Existing Buildings*. Reston, VA: American Society of Civil Engineers, 2014. doi: 10.1061/9780784412855.
- [44] C. Xuewei, H. Xiaolei, L. Fan, and W. Shuang, “Fiber Element Based Elastic-Plastic Analysis Procedure and Engineering Application,” *Procedia Eng.*, vol. 14, 2011, doi: 10.1016/j.proeng.2011.07.227.
- [45] J. B. Mander, M. J. N. Priestley, and R. Park, “THEORETICAL STRESS-STRAIN MODEL FOR CONFINED CONCRETE,” 1988.
- [46] D. G. Lignos, “INTERACTIVE INTERFACE FOR INCREMENTAL DYNAMIC ANALYSIS PROCEDURE (IIDAP) USING DETERIORATING SINGLE DEGREE OF FREEDOM SYSTEMS Version 1.2 THEORY AND EXAMPLE APPLICATIONS MANUAL Interactive Interface for Incremental Dynamic Analysis Procedure Version 1.2,” 2014.
- [47] L. F. Ibarra, R. A. Medina, and H. Krawinkler, “Hysteretic models that incorporate strength and stiffness deterioration,” *Earthq. Eng. Struct. Dyn.*, vol. 34, no. 12, Oct. 2005, doi: 10.1002/eqe.495.
- [48] D. Lignos, “SIDESWAY COLLAPSE OF DETERIORATING STRUCTURAL SYSTEMS UNDER SEISMIC EXCITATIONS A DISSERTATION SUBMITTED TO THE DEPARTMENT OF CIVIL AND ENVIRONMENTAL ENGINEERING AND THE COMMITTEE ON GRADUATE STUDIES OF STANFORD UNIVERSITY IN PARTIAL FULFILLMENT OF THE REQUIREMENTS FOR THE DEGREE OF DOCTOR OF PHILOSOPHY,” 2008.

- [49] D. G. Lignos and H. Krawinkler, "Deterioration Modeling of Steel Components in Support of Collapse Prediction of Steel Moment Frames under Earthquake Loading," *J. Struct. Eng.*, vol. 137, no. 11, Nov. 2011, doi: 10.1061/(ASCE)ST.1943-541X.0000376.
- [50] R. P. Kennedy, "Risk based seismic design criteria," *Nucl. Eng. Des.*, vol. 192, no. 2–3, Sep. 1999, doi: 10.1016/S0029-5493(99)00102-8.
- [51] T. M. Frankie, B. Gencturk, and A. S. Elnashai, "Simulation-Based Fragility Relationships for Unreinforced Masonry Buildings," *J. Struct. Eng.*, vol. 139, no. 3, Mar. 2013, doi: 10.1061/(ASCE)ST.1943-541X.0000648.
- [52] M. A. Erberik, "Seismic Fragility Analysis," in *Encyclopedia of Earthquake Engineering*, Berlin, Heidelberg: Springer Berlin Heidelberg, 2015. doi: 10.1007/978-3-642-36197-5_387-1.
- [53] K. Kostinakis and A. Athanatopoulou, "Incremental dynamic analysis applied to assessment of structure-specific earthquake IMs in 3D R/C buildings," *Eng. Struct.*, vol. 125, Oct. 2016, doi: 10.1016/j.engstruct.2016.07.007.
- [54] E. Fereshtehnejad, M. Banazadeh, and A. Shafieezadeh, "System reliability-based seismic collapse assessment of steel moment frames using incremental dynamic analysis and Bayesian probability network," *Eng. Struct.*, vol. 118, Jul. 2016, doi: 10.1016/j.engstruct.2016.03.057.
- [55] P. Zarfam and M. Mofid, "On the modal incremental dynamic analysis of reinforced concrete structures, using a trilinear idealization model," *Eng. Struct.*, vol. 33, no. 4, Apr. 2011, doi: 10.1016/j.engstruct.2010.12.029.
- [56] J. W. Baker and) M Eeri, "Efficient analytical fragility function fitting using dynamic structural analysis."
- [57] C.-T. Dang, T.-P. Le, and P. Ray, "A novel method based on maximum likelihood estimation for the construction of seismic fragility curves using numerical simulations," *Comptes Rendus Mécanique*, vol. 345, no. 10, Oct. 2017, doi: 10.1016/j.crme.2017.06.011.
- [58] International Code Council., *International building code 2003*. International Code Council, 2002.
- [59] G. Fenves and F. Filippou, "Methods of Analysisfor Earthquake- Resistant Structures," in

Earthquake Engineering, CRC Press, 2004. doi: 10.1201/9780203486245.ch6.

[60] “Help 3Muri.”

[61] I. Giongo *et al.*, “Detailed seismic assessment and improvement procedure for vintage flexible timber diaphragms,” *Bull. New Zeal. Soc. Earthq. Eng.*, vol. 47, no. 2, Jun. 2014, doi: 10.5459/bnzsee.47.2.97-118.

[62] New Zealand Society for Earthquake Engineering (1998-), *Assessment and improvement of the structural performance of buildings in earthquakes : prioritisation, initial evaluation, detailed assessment, improvement measures : recommendations of a NZSEE study group on earthquake risk buildings.*

[63] K. Shahzada *et al.*, “Experimental Seismic Performance Evaluation of Unreinforced Brick Masonry Buildings,” *Earthq. Spectra*, vol. 28, no. 3, Aug. 2012, doi: 10.1193/1.4000073.

[64] P. Roca, C. Molins, and A. R. Mari, “Strength Capacity of Masonry Wall Structures by the Equivalent Frame Method,” *J. Struct. Eng.*, vol. 131, no. 10, Oct. 2005, doi: 10.1061/(ASCE)0733-9445(2005)131:10(1601).

[65] G. Rizzano, R. Sabatino, and P. D. Student, “AN EQUIVALENT FRAME MODEL FOR THE SEISMIC ANALYSIS OF MASONRY STRUCTURES SÍSMICA 2010-8° CONGRESSO DE SISMOLOGIA E ENGENHARIA SÍSMICA 1 AN EQUIVALENT FRAME MODEL FOR THE SEISMIC ANALYSIS OF MASONRY STRUCTURES,” 2010.